1999-09

Development of a helicopter vortex ring state warning system through a moving map display computer

Varnes, David J.

Monterey, California. Naval Postgraduate School

NAVAL POSTGRADUATE SCHOOL

Monterey, California

THESIS

DEVELOPMENT OF A HELICOPTER VORTEX RING STATE WARNING SYSTEM THROUGH A MOVING MAP DISPLAY COMPUTER

by

David J. Varnes

September 1999

Thesis Advisor: Russell W. Duren

Approved for public release; distribution is unlimited.

REPORT DOCUMENTATION PAGE

Form Approved
OMB No. 0704-0188

1. AGENCY USE ONLY *(Leave blank)*	2. REPORT DATE	3. REPORT TYPE AND DATES COVERED
	September 1999	Master's Thesis

4. TITLE AND SUBTITLE
DEVELOPMENT OF A HELICOPTER VORTEX RING STATE WARNING SYSTEM THROUGH A MOVING MAP DISPLAY COMPUTER

5. FUNDING NUMBERS

6. AUTHOR(S)
Varnes, David, J.

7. PERFORMING ORGANIZATION NAME(S) AND ADDRESS(ES)
Naval Postgraduate School
Monterey, CA 93943-5000

8. PERFORMING ORGANIZATION REPORT NUMBER

9. SPONSORING / MONITORING AGENCY NAME(S) AND ADDRESS(ES)
Office of Naval Research (Naval Science Advisory Program) Mr. Steve Kern, Science and Technology Advisor, Commander, Naval Air Force, U.S. Atlantic Fleet, 1279 Franklin St., Norfolk, VA 23511-2494

10.SPONSORING/MONITORING AGENCY REPORT NUMBER
CNAL-1.2-99-TSP

11. SUPPLEMENTARY NOTES
The views expressed in this thesis are those of the author and do not reflect the official policy or position of the Department of Defense or the U.S. Government.

12a. DISTRIBUTION / AVAILABILITY STATEMENT
Approved for public release; distribution is unlimited.

12b. DISTRIBUTION CODE

ABSTRACT

The need for improved pilot aids has become a high priority item for pilots and aircrews operating at sea and ashore. Pilot aids such as the moving map display, GPWS, collision, and vortex-ring state (VRS) warning systems will significantly enhance aircrew situational awareness and safety. Many more of today's aircraft mishaps are a result of pilot error, which includes a loss of situational awareness. The moving map display provides relatively easy incorporation of sophisticated pilot aids without operational flight program (OFP) modification. This thesis discusses, examines and selects a vortex-ring state prediction algorithm to be incorporated in the GADGHT unit. A program was written that manipulated required aircraft performance data from the ARINC 429 data bus and compared this data to vortex-ring state boundaries predicted by the algorithm. The GADGHT unit provides an audible and visual warning to the pilots when the aircraft has penetrated the VRS boundaries. This warning system will provide increased safety and situational awareness to helicopter crews operating in increasingly demanding operational environments.

14. SUBJECT TERMS	15. NUMBER OF PAGES
Vortex Ring State, Power Settling, Settling With Power, Pilot Aids, GADGHT, Ground Air Display for Geographical/Hydrographical Tracking	153
	16. PRICE CODE

17. SECURITY CLASSIFICATION OF REPORT	1. SECURITY CLASSIFICATION OF THIS PAGE	19. SECURITY CLASSIFICATION OF ABSTRACT	20. LIMITATION OF ABSTRACT
Unclassified	Unclassified	Unclassified	UL

NSN 7540-01-280-5500 Standard Form 298 (Rev. 2-89)

Prescribed by ANSI Std 239-18

Approved for public release; distribution is unlimited.

DEVELOPMENT OF A HELICOPTER VORTEX RING STATE WARNING SYSTEM THROUGH A MOVING MAP DISPLAY COMPUTER

David J. Varnes
Lieutenant Commander, United States Navy
B.S., Purdue University, 1989

Submitted in partial fulfillment of the
requirements for the degree of

MASTER OF SCIENCE IN AERONAUTICAL ENGINEERING

from the

NAVAL POSTGRADUATE SCHOOL
September 1999

ABSTRACT

The need for improved pilot aids has become a high priority item for pilots and aircrews operating at sea and ashore. Pilot aids such as the moving map display, GPWS, collision, and vortex-ring state (VRS) warning systems will significantly enhance aircrew situational awareness and safety. Many more of today's aircraft mishaps are a result of pilot error, which includes a loss of situational awareness. The moving map display provides relatively easy incorporation of sophisticated pilot aids without operational flight program (OFP) modification. This thesis discusses, examines and selects a vortex-ring state prediction algorithm to be incorporated in the GADGHT unit. A program was written that manipulated required aircraft performance data from the ARINC 429 data bus and compared this data to vortex-ring state boundaries predicted by the algorithm. The GADGHT unit provides an audible and visual warning to the pilots when the aircraft has penetrated the VRS boundaries. This warning system will provide increased safety and situational awareness to helicopter crews operating in increasingly demanding operational environments.

TABLE OF CONTENTS

LIST OF FIGURES

LIST OF TABLES

ACKNOWLEDGMENTS

I would first like to thank the Office of Naval Research for the generous funding they have provided in support of this important topic. It is indeed gratifying to see such financial efforts directed toward improving safety and situational awareness for the helicopter pilot and crew. Secondly, I must thank my thesis advisor, Dr. Russ Duren for his unparalleled patience and guidance as well as persistent enthusiasm in the completion of this endeavor. There was never a "Do not enter" sign on his door. I would also like to thank Dr. E. Roberts Wood for his superb assistance in matters of helicopter aerodynamics. He has essentially taught me his aerodynamics course in the many times I have sought him out. I would be negligent if I did not express tremendous gratitude for the assistance provided by Carl Zaslow and the VH systems engineering IPT team in getting the GADGHT unit, simulation, and user interface up and running. I owe a great deal of thanks to Mr. Herman Kolwey from Pax River who provided the original idea and got me started off on the right foot with the excellent work he has already done. He has devoted a significant amount of his own time studying and educating people about vortex-ring state and its dangers. I also must acknowledge with sincere appreciation LCDR Don Lawson who provided numerous safety points of contact and expended great effort to assist me in obtaining safety information regarding vortex-ring state.

Last but not least, I especially would like to thank my wife, Kathy, and my sons, Michael and John, for supporting and tolerating me during this extremely busy time. They never once complained about the many hours I spent at home undisturbed in front of the computer. Despite what many may say, a thesis is truly a "family" affair.

I. INTRODUCTION

A. PURPOSE

The development of a personal computer (PC) based GADGHT (Ground/Air Display for Geographical/Hydrographic Tracking) and other similar commercial moving map display systems and software have hastened the implementation of numerous pilot aid features without the complexity of operational flight program (OFP) or avionics structural changes. Some of these features include flight-planning aids such as fuel consumption calculation, navigational aid (NAVAID) identification, emergency landing field and airspace identification, route construction, and flight time calculation. This thesis proposes utilizing the GADGHT system as a mechanism for providing warning to helicopter pilots on a little recognized aerodynamic phenomenon known as vortex-ring state (VRS).

B. TERMINOLOGY

Throughout academic and military literature as well as in numerous flight manuals and publications, vortex-ring state is synonymous with different phrases and terms. Some of these phrases and terms, however, refer to other phenomena depending on the source ones consults. This terminology inconsistency breeds confusion and leads to misunderstanding of the phenomena they were intended to represent. For instance, the Navy refers to vortex-ring state as power settling, whereas the Army refers to vortex-ring state as settling with power. The Navy uses settling with power to describe an aerodynamic phenomenon that differs from vortex-ring state. Likewise, the Army, and, in fact, many academic references, associate the term power settling with a flight condition dissimilar to vortex-ring state. It is the intention of this thesis to consider the Navy's term of power settling to be synonymous with

vortex-ring state. A brief and generally accepted definition of these terms is provided as follows:

Vortex-ring state or power settling: This is a condition of powered flight where the helicopter settles into its own downwash. This unsteady flight condition can be characterized by severe thrust fluctuations, vibrations, rapid rates of descent, sluggishness and vibrations of the controls and can result in a temporary loss of helicopter control. Conditions conducive to vortex-ring state are a vertical or nearly vertical rate of descent of at least 300 feet per minute (fpm) and low horizontal (forward) airspeed. The rotor system must be using some of the available engine power with either insufficient power *or* lack of immediate power application to retard the sink rate. These conditions can occur during steep approaches, approaches with a tailwind, poor altitude control during high hover conditions, or situations where an engine has failed or lack of available power exists. [Ref. 1]

Settling with Power: The Naval Air Training and Operating Procedures Standardization (NATOPS) manuals define settling with power to be an occurrence where the power required from a helicopter exceeds the power that is available. Conditions that are conducive to settling with power are high gross weights, high-density altitudes, and low rotor speed (RPM). Additional factors that may contribute to settling with power include significant angle of bank, and atmospheric instability [Ref. 2]. It may not be possible to maintain level flight due to the lack of power, causing settling or a descent to occur. [Ref. 3]

It is important to further clarify that these phenomena are two distinctly different flight conditions. A condition often described erroneously as power settling, or vortex-ring state, is merely a high sink rate as a result of insufficient power to reduce a rate of descent or terminate an approach. However, a settling with power condition *can* precipitate vortex-ring state if the rate of descent and airspeed

combination is adequate. It could also be said that vortex-ring state is likely to be encountered inadvertently when sufficient power is *not* available to prevent a descent. A comprehensive review of vortex-ring state may be found later in this thesis. [Ref. 4]

C. RESEARCH CONTRIBUTION

It is hoped that this research will, at minimum, raise the reader's awareness to the complexity of the vortex-ring state phenomenon. In addition to addressing the terminology differences that exist, this research attempts to use an existing study that combines theoretical and empirical data to predict the airspeed and rate of descent boundaries that define the existence of vortex-ring state. Actual aircraft and airspeed data will be fed into the GADGHT computer and compared against the theoretical vortex-ring state boundary. The aircraft's current position in terms of airspeed versus rate of descent will be compared to the theoretically computed boundary. Any penetration of the theoretical boundary will trigger an aural and visual alarm to the pilot that he/she is approaching vortex-ring state conditions. In addition to this endeavor, there has been a significant amount of research devoted to analyzing safety data from the military services, Federal Aviation Administration (FAA), and the National Transportation Safety Board (NTSB). Review of accident data supplied by the aforementioned agencies revealed that accidents involving vortex-ring state as well as settling with power were usually misdiagnosed or unrecognized by the pilots. Though vortex-ring state is not an everyday occurrence, today's modern helicopter and its missions dictate operations in an environment where the occurrence of either vortex-ring state or settling with power are increasingly likely. The result of this cumulative effort will be to enhance aircrew situational awareness and safety by providing pilots adequate warning of the approach or existence of vortex-ring state. This warning will ensure accurate identification of the current

flight condition and permit subsequent correct recovery or avoidance procedures to be made with confidence and without delay preventing mishaps and accidents.

D. ORGANIZATION OF THESIS

This thesis will first introduce the reader to the moving map display system (GADGHT) currently in use by some Navy helicopter squadrons as well as a multitude of other units across all services. Following the discussion of the GADGHT unit a more detailed analysis of past and current vortex-ring state theory, including the comparison and contrast of reviewed algorithms, is presented. Prior to the vortex-ring state theory, however, safety statistics compiled in the research of this thesis will be presented. H-34 partial power descent flight data will be plotted against the algorithm boundaries to show the closest correlation to the indicated vortex-ring state data points found in the partial power descent flight testing. An algorithm selection will be justified and other secondary methods of vortex-ring state indication will be discussed. Finally, the implementation and testing of the algorithm in working code for use within the GADGHT unit will be examined. Conclusions and recommendations for further action will complete the thesis.

II. THE GADGHT SYSTEM AND PILOT AIDS

A. GADGHT SYSTEM

The Ground/Air Display for Geographical/Hydrographic Tracking (GADGHT) system is a series of moving map and information technology information or display systems that are small, lightweight, inexpensive, flexible and highly supportable. The system was developed by Mr. Jim Tomasic, Mr. Steve Brown, and the VH Systems Engineering IPT staff at Patuxent River, MD. The GADGHT systems were originally conceived to allow older aircraft to incorporate newer technology within the constraints of budgets and time. Today, the systems are platform configurable for utilization on boats, ships, trucks and Humvees as well as numerous types of aircraft. The power and installation flexibility of these small systems permits them to significantly contribute to crew situational awareness as well as the enhancement of mission performance and effectiveness. The GADGHT system is based on commercial off the shelf (COTS) technology and is completely customer configurable for mission and vehicle installation. Furthermore, the GADGHT system will support the development of additional pilot aid features and other applications that can be used to gather, process, and display desired information, also configurable to the aircraft and mission needs of the users. Examples of these features include the display of digitized publications, the integration of other functionality, electronic indicators, as well as the incorporation and display of platform video. This would specifically include items such as NATOPS manuals, approach plates, ground proximity warning systems (GPWS), traffic collision and avoidance systems (TCAS), and forward looking infra-red (FLIR).

The system currently is comprised of four different models. The Atlas and Thor, Mercury, Gemini, and Apollo units.

1. Atlas Unit

The Atlas unit is a portable moving map system that has hot swappable battery power capability, and a commercial global positioning system (GPS), or a Thor box as a navigational source. The Thor box is a solid state interface capable of platform integration through a MIL-STD-1553B or ARINC 429/575 data bus. The purpose of the Thor box is to capture GPS navigational data from the aircraft rather than relying on a stand alone commercial receiver. The Atlas contains a 7.5-inch display diagonal with a pen based user interface. It weighs approximately 3.7 lb. and can be worn on the knee. The dimensions of the system are 11 X 7.5 X 1.6 inches. See Figures 1 and 2.

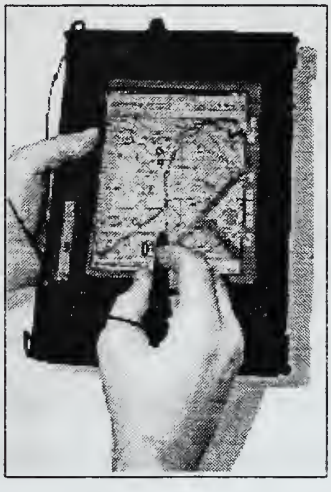

Figure 1. GADGHT Atlas Unit From Ref. [5]

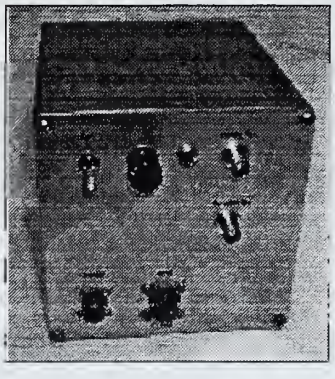

Figure 2. GADGHT Thor Unit From Ref. [5]

2. Mercury Unit

The Mercury Unit is a dual kneeboard design display coupled with a separate processor. The basic processor consists of a rugged enclosure that contains two PC-104 central processing cards and various interface cards. Another PC-104 format interface card provides the capability to produce an audible warning over the aircraft's intercom system. The weight of the mother unit is less than 7 lb. The two provided kneeboards can be produced in varying dimensions (6.5, 7.5, and 8.5 inches), and configured with additional displays. Each kneeboard's weight is estimated to be less than 2 lb. The Mercury Unit is capable of providing a mouse and keyboard, joystick, or pen based user interface. See Figure 3.

Figure 3. GADGHT Mercury Unit from Ref. [5]

3. Gemini Unit

The Gemini unit, like the Mercury Unit, is also a dual display design. Unlike the Mercury arrangement, the displays are no longer attached to the user. They can be affixed to a location within the user's area. Furthermore, the displays are offered in two additional sizes (10.5 and 12.5 inches). The Gemini unit contains the same basic processing system and user interfaces and has similar display weights to the Mercury unit. See Figure 4.

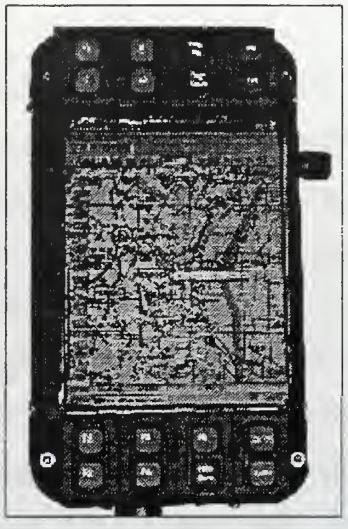

Figure 4. GADGHT Gemini Unit From Ref. [5]

4. Apollo Unit

Unlike the other GADGHT units, the Apollo unit utilizes the aircraft's multi-function display (MFD) rather than relying on a separate kneeboard or area mounted display. This design flexibility allows newer aircraft to incorporate the GADGHT system without imposing on limited space. The Apollo design requires essentially the same basic processing system as well as user interfaces used by the Mercury and Gemini implementations. The only exception is that the basic system for the Apollo design utilizes an 18-50 gigabyte hard drive to store its map information rather than a CD-ROM. See Figure 5.

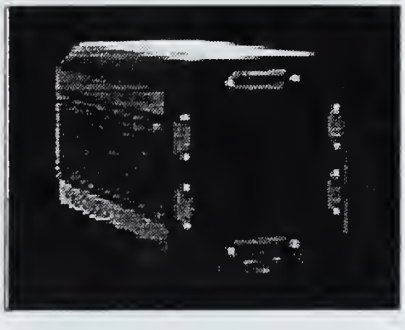

Figure 5. GADGHT Apollo Unit From Ref. [5]

The GADGHT system boasts of other features including sunlight readability and night vision goggle (NVG) compatibility. It also permits incorporation of platform video data, data interchange capability with other applications, object orientation, protected memory, symmetric multi-processing, dynamically loadable device drivers, and direct graphics access. GADGHT has also been developed for use in networking information tier architectures. Information tier one involves the enhancement of individual aircraft platforms and missions. Information tier two allows for information transfer between aircraft or platforms to provide operational coordination. Information tier three would support inter-service information transfers between air as well as ground forces to enhance operational coordination. However, the most significant advantage of the GADGHT system's adaptation to military applications is its unique ability to be installed and employed without modification to the platform's Operational Flight Program (OFP). Such OFP changes would result in costly and lengthy development, debugging and validation. Therefore, a GADGHT system is well suited to provide supplementary and powerful user applications particularly geared towards situational awareness and flight safety in aircraft platforms such as helicopters. [Ref. 5]

This thesis has utilized the Mercury unit for the purpose of implementing the vortex-ring state warning system. The necessity for obtaining required aircraft parameters through the MIL-STD-1553 or ARINC 429 data bus in order to run the vortex-ring state application was well suited to this design. The Mercury unit's ability to be integrated with the ARINC 429 and 1553 data bus allowed parameters essential for the vortex-ring state warning system implementation to be captured with only slight GADGHT system code modification.

B. FALCONVIEW AND OTHER FLIGHT PLANNING SOFTWARE

The advent of moving map and flight planning software has all but revolutionized modern day aviation. The ability to have an instantaneous aircraft position relative to a map displayed to the pilot has greatly simplified the navigational and administrative burdens of today's cockpit crews. It was a only a minor addition to expand moving map software to include functions relative to flight planning needs. Moving map/flight planning software such as Jeppesen's commercial FliteStar support a variety of map types, but primarily rely on CDs that contain sectional charts, topographical pilotage charts (TPC) and ONC charts to achieve world wide moving map coverage. The standard Jeppesen moving map presentation is a display of all ICAO low and high altitude airways, airports, airspace, navaids, and intersections. Additional data in IFR mode would include VORs, VORTACs, NDBs, geographical data as well as major cities. A Jeppesen display will also provide latitude/longitude, magnetic course, ground speed, and minimum safe altitude. Along with their moving map functionality, moving map software such as Jeppesen's also provide numerous flight planning aids. Weather briefings, automatic flight planning around restricted and prohibited airspace as well as class B and C airspace are examples of primary flight planning aids. Other flight planning aid functions include a built in flight recorder, emergency airport locator complete with detailed facilities information, conversion and winds aloft calculator, descent planner and pilot-defined checklists. Surprisingly, this amount of functionality does not require supercomputer capability. A 100 MHz system with as little as 4 MB RAM and 15 MB disk space and a CD-ROM would be sufficient to run the Jeppesen FliteStar. Hardware of this capability is relatively inexpensive for the amount of increased pilot assistance furnished by the moving map/flight planning software. The software itself is also quite affordable with costs well below one thousand dollars. [Ref. 6]

The GADGHT systems were developed to use FalconView Flight Planning Station Software. FalconView was originally developed by the U.S. Air Force Reserve, Air National Guard, and the Georgia Tech Research Institute for the U.S. Air Force. It permits its pilots and aircrews to flight plan through the use of a laptop anywhere in the world. It is currently used by over 13,000 aircrew members worldwide, including the 89th Airlift Wing at Andrews AFB, Maryland, which provides airlift and logistical support for the president, vice president, cabinet and other government officials. FalconView, along with other commercially available flight planning software runs on a Windows 95/NT based system. It allows the user to follow the aircraft's position, overlaid on a digitally presented map. It also includes overlay tools that allow the pilot to mark no-fly zones and restricted or prohibited flight areas as well as to download, via modem, the latest updates on the ever-growing number of towers, and antennas that could pose flight hazards. FalconView has the capability of displaying a five-meter image base resolution, which has been recently declassified. This is twice the resolution of the previous imagery. FalconView can also present detailed threat information that considers topography, flight elevation and the range of a threat's radar system to inform the pilot of his plane's detectability. FalconView utilizes National Imaging and Mapping Agency (NIMA) Compressed Arc Digitized Raster Graphics (CADRG) maps. This group of map types include Global Navigational Charts (GNC), Operational Navigational Charts (ONC), Tactical Pilotage Charts (TPC), Joint Operations Graphic (JOG), Topographic Line Map (TLM), and Controlled Image Base (CIB) – five and ten meter charts. Also supported are Digital Aeronautical Flight Information File (DAFIF), Digital Terrain Elevation Data (DTED), and Electronic Chart Upgrades (E-CHUM) information sources. FalconView has given the military vitally increased capability that is of an expandable, inexpensive and adaptable nature. [Ref. 7]

THIS PAGE INTENTIONALLY LEFT BLANK

III. VORTEX-RING STATE THEORY

A. EARLY STUDIES

The aerodynamic phenomenon known as vortex-ring state has been a concern to pilots and designers since the advent of the helicopter. It was studied heavily particularly in the 1940s and 1950s. Much of the literature that exists today was written many decades ago. Several of these earlier studies were written to simply verify the existence of vortex-ring state, study its effects, and to roughly define conditions when its occurrence may be likely. Even with the technology limitations of the time, their approach to the vortex-ring state problem has yielded results and observations that are consistent with today's data. An early and particularly thorough study of helicopter vortex-ring state and its effects is presented below:

1. Helicopter Behavior in the Vortex-Ring Conditions

W. Stewart published this comprehensive study in 1959. His report describes the flight experiences in the vortex-ring state conditions with the Sikorsky R-4B, R-6 and S-51, Bell 47 and Bristol 171 helicopters. He describes the working conditions of the helicopter as the propeller-working state, vortex-ring state, and the windmill-brake state. [Ref. 8]

a. Propeller-Working State

The propeller-working state is considered by Stewart to represent vertical climb. The rotor disc is moving in the direction of thrust and the airflow is directed downward through the rotor. The limiting condition for the propeller working state is the static-thrust case, or hovering. [Ref. 8]

b. Vortex-Ring State

As the helicopter descends from a hovering condition, it enters the vortex-ring state and the rotor disk is now moving in the opposite direction to the thrust that it produces. In this state, the rotor is still pushing air downwards through the rotor disk but the free air is moving upwards relative to the rotor and the air below the rotor is forced out radially. Thus, the air associated with the rotor disk does not form a regular slipstream development, but exists as a circulation of air in a very turbulent state. The flow is directed downwards through the rotor, then radially outwards and upwards outside the rotor disk. Some of the air passes upward above the rotor is again drawn inward and downward through the rotor, circulating in a manner from which this state derives its name. [Ref. 8]

c. The Windmill-Brake State

Beyond the vortex-ring state exists the windmill-brake state. This is a condition in which the rotor derives its energy from the air. The flow is upward through the rotor. The slowing of the air as it passes through the rotor disk produces the thrust. The boundary condition between the vortex-ring and windmill-brake states is the condition where the upward flow of air is brought to rest at the rotor disk. This condition of no flow through the disk is referred to as ideal autorotation. [Ref. 8]

2. Observations

As was previously mentioned, Stewart conducted his observation of the effects of the vortex-ring state on the Sikorsky R-4B, R-6 and S-51, Bell 47 and Bristol 171 helicopters. The region of roughness developed from Stewart's flight testing as well as his interpretation of the vortex-ring state boundary region is shown in Figure 6.

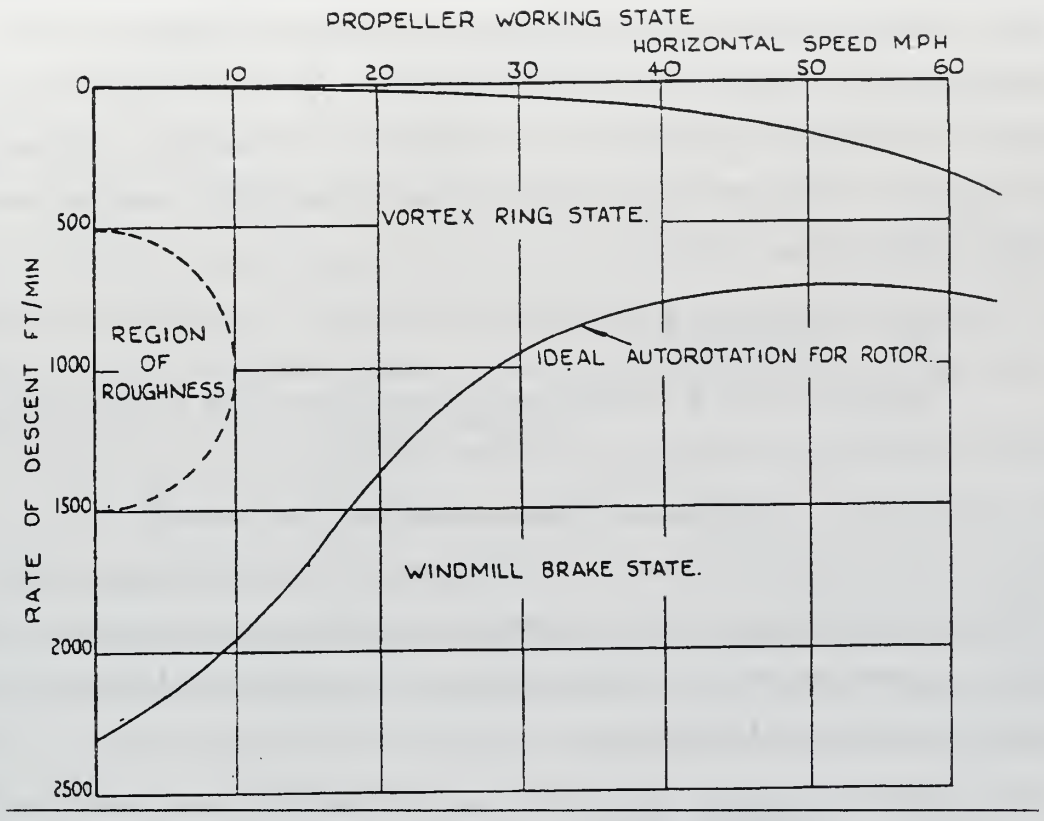

Figure 6. Stewart's Airflow Conditions For A Typical Helicopter From Ref. [8]

The observed effects of vortex-ring state are discussed below:

a. Sikorsky R-4B

When the Sikorsky R-4B approaches the region of roughness as detailed in Figure 6, "There is a great deal of wallowing or unsteadiness of the helicopter accompanied by random yawing moments and a considerable increase in the vibration level." [Ref. 8] Immediately following the yawing and vibrations is a loss of control manifested in the form of a violent nose-down pitch angle. Stewart further comments that complete aft cyclic cannot prevent this nose down pitch that eventually attains an angle of 40 degrees. Accompanying the nose low pitch angle is a rapid airspeed increase to approximately 40 knots with a significant altitude loss. Unfortunately Stewart does not stipulate the starting altitude

of the flight or the loss of altitude that resulted after encountering vortex-ring state. He continues to comment that a decrease of collective as the helicopter nears the unsteady conditions precipitates the nose-down pitching. An immediate *application* of collective may suppress the loss of control, but the effect was only temporary due to the R-4B's lack of power to climb in this region. [Ref. 8]

b. Sikorsky R-6

The Sikorsky R-6 exhibited general wallowing accompanied by harsh vibration and moderate nose-down attitudes of 5 to 10 degrees when in the region of roughness. Also noticed was the helicopter's tendency to turn towards the left. As with the Sikorsky R-4B a decrease in collective pitch precipitates the nose-down attitude. An increase in collective suppresses the nose-down attitude and permits the helicopter to fly clear of the region. [Ref. 8]

c. Sikorsky S-51

The Sikorsky S-51 displayed much of the same behavior characteristics as the R-6 and R-4B, but with significantly less tendency to yaw and less noticeable increase in vibration level. It still attains nose-down attitudes that are not as severe as the R-4B, but greater than the S-6. [Ref. 8]

d. Bell 47

The Bell 47 also showed an increase in vibration levels as well as some lateral and longitudinal wallowing accompanied by a fair amount of yawing. It did not react with violent nose-down pitching, as did the Sikorsky R-4B and S-51. [Ref. 8]

e. Bristol 171

The Bristol 171 demonstrated the least severe effects to the region of roughness depicted in Figure 6. Like the other helicopters, the Bristol 171 experienced an increase in vibrations accompanied with a certain amount of wallowing, however, it did not show the sensitivity that the other helicopters seemed to have possessed. Stewart attributes this decreased sensitivity to lower blade angles and higher kinetic energy. He states that these qualities result in the re-establishment of smooth flow conditions in an easier manner. [Ref. 8]

3. Stewart's Conclusions and Discussion

Helicopter behavior in the vortex-ring state ranges from complete loss of control to general wallowing instability coupled with an increased vibration level. The region of roughness shown in Figure 6 indicates that slow and steep approaches would be extremely difficult on the majority of the helicopter models flight-tested in his study. Stewart attributes the nose-down pitching attitudes of the helicopters to the flow effects on the fuselage. This assumption was verified by attaching wool tuffs to the fuselage of the helicopter as it neared the region of roughness. Stewart observed that the flow around the fuselage was very turbulent but that the general direction of flow was downward over the rear of the fuselage when the region of roughness was reached. Significant changes in flow direction were noticed when the helicopter was exhibiting wallowing characteristics. It was further observed that immediately prior to the violent nose-down pitch, the flow had completely reversed becoming upward and rearward over the fuselage. The Bristol 171 and Bell 47 which demonstrated much less pitching tendencies, have very slim tailcones and consequently have the best flight characteristics in the vortex-ring state. Stewart states that proper design of the fuselage, especially that of the tail cone can minimize the effects of vortex-ring

state on the helicopter. However, the rapid and randomly changing flow conditions and load distribution changes associated with vortex-ring state will always produce some vibrations and wallowing instability. Stewart stated that the regions of roughness exists in helicopter flight at very low airspeeds and in descents between 500 and 1,500 fpm with instability, control difficulties and increased vibration levels. Stewart additionally concluded that an application of power or collective pitch had a beneficial effect of helicopter behavior in the vortex-ring state. Even with this observation it is important to note that the application of collective *is not* a commonly accepted means of recovery from vortex-ring state and is typically cautioned against in many of today's flight guidance resources.

B. SAFETY DATA

With some appreciation for the nature of vortex-ring state as described in the Stewart observations the next logical step was to collect and assimilate existing modern helicopter safety data regarding this phenomenon. Data was gathered from the United States Navy, Marine Corps, Army, National Transportation Safety Board (NTSB), and the Air Accidents Investigation Branch (AAIB) from the United Kingdom. The U.S. Air Force refused to provide meaningful safety data for this research citing concerns over "privileged" information and its utilization for purposes that they claimed were not directly related to supporting increased helicopter safety [Ref. 9]. It should also be noted at this point that the U. S. Coast Guard was unable to locate any accident or mishap data related to the occurrence of vortex-ring state, power settling or settling with power [Ref. 10]. The acquisition of this safety data required the utilization of all known terms that are considered synonymous with vortex-ring state. As discussed in the introduction, these terms do not all contain the same meaning across civilian and military helicopter communities. The definition of vortex-ring state itself is fairly

consistent, but will invoke different words or phrases meant to be synonymous with it. For example, a search of the Army's safety database for vortex-ring state accidents would require one to search using vortex-ring state, settling with power or even dead air. The Navy, however, would produce vortex-ring state related mishaps under searches for vortex-ring state or power settling, but not settling with power. The same logic can be applied to the NTSB who, like the Army, accepts the term settling with power to be synonymous with vortex-ring state. Other difficulties encountered in the search for vortex-ring state data were the limitations of the databases searched. Many of the databases have not been digitized to the point that they allow word searches that are familiar in the use of today's word processors. Instead, the user is restricted to pre-programmed words or phrases. This, in some cases, requires reading entire classes of mishaps to obtain desired information. No small task indeed. The data presented in this thesis was obtained with the gracious assistance of many data analysts and safety personnel. It became quite apparent early in this research that vortex-ring state does not appear to be a well-tracked category of its own. Using available research capabilities, personnel assisting in locating the desired statistics were still able to provide helicopter mishaps or accidents that were attributed to vortex-ring state including vortex-ring state on the tail rotor. After careful review of the data provided the following brief conclusions can be made:

- Between 1982 and 1997, 33 incidents of vortex-ring state causing accidents have occurred. Four of these were attributed to vortex-ring state of the tail rotor. One of these incidents resulted in 11 fatalities.
- Most occurred at altitudes less than 200 ft at low airspeeds.
- Two incidents specifically comment on aircraft shudder and lateral vibrations.

- Several mishap narratives state that vortex-ring state was unrecognized by the pilot(s).
- In many instances application of collective was not only ineffective in escaping vortex-ring state, but served to further exacerbate the effects as well as to increase an undesired rate of descent.

A summary of the source statistics is provided in the following tables: TR refers to the tail rotor and MRB refers to the main rotor blade.

US Navy/Marine Corps		
Type	**Helo**	**Researcher's Comments**
TR-VRS	CH-53	None
TR-VRS	SH-2F	None
TR-VRS	SH-2F	None
MRB-VRS	CH-53D	Unrecognized -External Load at Night

Table 1. US Navy/Marine Corps Vortex-Ring State Safety Statistics

US ARMY		
Type	**Helo**	**Researcher's Comments**
MRB-VRS	Unknown	Vibration Noted - Large Rate of Descent
MRB-VRS	Unknown	Multi -Ship NVG Operation - Recovered at 50' AGL

Table 2. US Army Vortex-Ring State Safety Statitics

NTSB - NATIONAL TRANSPORTATION SAFETY BOARD			
Type	**Date**	**Helo**	**Researcher's Comments**
VRS-MRB	Apr-99	Robinson R-22	Initiated Flare at 20' and decreased airspeed to 20 kts
VRS-MRB	Dec-97	AS-355	Tailwind
VRS-MRB	Oct-97	HU-269B	Airspeed Decayed to 0 kts at 150' AGL
VRS-MRB	Oct-97	AS 316-B	**Aircraft Shuddered** - Initial ROD of 200 fpm
VRS-MRB	Jul-97	R-22-Beta	Unrecognized
VRS-MRB	Aug-95	Bell 47-G4A	None
VRS-MRB	May-95	Bell 47-G5A	VRS began at an altitude of 30-35ft AGL
VRS-TR	Oct-94	Enstrom F-28	Began to spin at 150-250' AGL
VRS-MRB	Oct-94	Enstrm F28-C	2500 ft MSL
VRS-MRB	Aug-94	Bell 230	MEDEVAC Flight - Steep Approach
VRS-MRB	Aug-94	Robinson R-22	Witnesses stated that helo "dropped" to the ground
VRS-MRB	Feb-94	Hiller UH12-H23D	Descent began *after* load release
VRS-MRB	Sep-93	HU-369-D	Stabilized 500 ft Hover - Violent Vertical Descent
VRS-MRB	Nov-92	HU-369-HS	None
VRS-MRB	Sep-92	Super Puma	High Winds - 11 Fatalities
VRS-MRB	Sep-92	Bell 47-G4A	None
VRS-MRB	Jun-91	HU-269-A	Descent began at 150ft AGL
VRS-MRB	Jun-91	Bell 47-G2A	None
VRS-MRB	May-91	Bell 47-G	Crosswind - Witnessed by NTSB Investigator/USCG Pilot
VRS-MRB	Jun-90	Hughes 269C	Utility Line Observation - Right Turn - Uncont Descent
VRS-MRB	Jan-90	R-22-Alpha	Final Approach to Helipad - 180 Wind Shift
VRS-MRB	Feb-89	SK-76-A	In Flight while maneuvering around IMC conditions
VRS-MRB	Aug-87	Bell-47G	Tailwind - Airspeed decreased to 0 in turn
VRS-MRB	Jun-84	Bell 47G-2	Airspeed Decayed - Helicopter Descended
VRS-MRB	Jul-83	R-22-XXX	**Lateral Vibrations Felt** Short Final at 75ft AGL
VRS-MRB	May-83	Enstrm F28-C	30-35 ft AGL crossing runway

Table 3. National Transportation Safety Board (NTSB) Vortex-Ring State Safety Statistics

AAIB - AIR ACCIDENTS INVESTIGATION BRANCH - UK			
Type	**Date**	**Helo**	**Researcher's Comments**
VRS-MRB	Dec-94	Bell 214ST	Night landing on vessel helo pad - Turbulent Weather

Table 4. Air Accident Investigations Branch – United Kingdom – Vortex-Ring State Safety Statistics

As stated previously, the statistics presented thus far are ones in which the occurrence of vortex-ring state has resulted in helicopter accidents or mishaps of varying severity. It is likely that this is not entirely representative of the frequency of occurrence of this phenomenon.

Informal discussions with several pilots have prompted many of them to recall with great fervor instances in which they have encountered vortex-ring state and have successfully flown clear of it without damage to the helicopter or injury to the crew. Oftentimes, these instances go unreported and, therefore, not discussed. Either embarrassment or a lack of appreciation for the potential consequences of vortex-ring state has prevented these circumstances from being reported in an appropriate form such as a military hazard report.

C. SAFETY IMPLICATIONS

The safety data and informal discussion with numerous pilots were not, alone, the only motivating factors for this vortex-ring state study. It became apparent that there was not only confusion over the various terms used synonymously with vortex-ring state, but widespread misunderstanding of the fundamental nature (using the Navy terminology earlier described) of vortex-ring state or power settling and settling with power. Though settling with power may certainly precipitate vortex-ring state they are two distinctly different phenomena requiring dissimilar recovery techniques. This misunderstanding points to a lack of training and awareness, which are crucial to either phenomenon's prevention. An article appearing in the May 1999 edition of *Rotor & Wing* attempted to address the misconceptions that abound between the two phenomena. The article stresses proper preflight planning as well as a heightened awareness of the performance limitations of one's helicopter as key to avoiding disaster [Ref. 2]. While this is particularly true for situations of settling with power (power required exceeds power available) it does not necessarily assure that one will forestall vortex-ring state. The best flight planning cannot prevent an engine failure or the possible rate of descent incurred because of such a failure. This critical distinction provides impetus for the development of a vortex-ring state warning system to

provide the pilot added safety and elevated awareness of the vortex-ring state boundary. Also, with the onset of increasingly demanding helicopter missions in less than ideal environments, the occurrence of vortex-ring state is likely to become more frequent. Given fixed and current flight information including rotor radius, weight, and air density, a vortex-ring state boundary can be plotted and displayed to the pilot. While airborne, the aircraft's rate of descent and airspeed data are compared to the boundary formulated from the current conditions. A visual and aural warning is presented to the pilot when the vortex-ring state boundary is penetrated. This system will provide a means of warning the pilot of potential impending danger that the best pre-flight planning may not prevent. It will ensure correct identification or recognition and permit subsequent recovery procedures to be made with confidence and without delay preventing injurious and costly accidents.

Figure 7, shown below for reference, illustrates how a settling with power incident, i.e. an engine failure, can easily lead to a vortex-ring state condition. A situation where available power is reduced due to an engine failure, especially in a take off or landing scenario, can deteriorate to a point on the chart that lies within the vortex-ring state boundary. Not a very desirable situation, but nevertheless possible. If the helicopter's airspeed is below the minimum single engine airspeed, the helicopter will descend. The minimum single engine airspeed according to Figure 7 is approximately 26 knots, quite low. The maximum airspeed associated with the vortex-ring state boundary is about 17 knots. Figure 7 reveals that a descent with a single engine airspeed of less than 26 knots will likely result in a penetration of the vortex-ring state boundary.

Figure 8 shows another slightly different perspective that, perhaps, may seem a bit more tangible to the average pilot. It is a two-engine performance plot of the rate of climb for varying gross weights versus airspeed for an H-53. Overlaid on top of this information is the plot of

the vortex-ring state boundary using the theory that is the basis for the vortex-ring state warning system. The vortex-ring state boundary was calculated using a gross weight of 50,000 lb. and a sea level density of 0.002378 slugs per cubic foot. Increasing the gross weight in the calculation of the vortex-ring state boundary has the effect of adjusting the upper boundary to a greater rate of descent (sliding the boundary down) as well as increasing the airspeed at which vortex-ring state can occur. It can be noted from the plot that only rates of descent are possible for the majority of gross weights below certain airspeeds. For example, a rate of climb for a gross weight of 70,000 lb. is not possible below approximately 30 knots of airspeed. Should a decrease in airspeed below 30 knots occur for 70,000 lb gross weight, a penetration of the vortex-ring state boundary will occur. Furthermore, one could extrapolate this situation for single engine performance where climb rates at these gross weights would be drastically reduced if not eliminated. A situation such as this could much more rapidly result in a penetration of the vortex-ring state boundary. This is a frightening and often overlooked possibility. The 'Poly' in the legend refers to a polynomial curve-fitting algorithm used for each set of gross weight data points.

Settling with Power

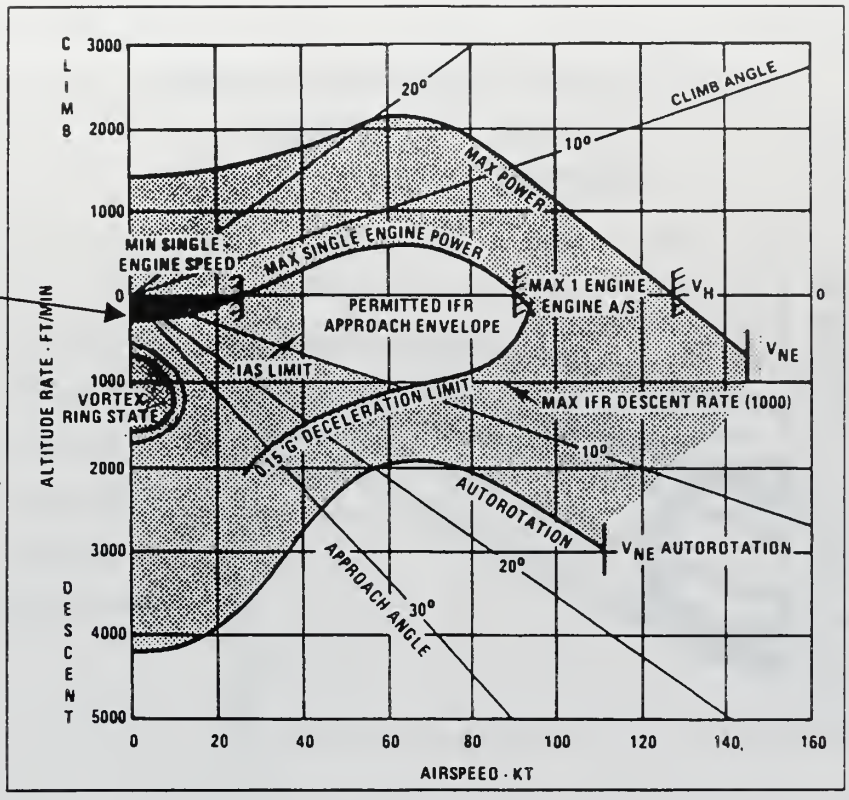

Figure 7. Typical Flight Envelope From Ref. [11]

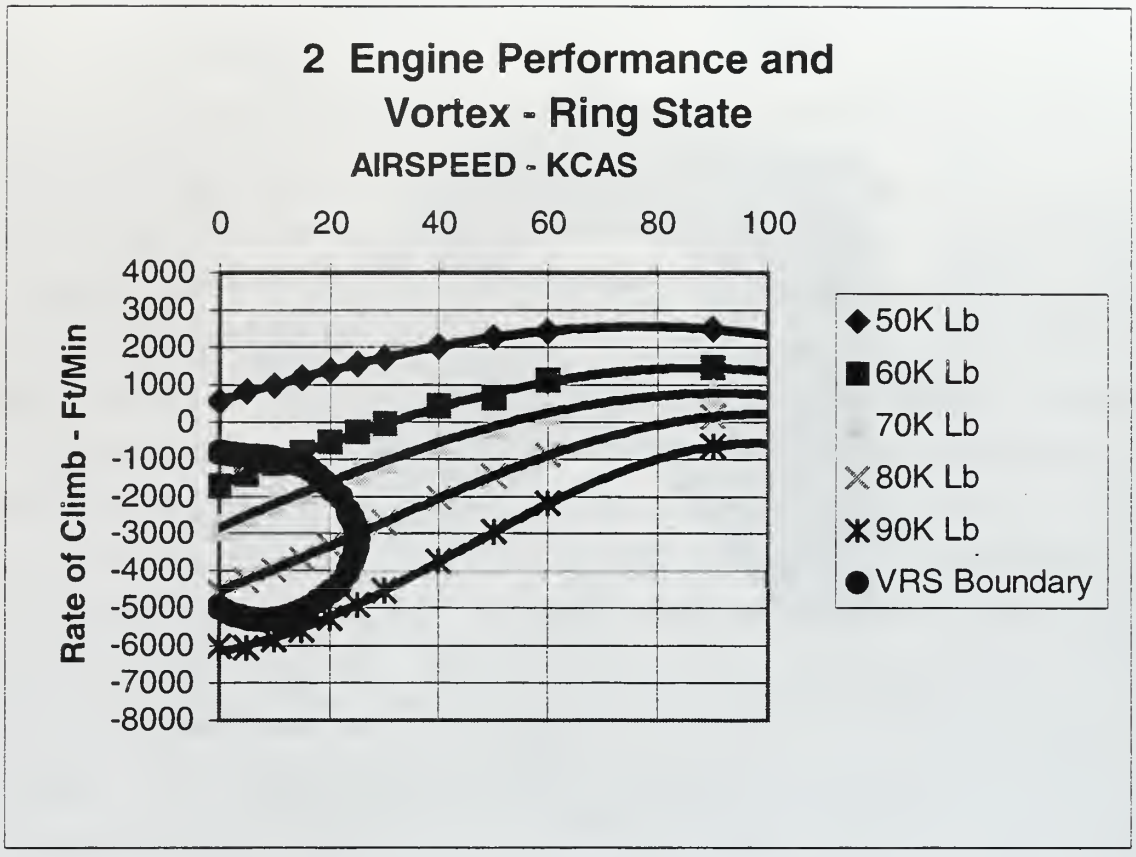

Figure 8. Vortex-Ring State boundary Overlaid On A Climb Performance Chart After Ref. [12]

D. MOMENTUM THEORY AND THE VORTEX-RING STATE

Momentum and blade element theory have been used by rotary wing aerodynamicists to analyze states of helicopter vertical flight known as the hover, climb, descent, vortex-ring state, and the windmill brake state. The flow conditions of these states are shown in Figure 9. Momentum theory applies the basic conservation laws of mass, momentum, and energy in analyzing the performance of the helicopter rotor system. Blade element theory, on the other hand, calculates the forces acting on an individual rotor blade due to it motion in the air as a means of analyzing the performance of the rotor system. It is the momentum theory in

combination with empirical data, however, that has been widely used in attempts to formulate boundaries that define vortex-ring state.

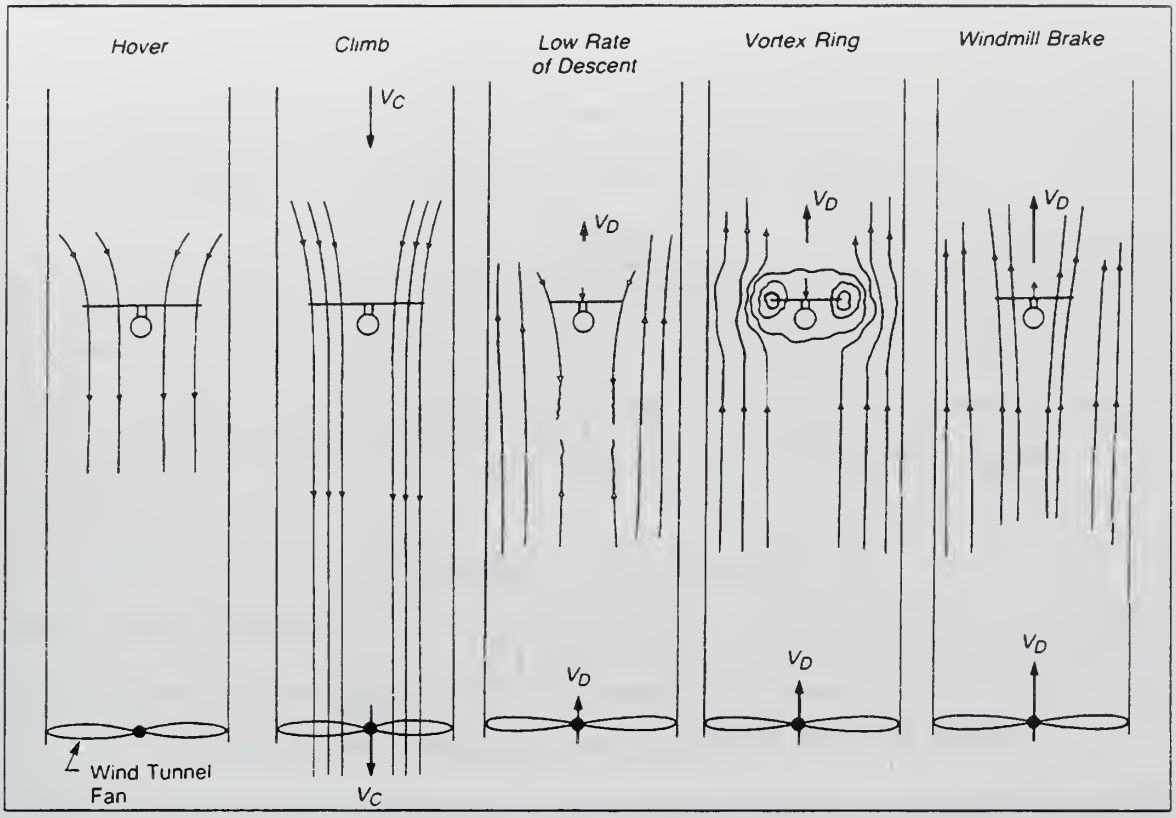

Figure 9. Helicopter Flow States From Ref. [13]

Any physical system must obey the laws of physics. Newton stated one such law: "For every action there is an opposite and equal reaction." This must be true for the helicopter as well. In the case of the helicopter in hovering flight, the action is the generation of thrust that is equal to the weight. The reaction is the acceleration of air mass from a motionless state at a large distance from the rotor to a condition where the air mass acquires a velocity increment in the wake below the rotor in a direction opposite to the thrust. This system is shown in Figure 10.

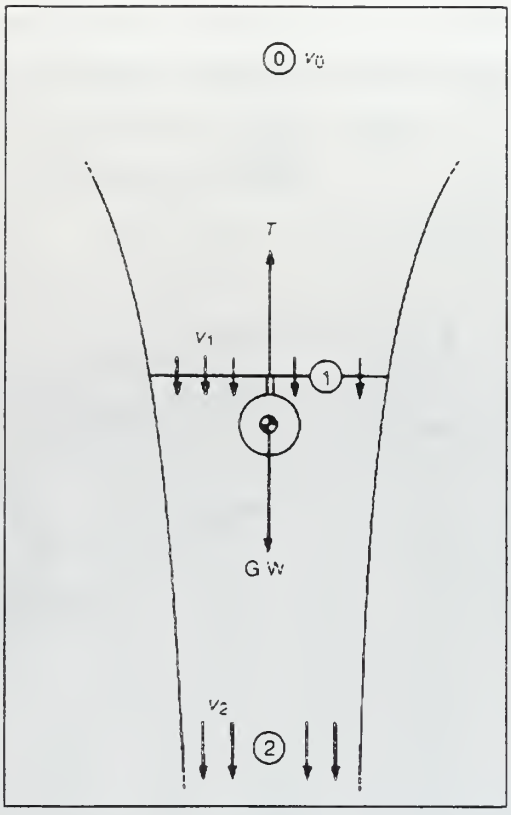

Figure 10. Flow Field Condition At The Rotor From Ref. [13]

The system behavior is governed by the relationship:

$$Force = (Mass)(Accleration)$$

This can be more specifically written for the helicopter as:

$$T = \dot{m}\Delta v$$

T is the rotor thrust, *m dot* is the mass flow, and $\in v$ is the change of velocity in the system. In momentum theory the helicopter rotor is modeled as an actuator disk with zero thickness that can support a pressure difference and thus accelerate the air through the disk. In his text, Prouty has numbered the regions of interest as 0 for high above the rotor, 1 for the plane of the rotor, and 2 for well below the rotor in the fully developed rotor wake. The mass flow in the plane of the rotor, or region 1, can be described as:

$$\dot{m} = \rho A v_1$$

Where Δ is the air density, normally given in slugs/ft^3, and A is the area of the rotor disk which is equivalent to πR^2. Given that the air in region 0 is motionless, we can say that v_0 is zero. The total change in velocity from v_2 to v_0 is simply v_2. Substituting in *m dot* and $\in v$ gives us:

$$T = \rho A v_1 v_2$$

Energy conservation further allows us to equate the rate of energy transfer in order to present the same equation in a more usable form. This, of course, is done under the presumption that the rotor and its wake form a closed system. The rate of energy transfer can be defined using the following:

$$EnergyRate = Force \times Velocity$$

Substituting the thrust, T, for the force, and v_1 for velocity, we can obtain the equation representing the rate of energy dissipated by the rotor:

$$EnergyRate = \rho A v_1^2 v_2$$

The energy rate imparted to the wake is simply the total change in kinetic energy. Since the air is not in motion far above the rotor system the change in kinetic energy at region 2 is simply the value of the kinetic energy at region 2. This can be written as follows:

$$EnergyRate = \frac{1}{2}\dot{m}_2 v_2^2$$

After setting the energy rate equations equal to one each other we obtain:

$$\dot{m}_1 v_1 v_2 = \frac{1}{2}\dot{m}_2 v_2^2$$

The mass flow in region 1 must be the same as the mass flow in region 2 due to the Law of Continuity. Simplifying the above expression one obtains:

$$v_2 = 2v_1$$

This expression implies that the velocity in the rotor wake is equal to twice the velocity at the rotor itself. Anyone who has ever stood within the wake of a hovering helicopter can attest to the significant wind speeds felt in this area. Such velocities could be 53 knots or higher for a CH-53. Velocities of this magnitude could make an attempt to hover or land in dusty or sandy environments a difficult if not impossible task. Substituting this into the original thrust equation we get:

$$T = 2\rho A v_1^2$$

The induced velocity in the plane of the rotor is then:

$$v_1 = \sqrt{\frac{T}{2\rho\pi R^2}}$$

The induced velocity has units of feet per second or feet per minute. Therefore, momentum theory has provided a relationship between the induced velocity at the rotor disk and the rotor thrust that is produced. [Ref. 13]

1. Momentum Theory In A Hover

The previous discussion provided a relationship between the thrust generated by the rotor and the induced velocity in the plane of the rotor system. The equation for the induced velocity was developed under the assumptions of a well-defined slipstream, and uniform velocities v_1 and v_2 over the slipstream cross section. Also, any rotational energy in the wake due to the rotor torque is neglected. With these assumptions made, and a helicopter in a hovering flight regime, we can call the induced velocity, v_1, the hover induced velocity, v_h. The equation for the hover-induced velocity would appear as shown below:

$$v_h = \sqrt{\frac{T}{2\rho\pi R^2}}$$

Consequently, the induced power loss for hover is:

$$P = Tv_h = T\sqrt{\frac{T}{2\rho\pi R^2}} \text{ Or,}$$

$$\frac{P}{T} = v_h = \sqrt{\frac{T}{2\rho\pi R^2}}$$

This relationship essentially determines the basic characteristics of the helicopter. For a low inflow, or low induced power loss, the air must be accelerated through the disk by a small pressure differential. To hover efficiently requires a small value of *P/T*, which also necessitates that the disk loading, *T/A*, be small as well. Examining this carefully reveals that the primary influence in the induced power loss is the $T/(2\rho\pi R)$ term. The effective disk loading will increase with decreasing density, or increasing temperature and altitude. [Ref. 14] A listing of the hover power losses without any simplifying assumptions is shown in Table 5.

Type Of Power Losses	**Percent Loss**
Induced Power (Generate Thrust)	60
Profile Power (Turn The Rotor)	30
Nonuniform Inflow	5 to 7
Swirl In The Wake	<1
Tip Losses	2 to 4

Table 5. Hover Power Losses After Ref. [14]

2. Momentum Theory In Climbing And Descending Flight

A rotor system in a climb is moving upward with a velocity, as shown in Figure 9, of V_C. This would mean that the flow, V_C , is directed downward through the rotor disk. It is assumed that the induced velocities, v_1 and v_2, which are at the rotor and in the far wake respectively, are uniform. Provided that constant thrust conditions exist, the induced velocity at the rotor in a climb is:

$$v_{1_C} = -\frac{V_C}{2} + \sqrt{\left(\frac{V_C}{2}\right)^2 + v_h^2}$$

V_C is also referred to as the rate of climb and is often expressed in terms of feet per minute. Climbing as well as hovering flight are included in what is termed as the normal working state.

The descending case of vertical flight is not quite as intuitive. The freestream velocity, V_D, or rate of descent is now directed upwards as the rotor descends. In this case the flow is mixed. For low rates of descent the local flow near the rotor is dominated by the rotor-induced velocity, which is still pointing downward, but the remainder of the flow field is upward [Ref. 13]. This can also be seen in Figure 9. An equation representing the induced velocity of the rotor in a low rate of descent is given below:

$$v_{1_D} = \frac{V_D}{2} + \sqrt{\left(\frac{V_D}{2}\right)^2 + v_h^2}$$

3. The Vortex-Ring State

When the helicopter begins a descent, a well-defined slipstream ceases to exist. The flows inside and outside the slipstream in the far wake desire to be in opposite directions. This conflicting direction of flow results in unsteady and turbulent air. Because this condition essentially starts when the helicopter begins a descent, many define the entire region from descent to the windmill brake state as vortex-ring state. Even though this region may be classically defined as vortex-ring state, the flow in the vicinity of the rotor continues to be reasonably well represented by momentum theory. This is, as pointed out in the discussion of low rates of descent, due to the fact that the flow near the rotor continues to be dominated by the rotor induced velocity. In practice, momentum theory remains valid for some distance into vortex-ring state, generally until the rate of descent approaches a quarter to half

of the hover induced velocity. Beyond this point, there is no longer a way to analyze the induced flow in the far wake. The chief difficulty with the application of momentum theory to the vortex-ring state is that it is based on a wake model consisting of a definite slipstream with a well defined wake downstream (far below the rotor), with the air moving in the same direction throughout the flow field [Ref. 14]. This is simply not so in vortex-ring state as can be seen in Figure 9. In the case where the rate of descent is equal to the rotor induced velocity, there is mathematically no net mass flow of air through the rotor system. This would indicate, based on the momentum equations already presented, that the thrust is equal to zero. In actuality the rotor does have significant thrust capability even within this region [Ref. 13]. The inability of momentum theory to describe the flow in the vortex-ring state requires us to seek induced velocity equations through the use of empirical data from measured rotor performance.

a. Vortex-Ring State Characteristics

Vortex-ring state is typically characterized by erratic thrust variations, unstable and turbulent flow conditions, and mild to severe vibrations. Accompanying these characteristics is another condition commonly associated with vortex-ring state. This condition, often referred to as power settling, is the situation when more power is required to descend than to hover. These characteristics are detailed in Figures 11 and 12 shown below:

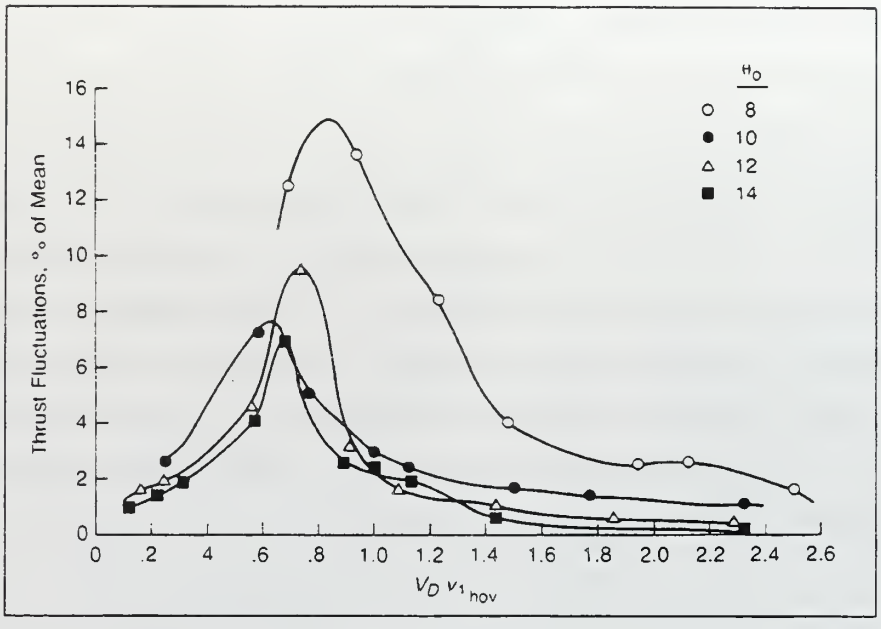

Figure 11. Thrust Variation In Vortex-Ring State From Ref. [13]

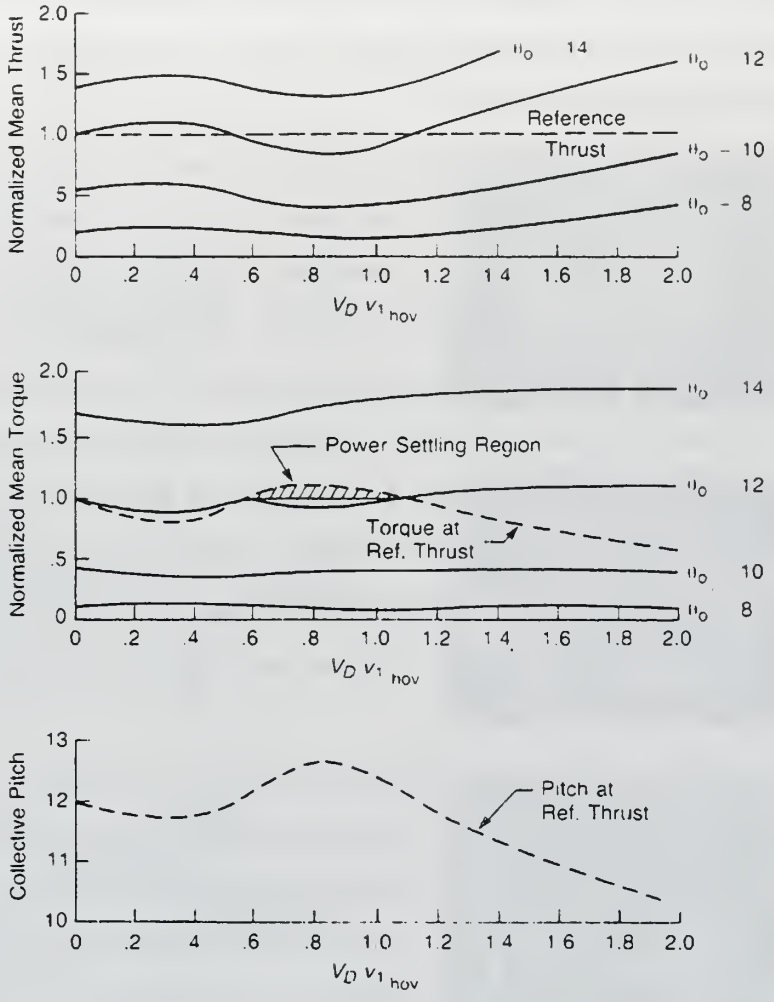

Figure 12. Power Settling Region Of Vortex-Ring State From Ref. [13]

Referring to Figure 11 it would appear that the most severe thrust fluctuations occur at a rate of descent that is approximately equal to 70 percent of the hover induced velocity. This result has been found to be in good agreement with flight tests. Examining Figure 12 reveals that the power settling region occurs between about 0.6 V_D/v_{1h} to 1.1 V_D/v_{1h} based on a reference thrust derived from a collective setting of 12 degrees. The power-settling region correlates not only to the requirement for increased torque but increased collective pitch as well. Following the figure carefully, it is observed that the torque and collective initially decrease

with the start of a descent, but begin to increase at about 0.5 V_D/v_{1h} in the region of maximum flow fluctuation before decreasing again as the rotor approaches the autorotation region.

Vortex-ring state has also been examined in the wind tunnel using a helicopter model and smoke generators. A particular film created by Drees and Hendal in 1951 shows incredible footage of the flow behavior in the vortex-ring state. Observations of the film show an airbody that appears to circle the helicopter rotor. As the rotor system continues to circulate air the airbody grows downward until its bursts releasing its accumulated energy into to the upward moving flow. See Figure 13. The airbody returns to its original shape before it grows again. After reviewing the film, the airbody seems to burst on alternating sides, but is reported by Drees and Hendal to form and burst one side at a time in a completely random fashion.

The effect of forward flight on the vortex-ring state is to essentially shed the disturbed airflow behind the helicopter. This occurs with the introduction of a velocity component parallel to the rotor disk and acting in the rearward direction. Studies and flight tests have shown that forward velocities as low as 10-20 knots are sufficient to prevent the occurrence of vortex-ring state. As will be seen later, the forward velocity at which vortex ring state is no longer a threat is a function of the rotor radius, air density, and weight of the helicopter.

The flow fluctuation (seen in Figure 13) in the vortex-ring state region results in many of the common characteristics associated with this phenomenon including changes in the rate of descent, thrust variations, rotor blade flapping, vibrations, and a loss of control effectiveness. As stated previously the lack of a valid wake model to represent the vortex-ring state region prevents the momentum theory from precisely defining the limits of this region. This leads to the use of flow

visualization to better define the behavior and boundaries of the vortex-ring state region.

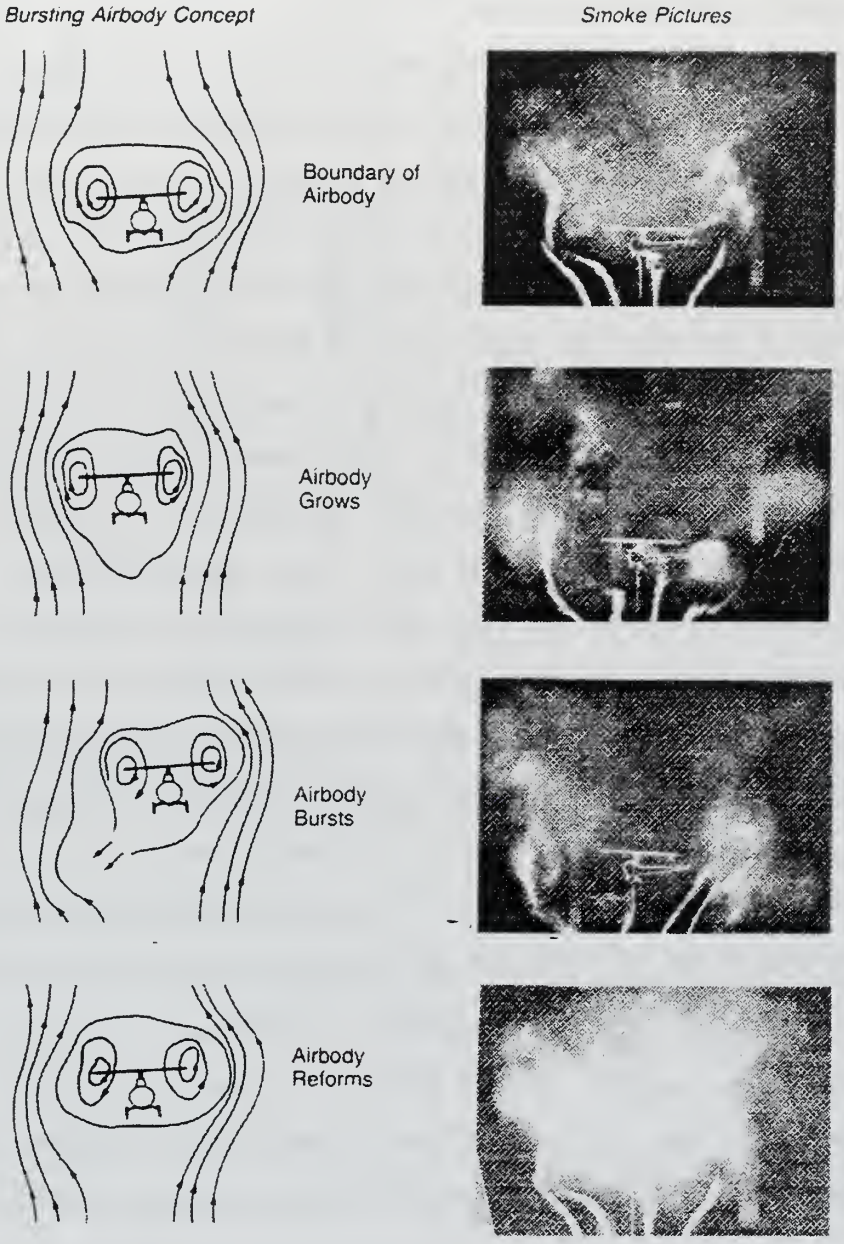

Figure 13. Vortex-Ring State Airbody Formation From Ref. [13]

4. Autorotation And The Turbulent Wake State

The autorotation, unlike the hover, climb, and descent, is a special case of vertical flight that is a power off descent. The source of power in the autorotation is simply the descent velocity upward through the rotor disk. The vertical autorotation actually occurs in the vortex-ring state region with the ideal vertical autorotation defined to be the case in which the rate of descent is equal to the hover induced velocity, $V_D = v_h$. This relationship indicates that there is no net mass flow through the rotor system. In fact, a review of the film made by Drees and Hendal showed that there appeared to be no smoke passing through the rotor during wind tunnel tests of a helicopter model in a vertical autorotation. The flow in the wake field above the rotor is turbulent, and there is even some recirculatory flow in the plane of the rotor. Even though vertical autorotation occurs in the vortex-ring state regime, it is a balanced, steady flight condition in which the rotor thrust is equal to the gross weight of the helicopter [Ref. 13]. Examining the autorotation from the perspective of blade element theory leads to defining the occurrence of the vertical autorotation to be when the lift vector of a blade is equal to the drag component in a given rate of descent. The combination of the momentum and blade element theory permits an approximation for the rate of descent of a helicopter in autorotation to be made as follows:

$$V_D = 1.97 v_{1_{hov}}$$

The result has given way to a rule of thumb that the rate of descent in a vertical autorotation is essentially twice the hover-induced velocity. [Ref. 13]

The turbulent wake state is a flight regime considered by some to lie between the vortex-ring state and the windmill brake state. Momentum theory is still not applicable in this condition because the wake is distorted by a nonuniform and turbulent flow. Even though there is a high degree of turbulence, there is some velocity upward through the disk,

therefore, much less recirculatory flow through the rotor. The rotor in this state experiences some roughness due to the turbulence, but it does not compare to significant vibrations that can accompany vortex-ring state. [Ref. 14] The following figure shows the rotor flow for the ideal autorotation and the turbulent wake state:

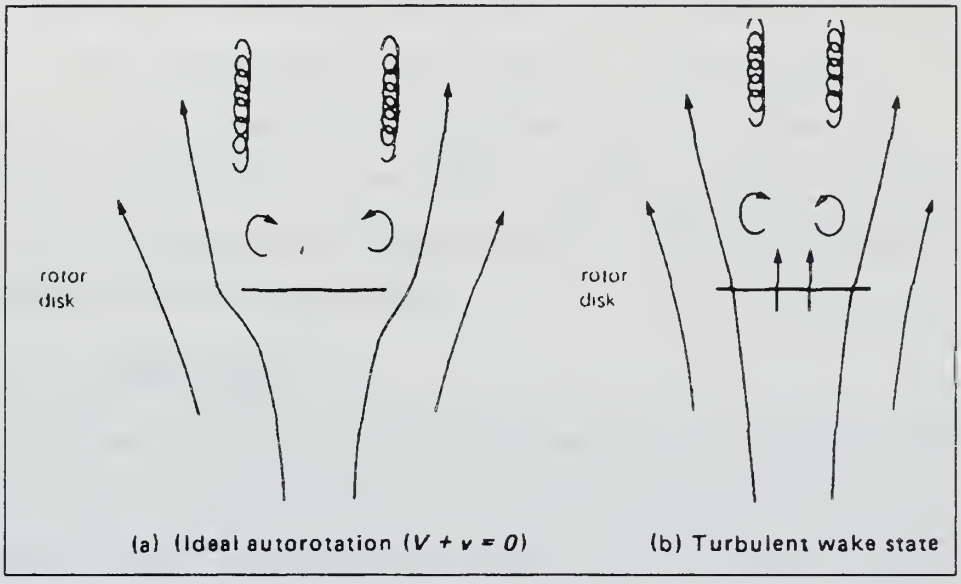

Figure 14. Rotor Flow - Ideal Autorotation And Turbulent Wake State From Ref. [14]

5. Windmill Brake State

At very large rates of descent i.e., higher than the rotor-induced velocity, the flow becomes upward at the rotor and at distances far from the rotor. The system again contains a definite slipstream. Since the flow is upward through the disk, the rotor is extracting power from the airstream in excess of the induced losses. The wake is well behaved above the rotor, which allows momentum theory to be applied in analyzing this flow state to obtain estimates of rotor performance. The equation for the induced velocity at the rotor in the windmill brake state is therefore:

$$v_{1_{WB}} = \frac{V_D}{2} - \sqrt{\left(\frac{V_D}{2}\right)^2 - v_{1_h}^2}$$

IV. VORTEX-RING STATE BOUNDARY PREDICTION ALGORITHMS

A. ALGORITHMS REVIEWED

Three different theories concerning vortex-ring state boundary prediction were examined for potential use in the vortex-ring state warning system. The theories, or algorithms, were reviewed for several attributes including the use of wind tunnel testing in support of conclusions, conformity to known flight test data, and their adaptability for use in the warning system implementation. Each of the theories is described in the following sections:

1. Wolkovitch

The most commonly referenced or, perhaps, even most widely utilized vortex-ring state prediction algorithm is that of Dr. Julian Wolkovitch. He presented a paper published in the *Journal of the American Helicopter Society*, in July, 1972 titled, "Analytical Prediction of Vortex-Ring State Boundaries for Helicopters in Steep Descents." This article appears to be one of the first theories published that made an attempt to utilize momentum theory in combination with empirical data to predict the location of the vortex-ring state boundary. Wolkovitch's motivation for better defining the problematic vortex-ring state boundaries was twofold. First, was the requirement to design helicopters that could perform steep descents with normal engine functioning. Second, knowing the vortex-ring state boundaries was important for ensuring that a twin engine helicopter experiencing a single engine failure could safely descend.

a. Upper Boundary

The flow model that Wolkovitch uses to define the occurrence of vortex-ring state is shown below in Figure 15.

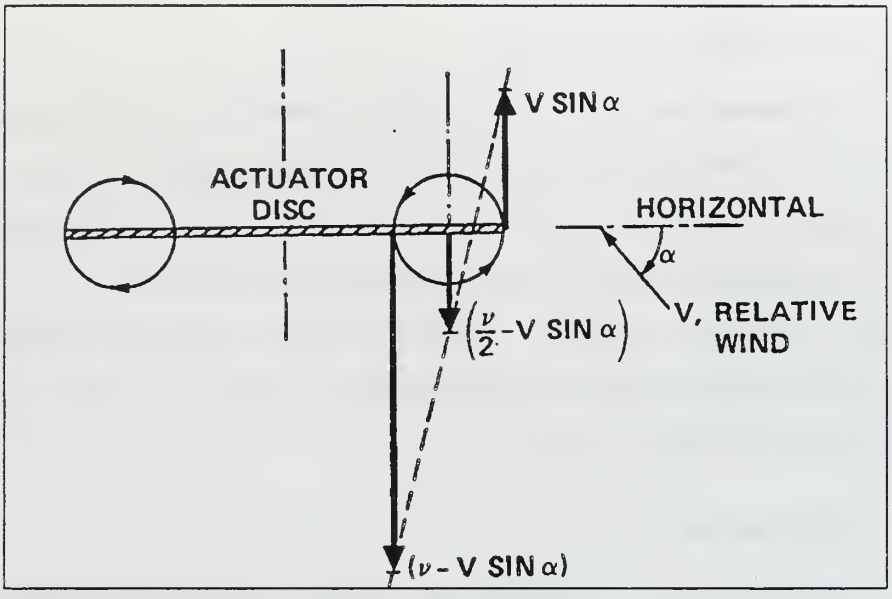

Figure 15. Wolkovitch's Flow Model From Ref. [15]

V represents the relative wind, v is the induced velocity at the actuator disk, which is considered positive in the downward direction, and α is the inclination of the plane of the actuator disk to the flight path, defined as degrees positive for a descent. The flow model consists of a slipstream with a uniform flow at any cross section. The slipstream is surrounded by a tube of vorticity and is separated from the relative wind. The upward component of the slipstream – outside the vortex tube, is Vsinα. The velocity inside the vortex is downwards and is defined by v-Vsinα. The average of these two velocities is equivalent to the rate of descent of the center of the vortex cores, or v/2-Vsinα. Wolkovitch concludes that vortex-ring state will occur when the relative velocity of the vortex cores, or their rate of descent is zero. Unsteady flow will result, as the vortex cores have no movement away from the plane of the rotor disk. Solving for V in the velocity equation of the vortex cores gives us the critical relative velocity at which vortex-ring state will occur:

$$V_{crit} = \frac{v}{2\sin\alpha}$$

Using momentum theory, Wolkovitch expresses the critical velocity in terms of the horizontal and vertical velocities as well as the tip loss factor, B. The tip loss factor is included to account for non-uniform lift distribution across the rotor blade. Examining the lift distribution across the rotor blade would reveal that the lift rapidly falls off towards the last few percent of the span near the tip. This decrease in lift results in a decrease of the overall induced velocity that was calculated previously employing actuator disk concepts. The tip loss factor is a value of one or less that represents the effective radius of the rotor. A typical tip loss factor of 0.97 or 0.98 can yield between 10 and 15 percent lower thrust for a given blade pitch angle. Wolkovitch plots the rate of descent vs. the induced velocity as shown in Figure 16.

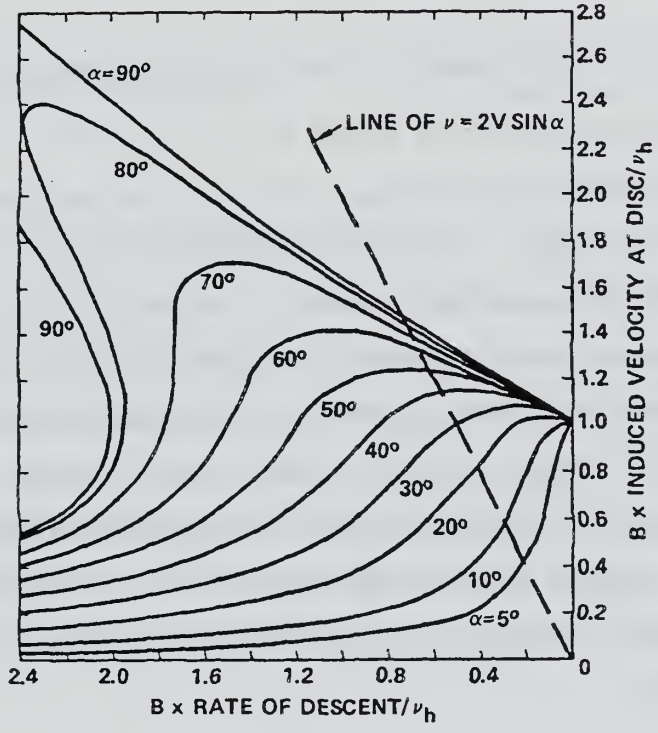

Figure 16. Induced Velocity Versus Rate Of Descent From Ref. [15]

The intersection of the dashed line with the curves indicates the critical rate of descent for a given B and α. This information is also presented in the following figure in terms of a nondimensional horizontal and vertical velocity component. Two different tip loss factor values are plotted with and without parasite drag.

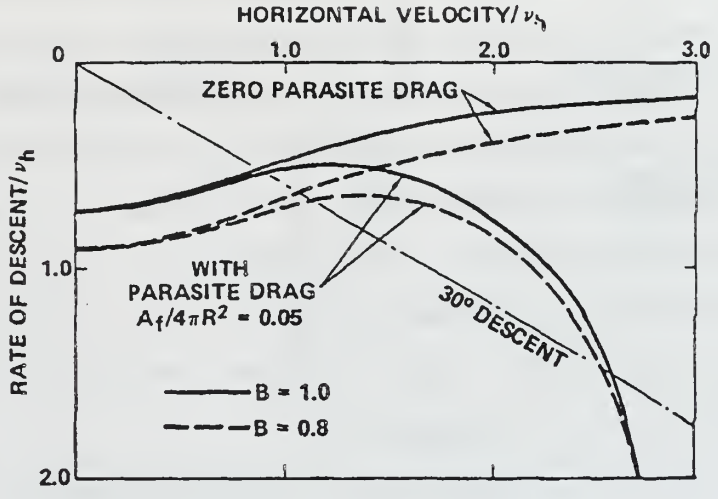

Figure 17. Upper Boundary Of Vortex-Ring State From Ref. [15]

Parasite drag is defined to be the drag associated with many parts of the helicopter including the fuselage, rotor hub, landing gear, tail rotor, tail surfaces, and cowlings. These items provide no direct contribution to the main rotor lift, and must be balanced by the main rotor thrust. Parasite drag increases with increasing airspeed and does not include the drag due to the rotor blades themselves. The drag attributed to the rotor blades is known as induced drag and profile drag. A graph depicting the relationship between the different types of drag and airspeed is shown in Figure 18. According to Wolkovitch, parasite drag causes the boundary of the vortex-ring state to occur at steeper angles of descent for a given airspeed. [Ref. 15]

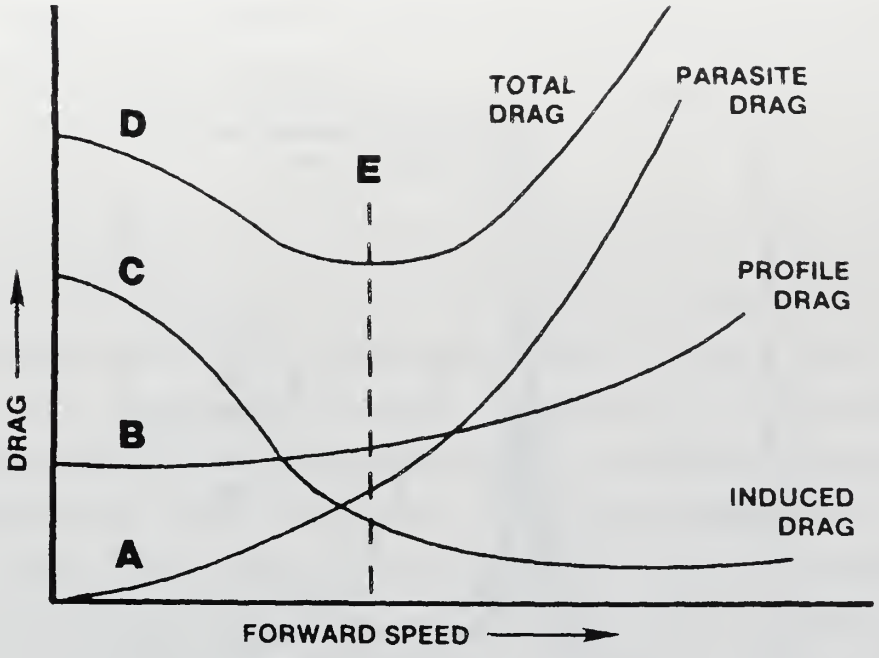

Figure 18. Drag And Airspeed Relationship From Ref. [1]

The line on Figure 18 labeled as E is the airspeed in which the lowest overall drag occurs. This point represents the minimum rate of descent for autorotation, maximum endurance, and the largest rate of climb. [Ref. 1]

b. Experimental Comparison

To confirm the upper boundary prediction with experimental results, Wolkovitch utilized limited experimental data that presented thrust fluctuations indicating the observed unsteady flow associated with vortex-ring state. He was able to show, as seen in Figure 19, that significant thrust fluctuations occur approximately at $V_{crit} = 0.707v_h$ for blade pitch angles of 8, 10, 12 and 14 degrees. The highest measured mean-to-peak thrust fluctuations were approximately 15 percent of the mean thrust.

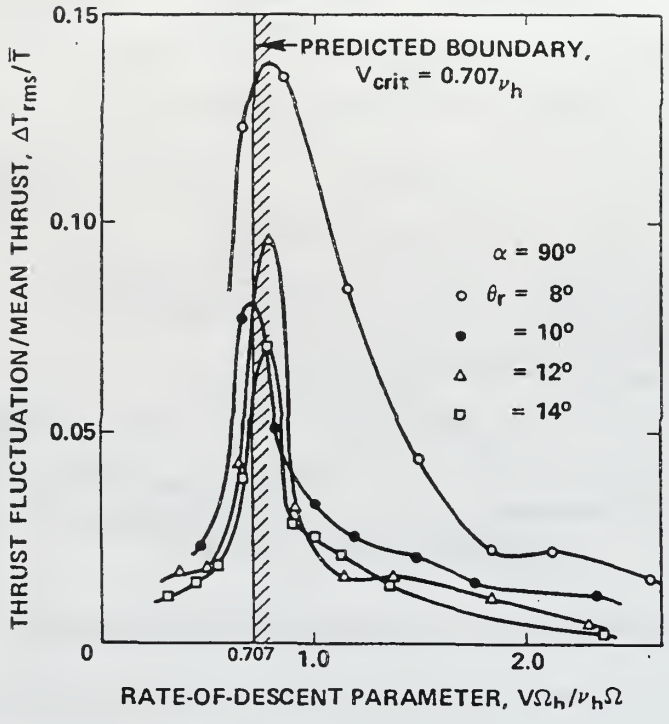

Figure 19. Measured Thrust Fluctuations – Vertical Descent From Ref. [15]

c. Inclined Descents

All of the previous analysis that Wolkovitch performed assumed a vertical descent for the rotor system. Using existing experimental data he was able to demonstrate that the upper boundary still corresponded with mean-to-peak thrust fluctuations of between 15 and 25 percent of the mean thrust for descent angles of 30 through 90 degrees.

d. Vortex-Ring State Lower Boundary

When the descent rate is increased far enough it eventually will reach a point in which steady flow is re-established. This regime is the windmill brake state as discussed previously. All of the velocities in the rotor system are now upwards and the rotor wake lies well above the plane of the rotor system. Wolkovitch defines the lower boundary of the vortex-ring state as the point in which the horizontal speed and rate of

descent reestablish this smooth, steady flow. He derives the critical condition for the lower boundary as:

$$V_{crit} = \frac{kv}{2\sin\alpha}$$

As before, α is defined to be the inclination of the rotor disk to the flight path, v is the induced velocity, and k is an empirical constant specifying the contraction of the wake. Wolkovitch uses k in his flow model, shown in Figure 20, to suggest that the lower boundary is not as sharply defined as the upper boundary. A value of k=1 refers to conditions at the rotor disk. On the other hand, a value of k=2 would imply conditions at infinity. Using a value of k=2, however, would not result in unsteady flow conditions being reflected back to the rotor system. Wolkovitch recommends that a value of k between 1.4 and 1.6 be used. Approaching vortex-ring state from the lower boundary would mean that the breakdown of the slipstream is occurring farther away from the rotor system. Momentum theory is also not particularly accurate at high forward speeds where other vortex interactions are occurring.

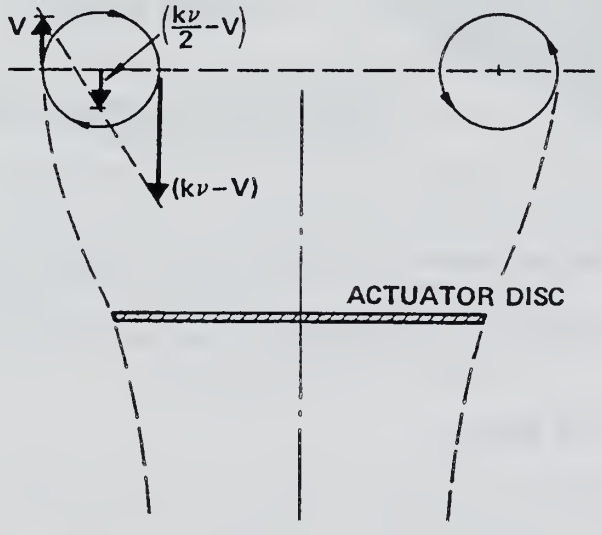

Figure 20. Flow Model For The Lower Vortex-Ring State Boundary From Ref. [15]

e. Predicted Vortex-Ring State Boundary

Combining Wolkovitch's upper and lower boundary prediction using k values of 1.41 and 1.54 leads to the final boundary presented in Figure 21. Overlaid on his upper and lower boundary predictions is a region of roughness obtained through flow visualization. In his concluding comments, Wolkovitch concedes that even though the upper boundary is sharply defined, some unsteadiness can occur at lower rates of descent. It is interesting to note that the upper and lower boundaries do not coincide. This would seem to imply that vortex-ring state is possible at all airspeeds.

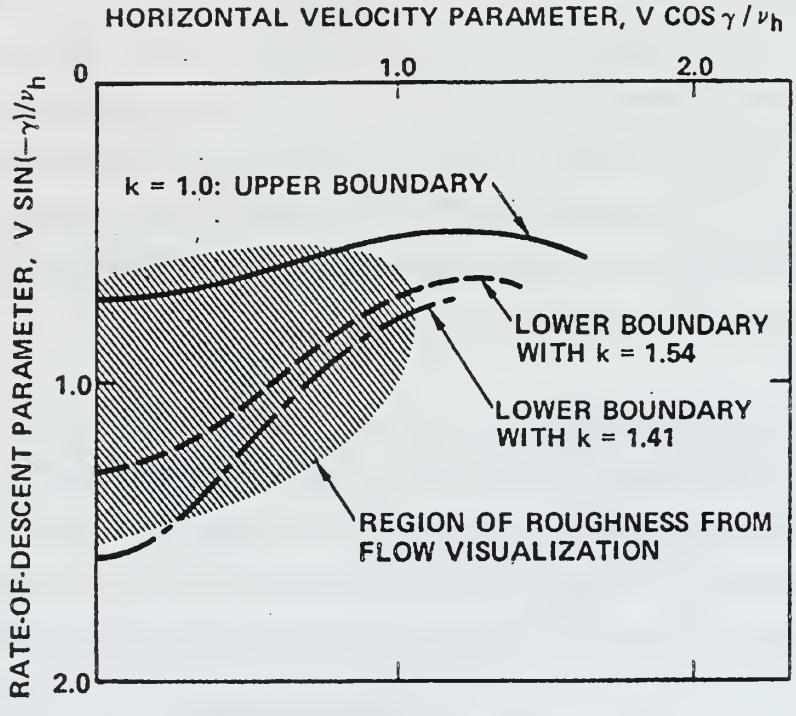

Figure 21. Predicted Vortex-Ring State Boundary From Ref. [15]

2. Peters And Chen

Another commonly referenced source for vortex-ring state prediction is that of Dr. David Peters and Shyi-Yaung Chen. Their paper was published in the *Journal of the American Helicopter Society* in July

1982. Peters' and Chen's motivation for conducting their study was to reexamine vortex-ring state boundary prediction criteria, as presented by Wolkovitch, and to extend the criteria to include a more consistent wake model [Ref. 16]. Peters and Chen introduce their discussion by defining the helicopter state, windmill state, and the vortex-ring state. They consider the helicopter state to be that flight condition where the rotor is imparting energy to the flow field via the induced flow. In the windmill state the rotor is extracting energy from the air by slowing the freestream. Vortex-ring state is defined to be the region in which the concept of a momentum supported slipstream is no longer valid, which, can include both the helicopter and windmill state. This is an important point to keep in mind when the vortex-ring state boundary is presented. [Ref. 16]

a. Background

Peters and Chen begin their study by reexamining momentum theory as it applies to rotors in yawed flow. Yawed flow is a term used to indicate that an inplane component of velocity exists. One could also describe this inplane component as either the horizontal component of velocity that the helicopter generates as it moves forward, or the horizontal velocity component of the wind it experiences, or both. They continue their discussion by deriving an equation that relates the normalized rate of descent η, horizontal velocity μ, and induced flow ν. Figure 22 shows the actual vs. normalized velocity components. The equation describing their relationship is shown below:

$$\eta = \nu \pm \sqrt{\frac{1}{\nu^2} - \mu^2}, \quad \nu\mu \leq 1$$

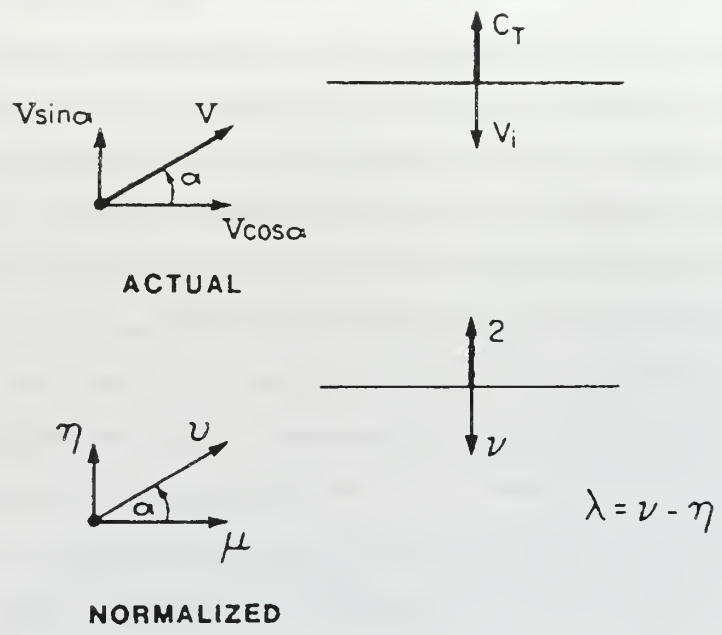

Figure 22. Velocity Components, Actual And Normalized From Ref. [16]

The normalized rate of descent, η, is equal to Vsinα, where α is the descent angle. The normalized horizontal velocity, μ, is equal to Vcosα, and the normalized axial flow at the rotor is λ=ν-η. The normalized value of the induced velocity, ν is defined by the following equation:

$$\nu = \frac{V_i}{\Omega R\sqrt{\frac{C_T}{2}}}$$

C_T is the thrust coefficient normal to the rotor plane. Figure 23 shows the induced flow, ν, plotted for a family of inplane or horizontal velocity values.

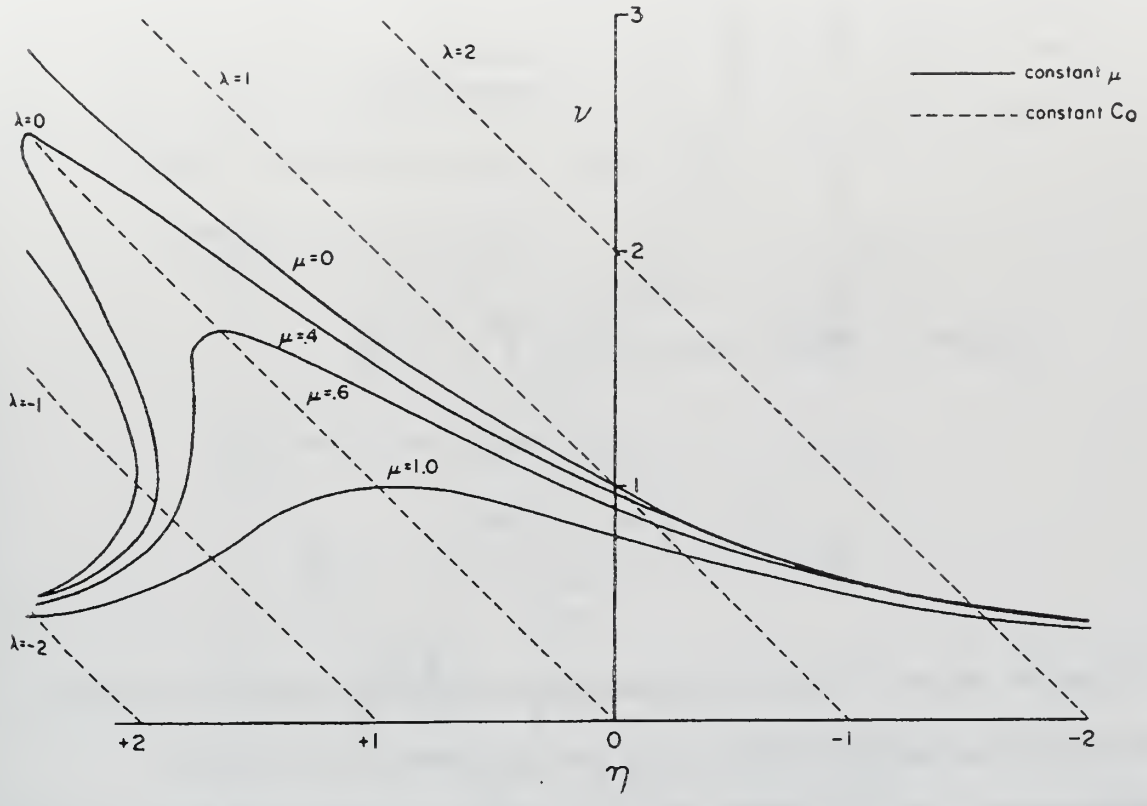

Figure 23. Induced Flow Versus Rate Of Descent For Various μ Values From Ref. [16]

Figure 23 reveals that each constant inplane velocity curve, μ, appears to peak on the line, λ=0, which is stipulated by Peters and Chen to be the crossover from the helicopter to the windmill states. They point out that the peaks do, in fact, lie on the λ=0 line by taking the derivative of the rate of descent with respect to induced flow. When this derivative is set equal to infinity, peaks form when λ=0. They further point out that the roots associated with the momentum equations describing Figure 23 are directly related to the vortex-ring state. These roots essentially are characterized by large and unsteady thrust fluctuations, and a loss of thrust as well as the increase in the power required to descend. The region in which the momentum equation contains three roots is presented in Figure 24.

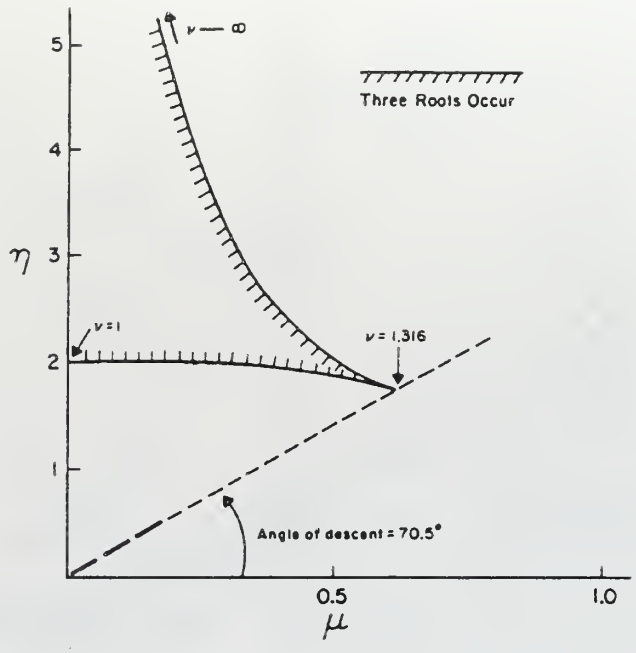

Figure 24. Region In Which Momentum Equation Has Three Roots From Ref. [16]

This figure appears to show that no multiple roots occur beyond approximately $\mu>0.62$. Peters and Chen draw the conclusion based on this result that the vortex-ring state does not occur for high values of inplane flow. They claim that this is consistent with the physical mechanism of vortex-ring state, in that large inplane flows act to sweep the vortices away [Ref. 16]. Therefore, a maximum normalized inplane or horizontal velocity has been specified for their vortex-ring state boundary.

b. Upper And Lower Boundary

One of the main criticisms of Wolkovitch leveled by Peters and Chen is that the theory does not take into account a wake propagation angle. Instead, Wolkovitch's flow model assumes the flow to propagate directly down. There would appear to be no maximum inplane velocity at which vortex-ring state does not occur. This is not consistent with experimental or actual flight test data. In fact, one of the primary methods often discussed for escaping vortex-ring state is an application of forward cyclic to increase the airspeed. This velocity is the same as an

increase in the inplane velocity component, thus sweeping the unsteady flow behind the helicopter. Therefore, Peters and Chen suggest a new flow model, shown in Figure 25 that considers the propagation angle of the wake due to an inplane velocity component.

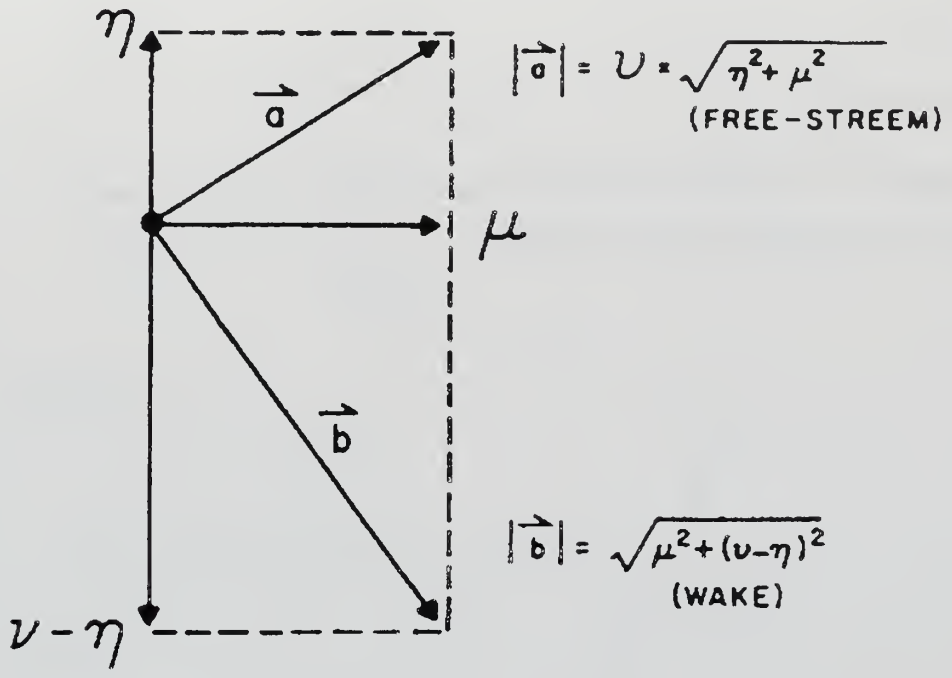

Figure 25. Wake Propogation Flow Model From Ref. [16]

The component of the freestream velocity in the direction of the wake is:

$$\frac{a \bullet b}{|b|} = \frac{\mu^2 + \eta^2 - v\eta}{\sqrt{\mu^2 + (v-\eta)^2}}$$

If the average velocities inside and outside of the wake are set equal to zero, one obtains:

$$\frac{\mu^2 + \eta^2 - v\eta}{\sqrt{\mu^2 + (v-\eta)^2}} + \sqrt{\mu^2 + (v-\eta)^2} = 0$$

Combining the previous equation with the momentum result for rotors in yawed flow,

$$1 = v^2\left[\mu^2 + (v-\eta)^2\right]$$

leads to a set of three equations that define the Peters and Chen vortex-ring state boundary:

- $\mu^2 = \frac{1}{v^2} - \frac{1}{v^6}$
- $\eta = v \pm \frac{1}{v^3}$
- $\lambda = v - \eta = \pm \frac{1}{v^3}$

These equations give rise to the Peters and Chen vortex-ring state boundaries shown in Figures 26 and 27.

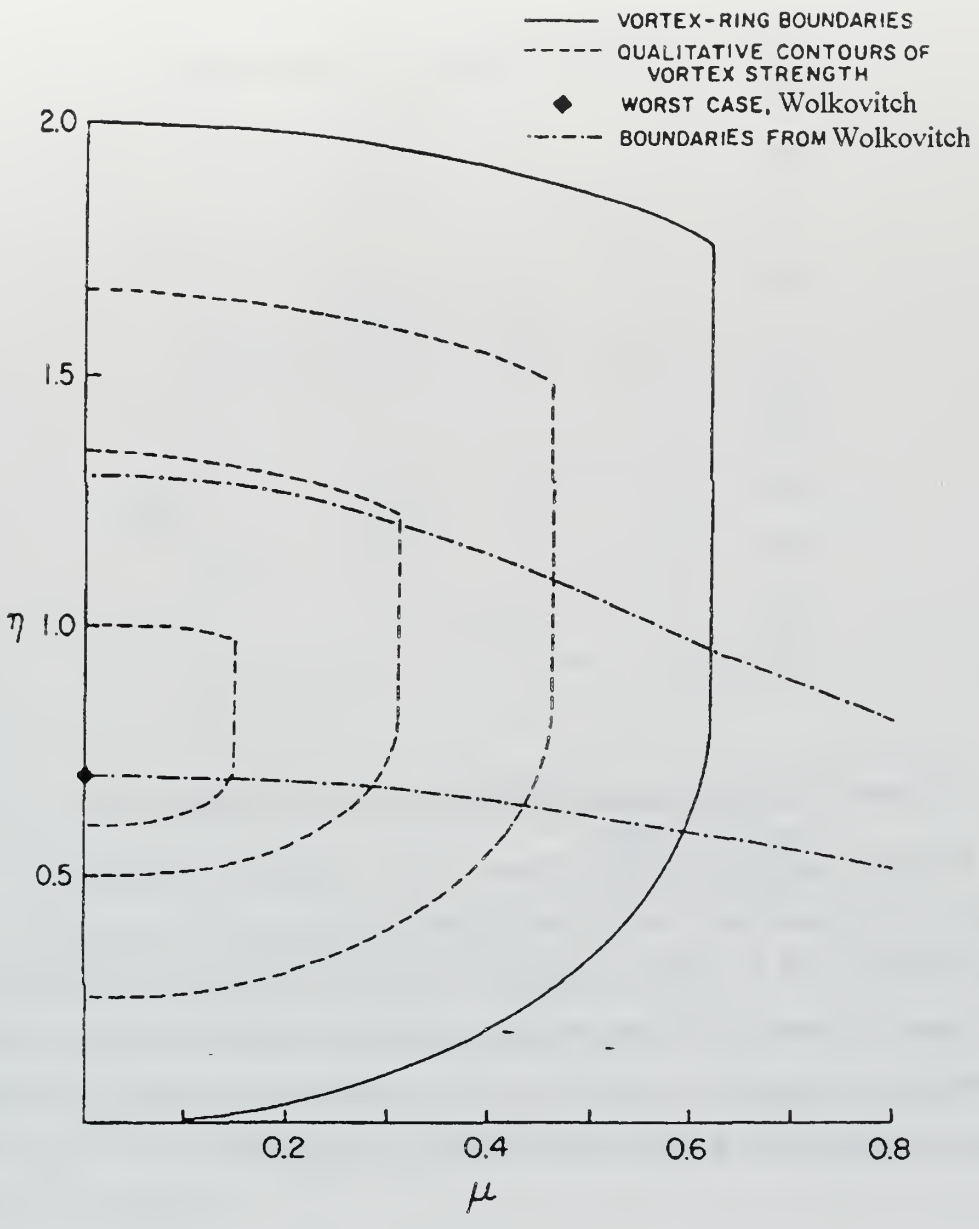

Figure 26. Vortex-Ring State Boundary From Ref. [16]

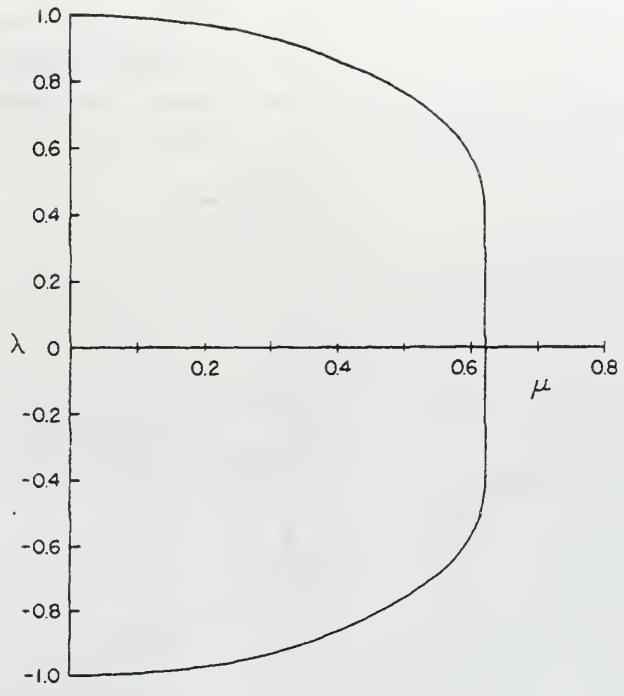

Figure 27. Vortex-Ring State Boundary Of μ Vs. λ From Ref. [16]

Figure 26 presents the Peters and Chen vortex-ring state boundary overlaid by the upper and lower boundaries of Wolkovitch as well as qualitative contours of vortex strength. Note that the plot is inverted to what Wolkovitch presented showing increasing descent rate in the positive y rather than the negative y direction. An orientation showing the rate of descent in the negative y direction is shown in Figure 28.

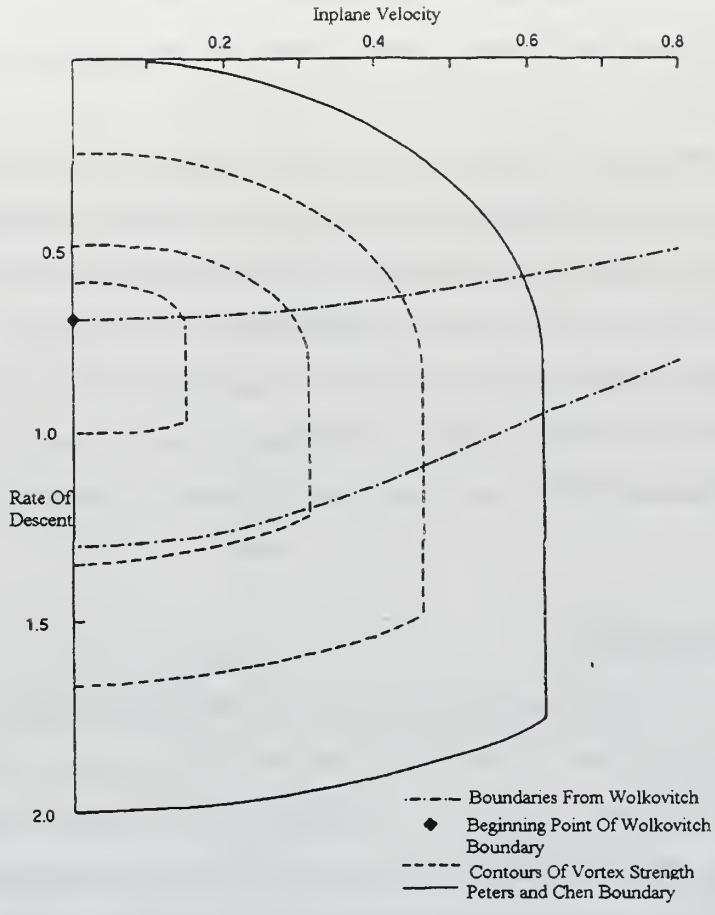

Figure 28. Vortex-Ring State Boundaries With Negative Y Axis Orientation

Figure 27 expresses the vortex-ring state boundaries in terms of the relationship between the inplane velocity and the normalized axial flow. Recall that the axial flow is the normalized rate of descent subtracted by the induced velocity.

c. Concluding Remarks

The following remarks can be made concerning the Peters and Chen vortex-ring state boundary:

- Peters and Chen show no existence of vortex-ring state above a normalized or inplane velocity component of 0.62.
- Vortex-ring state can occur over a wider range of rates of descent.

- The center, not the edge, of the vortex-ring state region is considered to be the point at which the normalized rate of descent is equal to 0.707.

The efforts of Peters and Chen were built upon the theory of Dr. Wolkovitch and were intended to remove what they considered to be inconsistencies of his theory. The most significant difference, perhaps, is the recognition of the effect of the inplane velocity component on the propagation angle of the wake. This lead to the result that the freestream velocity has a negative component in the direction of the wake. From this conclusion, a boundary for vortex-ring state on the helicopter side was obtained.

3. Gao And Xin

Professor Zheng Gao and his graduate student Hong Xin, both from the Institute of Helicopter Technology-Nanjing University of Aeronautics & Astronautics, published a paper in the First Russian Helicopter Society Annual Forum Proceedings titled, "An Experimental Investigation On Vortex-Ring State Boundary," published in 1994. A motivating factor cited by the authors, for researching this problem were the numerous helicopter accidents in China attributed to vortex-ring state. The lack of existing satisfactory methods for determining the vortex-ring state boundaries prompted Gao and Xin to take a more experimental approach to solving this dilemma.

a. Experimental Set Up

It was essential that if a vortex-ring state boundary was to be obtained experimentally the test apparatus used in the study must be highly reliable and free of common wind tunnel testing limitations. With this in mind, Gao and Xin developed a test apparatus free from two main limitations associated with the typical wind tunnel. The first wind tunnel limitation is that it is difficult to account for the severe interference

effects from the wind tunnel wall because of the size of the fluctuating air body around the rotor system, which can extend to a distance of several rotor diameters in the vortex-ring state. Second, many wind tunnels demonstrate poor low speed characteristics in the low speed region required to study vortex-ring state. Gao and Xin developed a six-meter long whirling beam mounted with a model rotor driven by an a/c. motor and attached to a scaled model fuselage of a Bell 206. The model rotor had the ability to be fixed on the beam in several radial locations. Additionally, level, vertical and oblique flight conditions were modeled by changing the orientation of the axis of the model rotor. The whirling beam could be adjusted to rotate anywhere from 0 to 30 rpm allowing several descent velocities to be examined. See Figures 29, 30, and 31 for diagrams of the testing apparatus. Three sets of rotor blades with varying characteristics were utilized in the experimental studies. See Table 6.

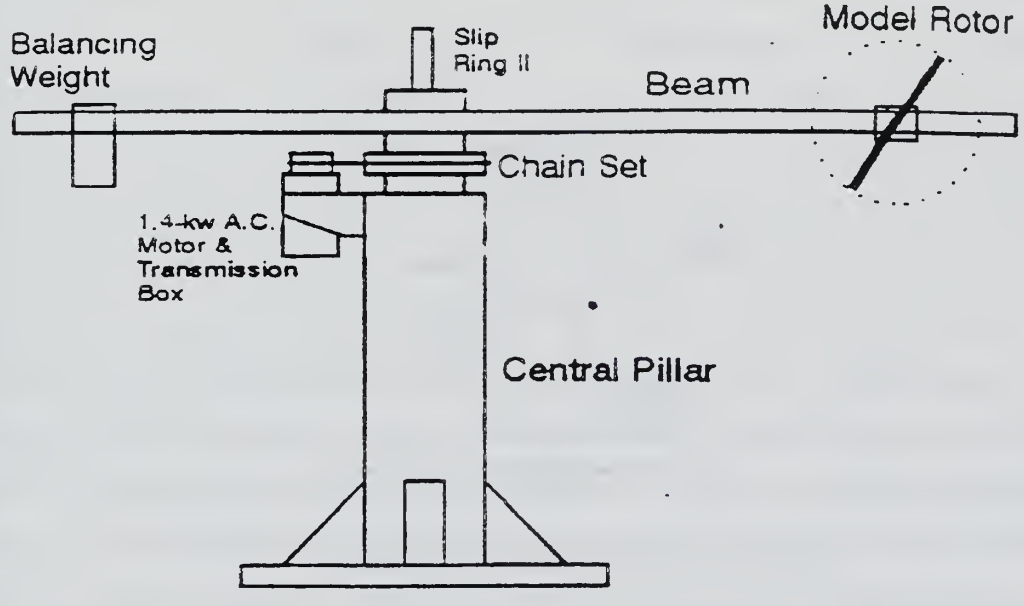

Figure 29. The Whirling Beam From Ref. [17]

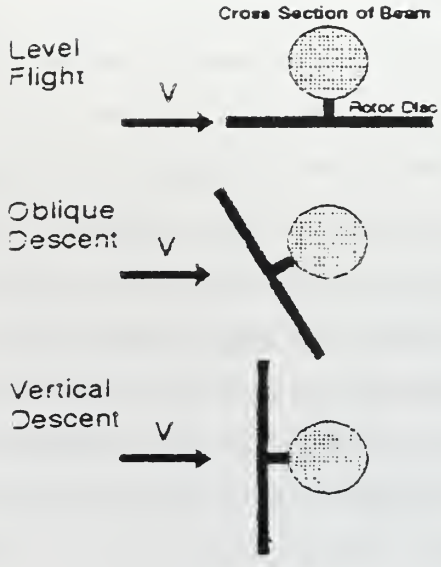

Figure 30. Conditions Of Flight From Ref. [17]

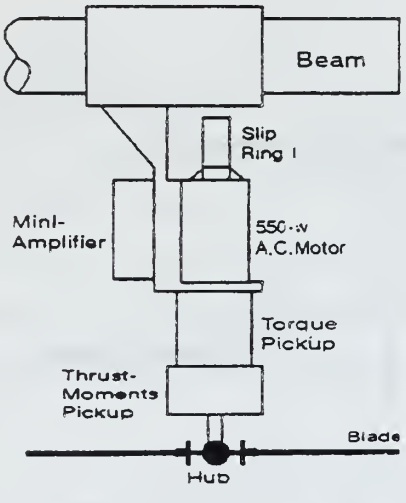

Figure 31. Rotor System From Ref. [17]

The function of the whirling beam was to measure the torque and thrust experienced by the rotor system. This was accomplished with the use of a strain-gauge balance system located between the motor and the hub of the rotor. Four leaf springs were used to sense the thrust, and a torsion tube was used to gather the torque data. After passing through an amplifier the

signals were sent to a computer where they were sampled and converted to digital data to be graphed as output. [Ref. 17]

Blade Sets	No. 1	No. 2	No. 3
Airfoil	NACA 0012	NACA 23012	OA 212
Blade Twist	0	-5.5°	-9.22°
Chord (mm)	60	73	73
Weight (grams)	150	240	240

Table 6. Rotor Blade Properties After Ref. [17]

b. Testing And Reduction Of Data

Fourteen groups of tests were conducted using the various blade sets as described in Table 6. The model rotor was fixed on the whirling beam at a radial location of five meters. For each testing group the rotational speed of the whirling beam was increased incrementally at each testing point. The first and last testing points of each group were for hovering conditions. Gao and Xin point out that at each test point the rotor was not started until the beam had been adjusted to rotate steadily at the desired speed. Once this stability was achieved data points were then sampled and the time histories of the torque and thrust were recorded. Sampling was also completed before and after the rotor was engaged while the whirling beam was rotating in order to obtain the fore and aft zeroes of the measurements at that test point. The zero drifts of each channel were monitored by checking the repeatability of the fore and aft zeroes of each test point as well as the first and last hovering values of the test group. [Ref. 17] The conditions of testing are shown in Table 7.

Test Group No.	Blade Sets Used	Blade Pitch Angle (deg)	Fuselage	Angle Of Descent	V_h	Number of Test Points	V_{max}/V_h
1	1	6	No	90	3.15	21	1.94
2	1	8.5	No	90	3.63	17	
3	1	10	No	90	4.03	21	1.39
4	2	10	No	90	4.28	21	1.18
5	2	10	Yes	90	4.25	21	1.23
6	3	10	No	90	4.20	21	1.25
7	3	10	Yes	90	4.20	21	1.26
8	3	10	No	90	4.20	16	1.11
9	3	10	No	75	4.20	22	1.33
10	3	10	No	60	4.20	12	1.11
11	3	10	No	45	4.20	22	1.34
12	3	10	No	30	4.20	12	1.13
13	3	10	No	15	4.20	22	1.34
14	3	10	No	0	4.20	7	0.90

Table 7. Test Conditions From Ref. [17]

For each test point, the average value of the pair of fore and aft zeroes was used as the mean zero and subtracted from the sampled data when the rotor was running. Furthermore, the data was averaged over the sampling period in order to obtain mean values at that particular velocity. [Ref. 17]

Gao and Xin eliminated centrifugal force effects by subtracting the zeroes that were measured, as described before, when the beam was rotating. Other sources of error included a flapping motion of the rotor blades that was introduced as a result of inplane component of the freestream velocity as well as a Coriolis moment acting on the rotor blades. This Coriolis moment resulted from the rotor axis not being

parallel with the central pillar. Both of these errors were analyzed and expressed in terms of tilt angle errors of the rotor system. Because of the tilt angle errors, the measured thrust was slightly less than the actual value. A thrust correction was applied utilizing the angle errors and is shown below:

$$T_{Real} = \frac{T_{Measured}}{\cos\beta_0 \cos\beta_\sigma}$$

β_0 represents the tilt angle error from the flapping motion of the rotor blades and β_σ was the tilt angle error introduced from the Coriolis moment.

Other data validity concerns that were addressed included possible electrical interference and mechanical vibration. Gao and Xin reported that the mean square deviations of the zeroes caused by the electrical interference and mechanical vibrations were less than one percent of the corresponding mean values. [Ref. 17]

c. Results

Gao and Xin discovered, like Wolkovitch, that the most severe region of the vortex-ring state in a vertical descent was the region in which the descent velocity was 0.6 to 0.8 of the rotor-induced velocity. ($0.6v_h < V < 0.8v_h$) The relationship between the torque, thrust and the nondimensional velocity is shown in Figure 32 and 33. Gao and Xin also determined that, according to their power spectra data shown in Figure 34, the period of the aerodynamic fluctuations was approximately one to two seconds; the same as was reported by the makers of the smoke study films shown earlier in this thesis in Figure 13.

One of the most significant findings highlighted by Gao and Xin was the correlation of their mean torque data to what many call the power settling phenomena of vortex-ring state. This phenomenon is, again, described as the situation where an increase in torque is observed

for increasing descent velocity. In this region pilots find that an increase in collective is required even though they are in a descent. As can be seen from Figure 35, the mean torque is a minimum at a low descent velocity of about $V=0.28v_h$. Beyond this point the trend for the mean torque begins to rise and comes fairly close to leveling off at a descent velocity of $V=0.8v_h$. Beyond this point the mean torque rises again. Gao and Xin speculate that this second increase is due to local blade stall. After $V=0.8v_h$ the torque fluctuations, however, gradually decrease as the rotor moves towards the windmill brake state. The point at which the mean torque begins to increase with an increasing descent rate is defined by Gao and Xin to be the critical descent velocity. They have experimentally defined this value to be $Vcrit = 0.28v_h$. $Vcrit = 0.28v_h$ is considered to be the worst case scenario or, in other words, the lowest descent velocity for which this behavior will commence. The value for which this power settling region begins varies from 0.28 for the vertical descent to 0.55 for a descent angle of 45 degrees. Descent angles shallower than 40 degrees do not indicate a mean torque behavior of this sort. Additionally, no evidence of the vortex-ring state was found for angles of descent less than 30 degrees. Therefore, Gao and Xin conclude that vortex-ring state cannot be entered for descent angles less than 40 degrees.

Another interesting result reported by Gao and Xin was that for angles of descent between 60 and 75 degrees, the torque and thrust fluctuations are greater than those for the vertical descent. This would indicate that the turbulence associated with the vortex-ring state is the highest when the descent angle is between 60 and 75 degrees. See Figures 36 and 37. For angles of descent less than 60 degrees, the fluctuations drop of until they finally disappear below 30 degrees.

Gao and Xin also utilized the boundary equation formulated by the Peters and Chen model, and, instead, set it equal to their empirically determined descent velocity of $0.28v_h$. The entire equation is shown as follows:

$$\frac{V.W}{|W|} = \frac{V_x^2 + (v - V_Y)^2 - v(v - V_Y)}{\sqrt{V_x^2 + (v - V_Y)^2}} = -0.28v_h$$

Gao and Xin were also able to empirically define that the descent velocity, or V_Y, for vortex-ring state lies between $-0.28v_h$ and $-1.8v_h$. Using this result and the previous equation, the maximum horizontal velocity in which vortex-ring state can exist is $V_X=0.91v_h$. This corresponds to a limiting descent angle of 40 degrees. The entire vortex-ring state boundary appears in Figure 38.

One final remark made by Gao and Xin was a conclusion regarding disk loading, blade twist and fuselage effect. They concluded that the disk loading influenced the rotor behavior in such a manner that for the induced rotor velocity in a hover, rotors with different disk loading have the same variation of torque and thrust. Therefore, V_{crit}, or, V/v_h, must be constant for rotors of different disk loadings. Regarding the effects of the fuselage and blade twist, the authors simply stated that neither one had any significant effect on the vortex-ring state.

A superposition of the three vortex-ring state boundaries of Wolkovitch, Peters/Chen, and Gao/Xin is shown in Figure 39.

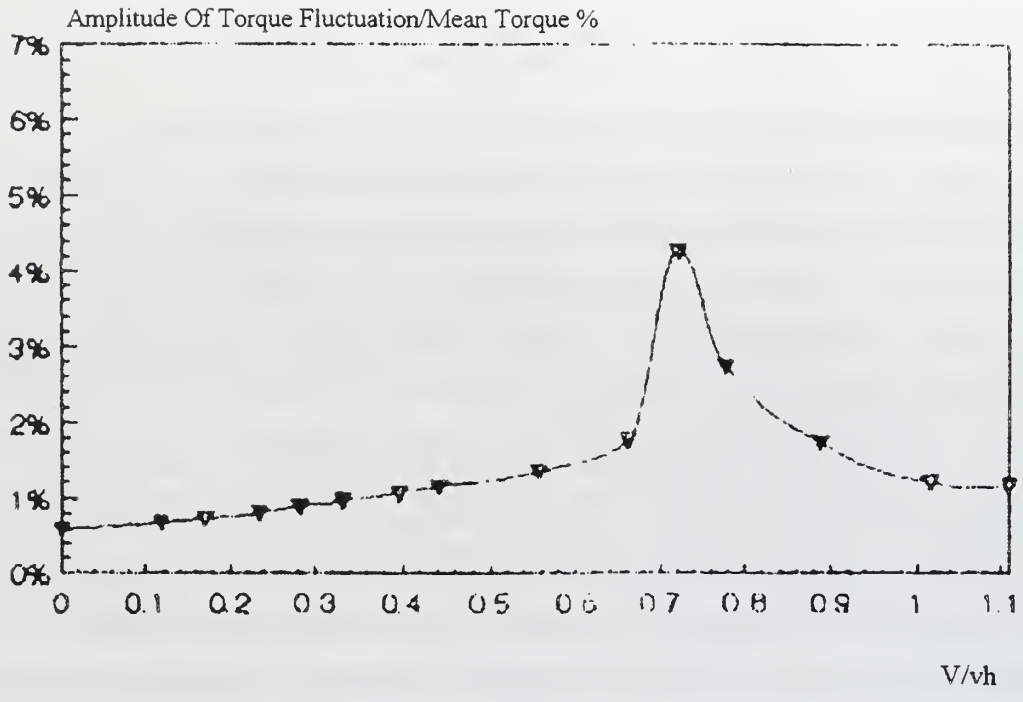

Figure 32. Torque Fluctuations In A Vertical Descent From Ref. [17]

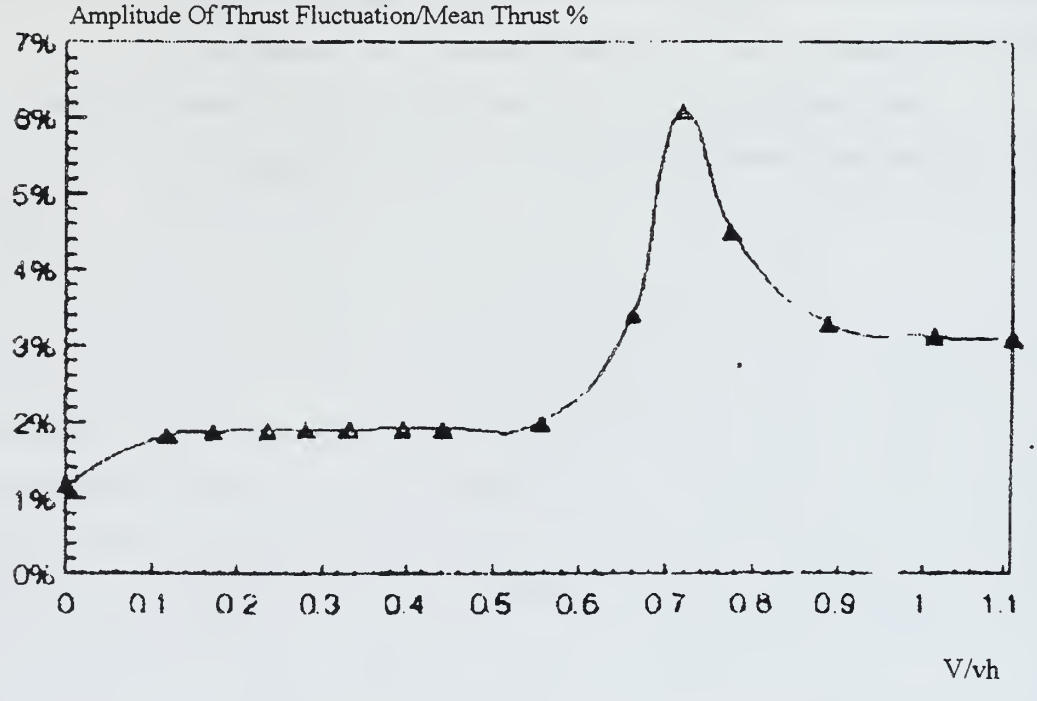

Figure 33. Thrust Fluctuations In A Vertical Descent From Ref. [17]

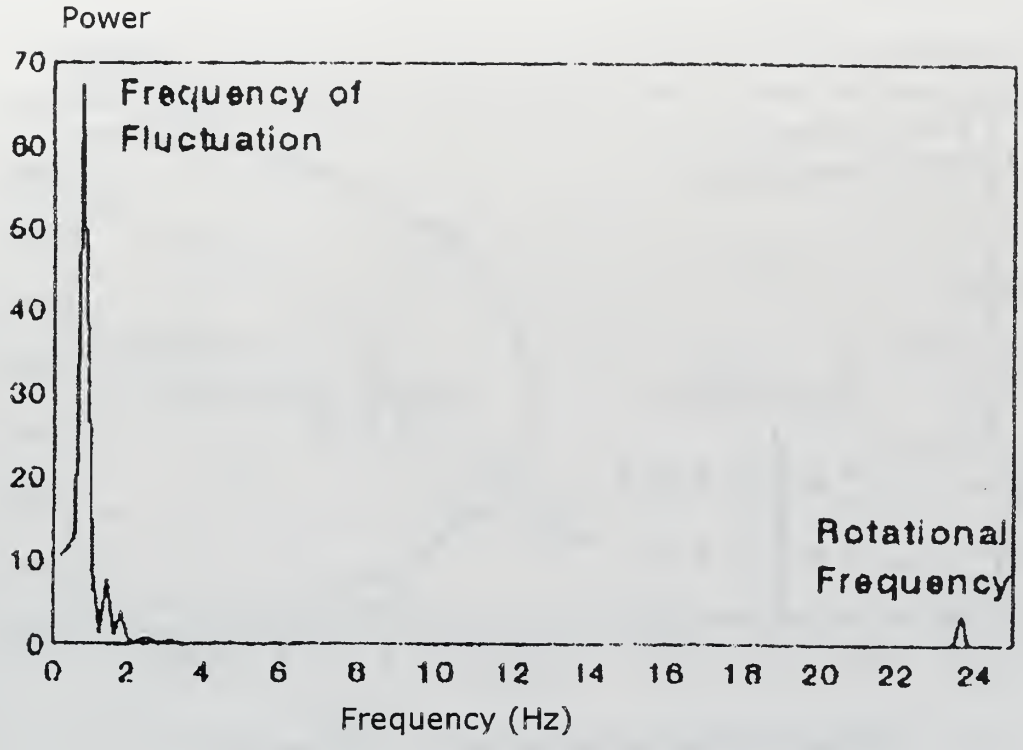

Figure 34. Power Spectrum From Ref. [17]

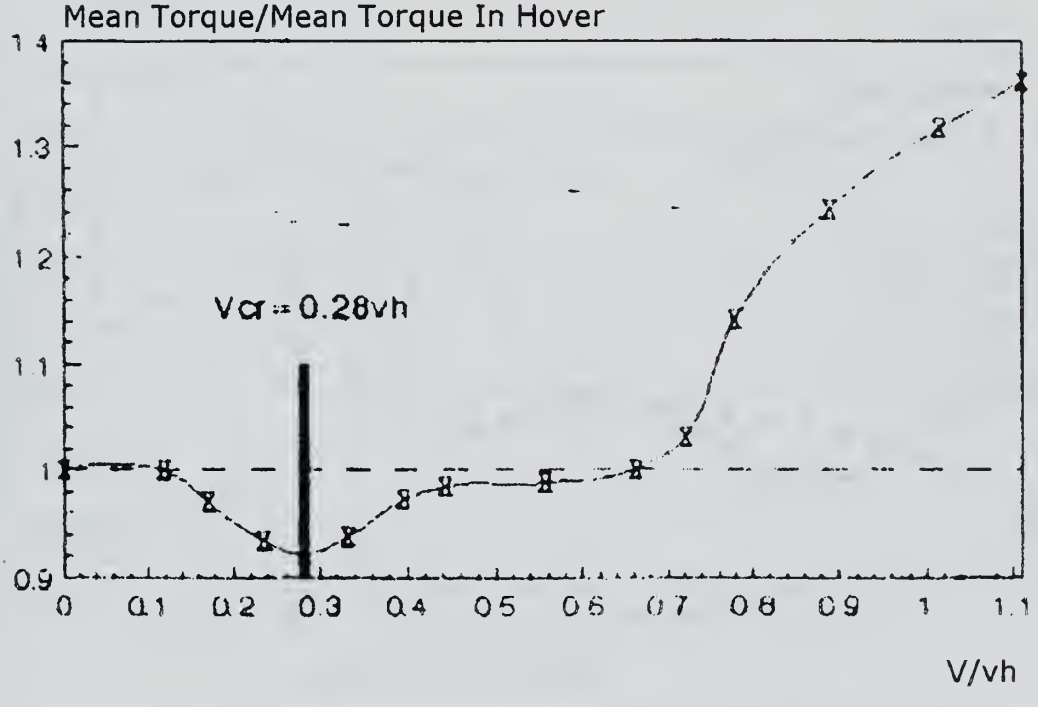

Figure 35. Mean Torque In A Vertical Descent From Ref. [17]

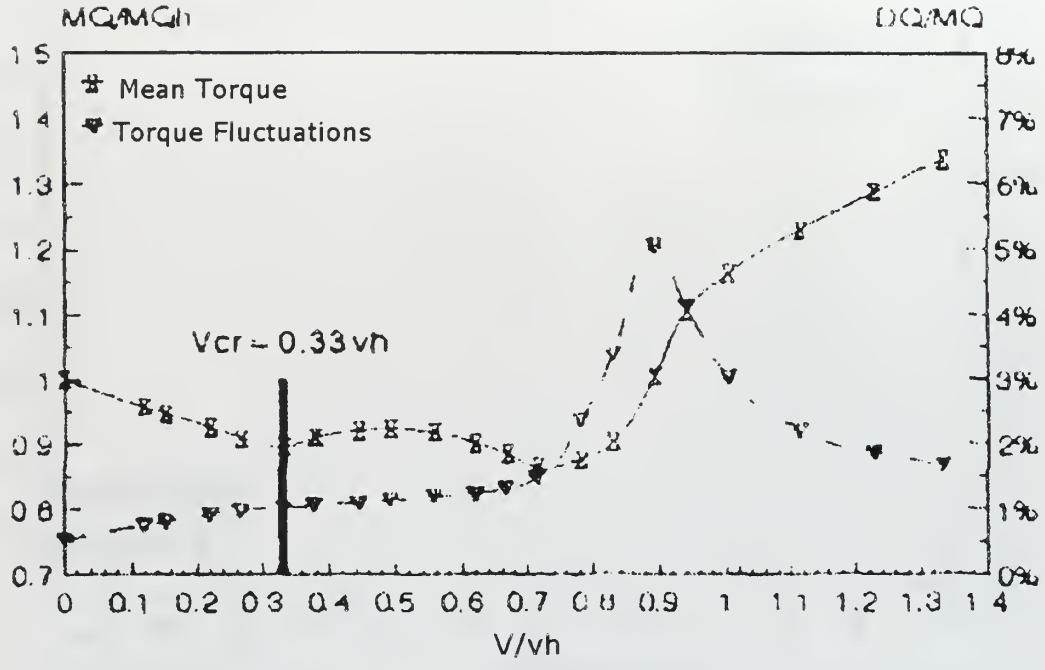

Figure 36. Torque Fluctuations For A 75° Descent

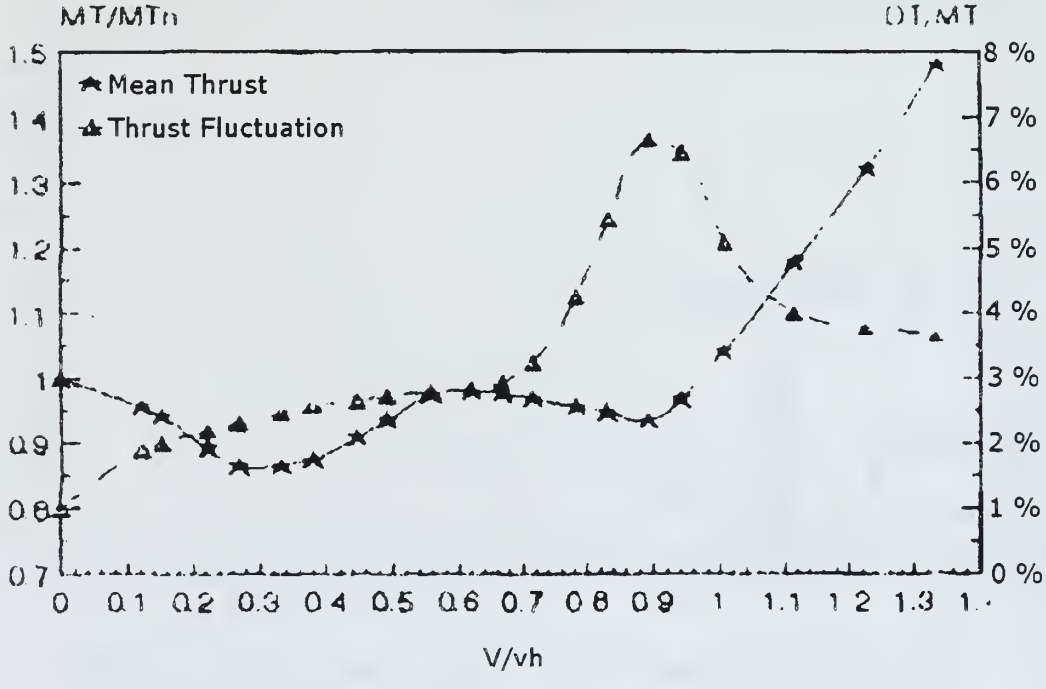

Figure 37. Thrust Fluctuations For A 75° Descent After Ref. [17]

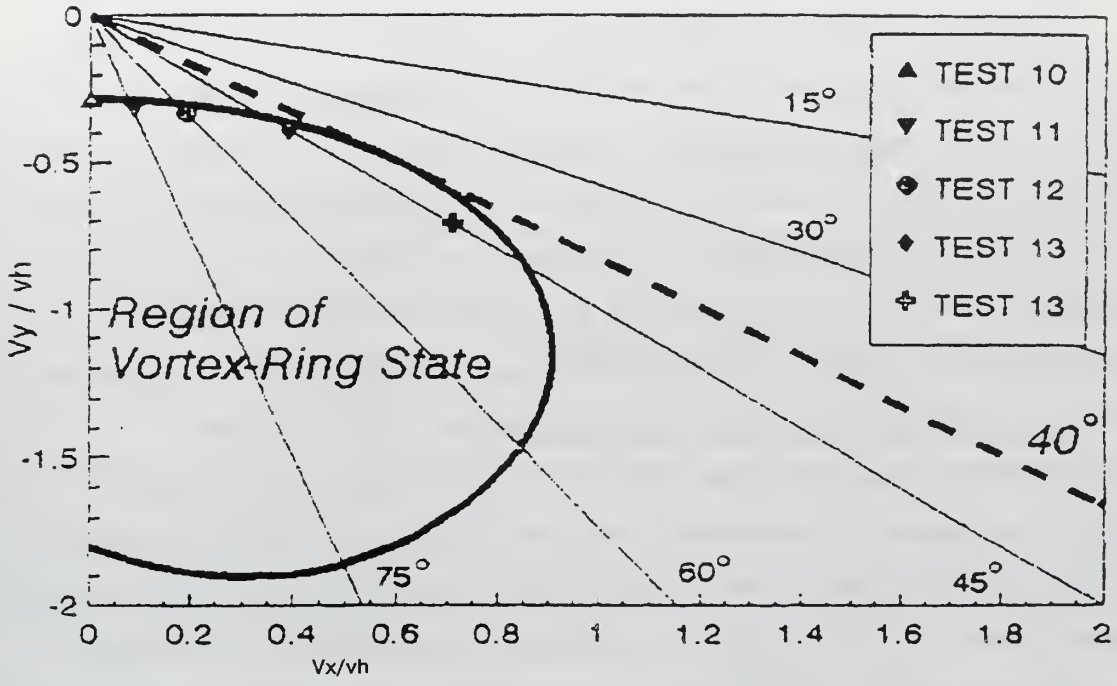

Figure 38. Gao And Xin Vortex-Ring State Boundary From Ref. [17]

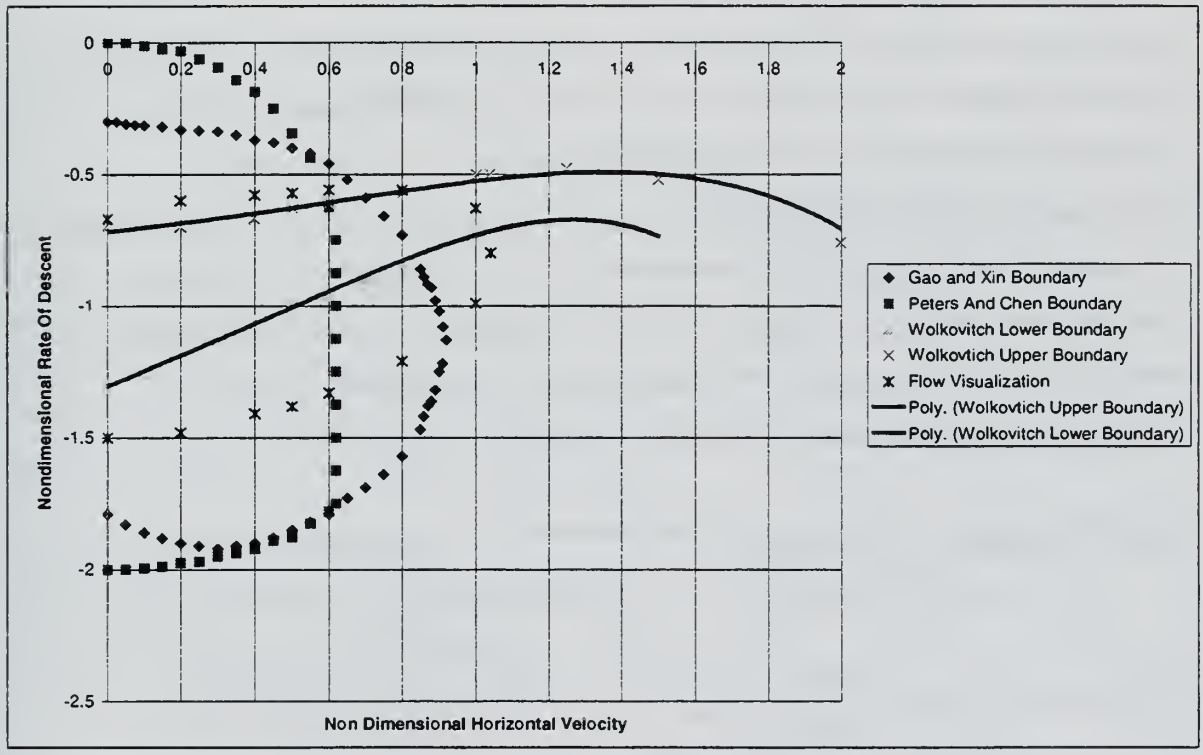

Figure 39. Superposition Of Vortex-Ring State Boundaries And Flow Visualization

B. EXPERIMENTAL COMPARISONS WITH H-34 DATA

In 1964, Langley Research Center, under the direction of James Scheiman, conducted an extensive flight test program to obtain rotor blade airloads, bearing moments, and blade motions as well as to measure numerous flight parameters. The purpose of the program was to provide additional experimental data on vibratory loads that was considered as lacking at that time. The tabulated data presented without analysis in the NASA Technical Memorandum X-952 was collected for forward flights from 0-120 knots, flights in and out of ground effect, climbs, autorotations, maneuvers, and operations with fore and aft center of gravity locations. This data was obtained through the instrumentation of a U.S. Army Sikorsky H-34. Of particular interest to this study was the partial power descent flight tests and the corresponding pilot remarks.

Partial power descent data was obtained for flight test numbers 55-76. Descents were initiated at airspeeds ranging from 0 to 113 knots. Actual descent rates varied from 0 to 2,600 feet per minute. The testing gross weight of the helicopter was reported to be between 11,200 and 11,805 lb. For calculations used in the vortex-ring state boundary determination an average weight of 11,502.5 lb. was used. Similarly, the air density for the partial power descent data varied from 0.00208 to 0.00244 slugs/ft^3. Averaging all of the reported air densities yielded a value of 0.00216 slugs/ft^3. The partial power descent data and corresponding comments are shown in Table 8.

Flight	Airspeed (knots)	Air Density (Slugs/ft^3)	Remarks Vd,i = Instantaneous Descent Velocity Vd,av = Average Descent Velocity (ft/min)
55	0	.00217	Vd,i = 700; Vd,av = 900
56	0	.00221	Vd,av = 1,200 ***Rough; Blades Flapping Erratically; Unsteady Flight***

Flight	Airspeed (knots)	Air Density (Slugs/ft^3)	Remarks Vd,i = Instantaneous Descent Velocity Vd,av = Average Descent Velocity (ft/min)
57	0	.00213	Vd,av = 1,350 ft/min ***Heavy Roughness***
58	7	.00217	Vd,av = 1,000
58	6	.00218	Vd,av = 1,800
59	≈8	.00214	Vd,av = 2,100 ***Helicopter Temporarily Out Of Control***
59	≈7	.00215	Vd,av = 1,850 ***Helicopter Temporarily Out Of Control***
60	10	.00209	Vd,av = 800 ***Moderate Roughness***
61	≈12	.00211	Vd,i = 400; Vd,av 1,700
62	≈14	.00211	Vd,av = 2,000 ***Unsteady Flight***
62	≈6	.00214	Vd,av = 2,600 ***Unsteady Flight***
63	15	.00244	Vd,av = 650
64	16	.00209	Vd,i = 400; Vd,av = 500 ***Moderate Roughness; Temporary Loss Of Directional Control***
65	17	.00211	Vd,i = 450; Vd,av = 250
66	16	.00208	Vd,av = 550
67	16	.00214	Vd,av = 700
68	18	.00212	Vd,av = 650
69	18	.00215	Vd,av = 700
70	20	.00214	Vd,av ≈ 0 ***Smooth; One Per Revolution; Blade Flapping***
71	21	.00223	Vd,av = 1,000
72	22	.00220	Vd,av = 1,000 ***Smooth***
73	24	.00213	Vd,i = 500; Vd,av = 250 ***Blades Flapping Erratically***
74	26	.00236	Vd,av = 450

Flight	Airspeed (knots)	Air Density (Slugs/ft^3)	Remarks Vd,i = Instantaneous Descent Velocity Vd,av = Average Descent Velocity (ft/min)
75	70	.00222	Vd,av = 200
76	112	.00212	Vd,i = 400; Vd,av = 600 ***One Revolution Only; Rough***
76	113	.00212	Vd,av = 550 ***Rough***

Table 8. Partial Power Descent Data After Ref. [18]

For each flight there is a corresponding airspeed, air density, and a rate of descent included in the remarks column. The rates of descent are labeled as Vd,i, and Vd,av. Vd,i represents the instantaneous rate of descent, which is obtained over a time interval of five to ten seconds. Vd,av is the average rate of descent obtained over a time interval of one to two minutes. Average rates of descent, Vd,av, were used for plotting this data.

Review of Table 8 reveals that many of the pilot remarks and associated airspeed and descent rate values show a close correlation even to the most general definition of vortex-ring state. Vibrations, flapping blades, high descent rates, unsteady and rough flight, and the loss of control are listed in the remarks section of the reported data. These comments are indicative of the characteristics of vortex-ring state that have been previously discussed and strongly suggest that the helicopter was in vortex-ring state during a majority of the partial power descent flight tests. Based on this observation it was felt that the H-34 would serve as a good metric to use in comparing the three previously studied vortex-ring state theories. All of the data points shown in Table 8 were plotted with an overlay of the vortex-ring state boundaries from Wolkovitch, Peters and Chen, and Gao and Xin. Also overlaid on each plot is the region of roughness obtained from flow visualization reported

by Drees and Hendal. Each H-34 data point with an associated comment related to vortex-ring state was enclosed by a box.

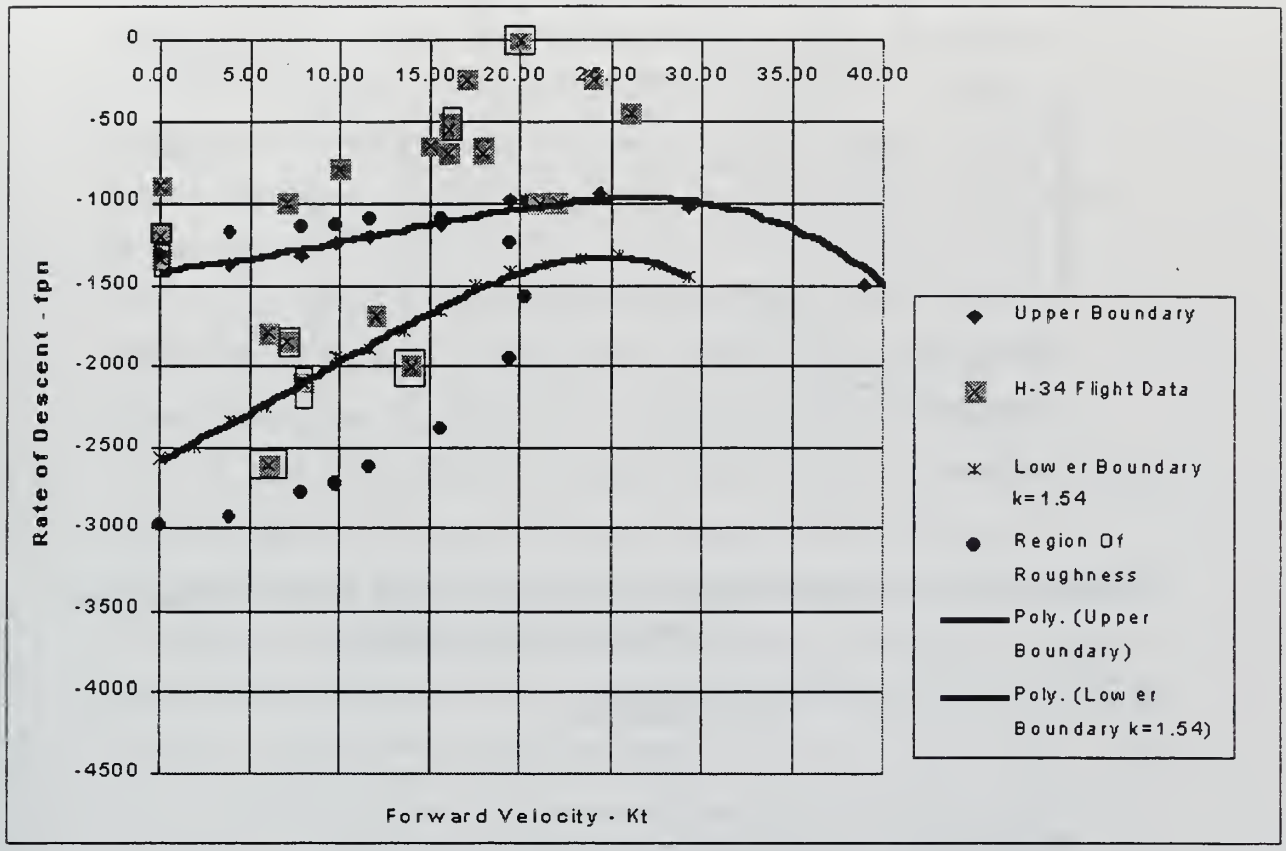

Figure 40. H-34 Partial Power Descent Data Overlaid With The Vortex-Ring State Boundary Of Wolkovitch After Ref. [19]

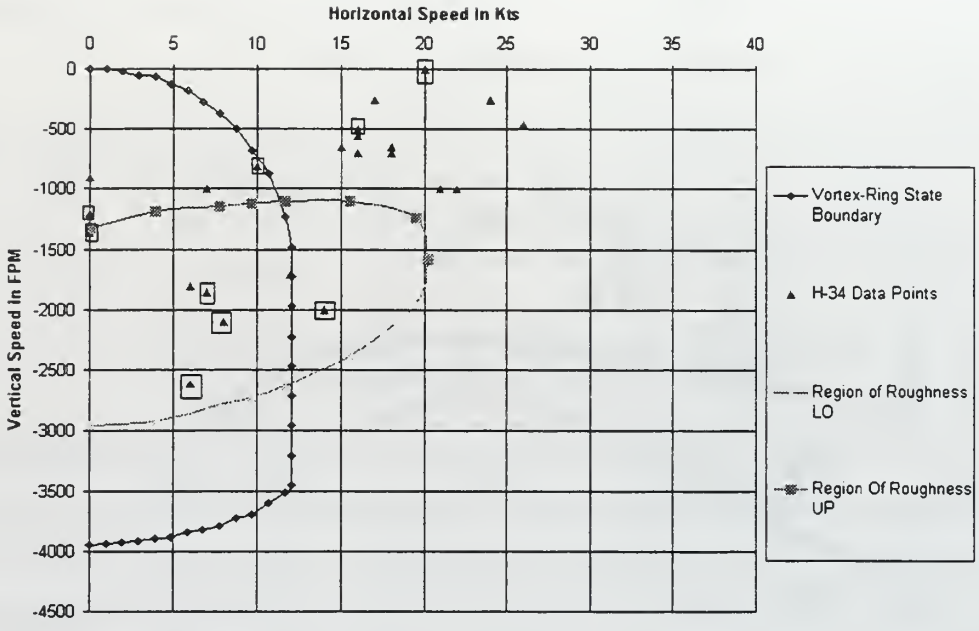

Figure 41. H-34 Partial Power Descent Data Overlaid With The Vortex-Ring State Boundary Of Peters And Chen

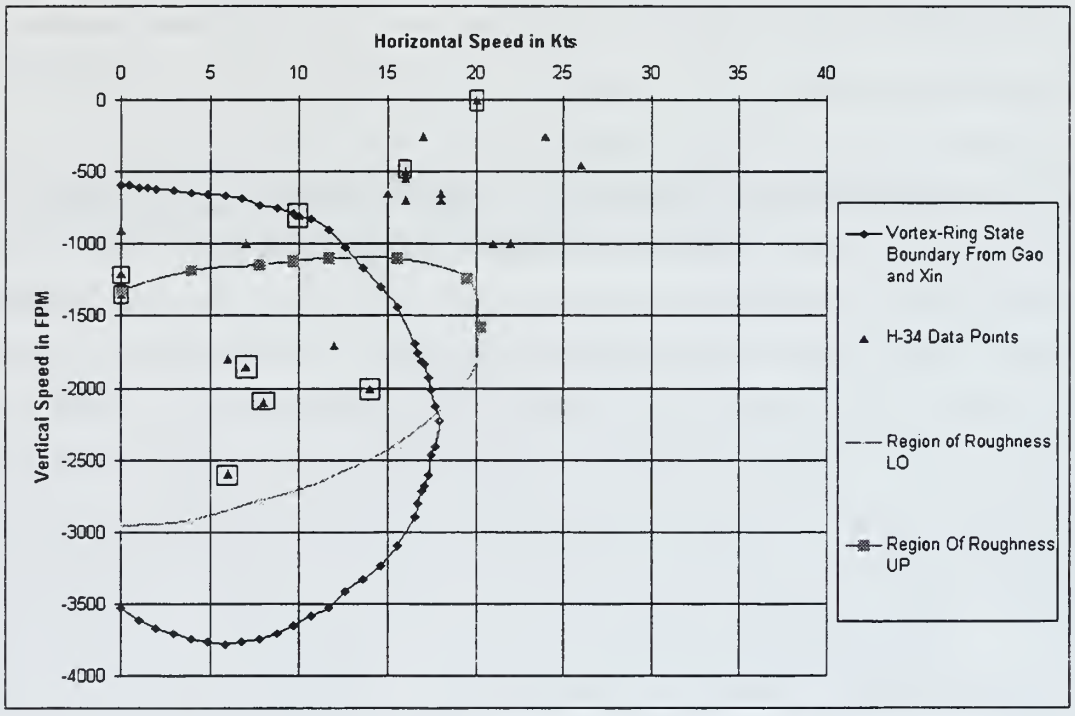

Figure 42. H-34 Partial Power Descent Data Overlaid With The Vortex-Ring State Boundary Of Gao And Xin After Ref. [19]

After examining the previous plots the following observations were made:

- The two remarks referring to the helicopter as temporarily out of control (Flight 59) are located within all of the boundaries. They are, however, more centrally located within the vortex-ring state boundaries of Peters/Chen and Gao/Xin. Since this is the most severe characteristic of vortex-ring state, one would expect this to be the case.
- The narrow region between Wolkovitch's upper and lower boundary results in the exclusion of a greater number of data points than either Peters/Chen, or Gao/Xin. Of particular note is flight 62. For each rate of descent and airspeed pair, the pilots remarked that they experienced "unsteady flight," again, another accepted characteristic of vortex-ring state. This seeming discrepancy refers to Wolkovitch's consideration in establishing a standard k (a wake contraction constant) value for defining the lower boundary. K was assigned a value of 1.54 in this plot.
- Peters' and Chen's boundary extends no farther than 12 knots and excludes one point from flight 62 as well. The result of this significantly shortened boundary in the airspeed axis is to effectively cut the region of roughness by approximately 40 percent.
- Two data points from flights 64 and 70 are not included in any vortex-ring state boundary. Even though the comments under flight 64 included moderate roughness, and temporary loss of directional control (vortex-ring state behavior) the airspeed and rate of descent did not fit the boundaries of any theory. This also includes the boundary describing the region of roughness from flow visualization. Under the remark for flight 70 a comment is made about blade flapping, another vortex-ring state characteristic.

However, the average rate of descent for this condition is zero, implying a cause other than vortex-ring state.

- The most inclusive boundary belongs to Gao and Xin. Its extends as far as approximately 17.5 knots, but begins at a higher rate of descent and ends at a lower rate of descent than does Peters and Chen.
- Increasing the gross weight of the helicopter increases the induced velocity and consequently increases the rate of descent at which the boundary begins and ends, and shifts the edge towards a higher airspeed. The only exception to this is the Peters and Chen boundary, which still begins at zero airspeed and zero rate of descent.
- Increasing the air density has the opposite effect of increasing the weight. An increase in the air density leads to boundaries beginning and ending at lower rates of descent. Additionally, the boundaries do not extend as far in airspeed, either. The effect of a change in air density is not as readily noticeable as one in weight. Examination of the hover induced velocity equation proves this fact.
- An increased rotor radius has the same effect as an increase in air density. The boundary begins and ends at a lower rate of descent and retracts to a lower airspeed.
- The region of roughness is affected similarly with changes to gross weight, air density, and rotor radius.

C. ALGORITHM CRITIQUE AND SELECTION

It was essential to choose a vortex-ring state boundary algorithm that would prove to be practical and reliable for implementation. A boundary that indicates vortex-ring state on any descent would be over-conservative and impractical to implement. On the other hand, a

boundary that does not adequately define the vortex-ring state region would not serve its intended purpose of providing a sufficient warning to the pilot. It was felt that the Gao and Xin boundary would best provide the combination of practicality, ease of implementation, and sufficient warning to function as a reliable safety/situational awareness tool in the warning system. A critique of the vortex-ring state boundary theories of Wolkovitch, Peters and Chen, and Gao and Xin is contained in the following sections:

1. Wolkovitch

One of the main deficiencies of the Wolkovitch boundary is that it does not account for the skew or propagation angle of the rotor wake at higher forward speeds. The flow model shown in Figure 20 indicates only a downward vertical velocity component for the vortex core. There are no horizontal or inplane velocity components considered in this wake geometry. Looking at Wolkovitch's predicted boundary shown in Figure 21 indicates that vortex-ring state is possible for all horizontal velocities, or highly yawed flows. This is not supported by available test data, and from a realistic viewpoint doesn't make sense. A higher horizontal velocity or inplane flow should have the effect of sweeping the disturbed air or vortices away from the rotor system. In fact, many flight manuals and publications list obtaining forward airspeed as a procedure for escaping vortex-ring state. The only effect of higher inplane flows in the vortex-ring state boundary appears to be manifested in Wolkovitch's consideration of the parasite drag as discussed previously from Figure 17. This figure suggests that the inclusion of parasite drag has the effect of changing the shape of the upper vortex-ring state boundary downwards. Figure 18 shows that parasite drag increases for increased airspeed, thus its effects should be more pronounced at higher airspeeds. [Ref. 16]

A second discrepancy of the Wolkovitch is that his lower boundary does not provide a sufficient bridge between the vortex-ring state and windmill brake state. An area still remains below the lower boundary that is not yet the windmill brake state. Vortex-ring state could realistically exist below the lower boundary. Revisiting Figure 40 it can be seen that there are two H-34 partial power descent data points that lie below the lower boundary described by k=1.54. These two data points have comments associated with them that suggest the helicopter was experiencing vortex-ring state, yet, they are not included in Wolkovitch's boundary. [Ref. 16]

A third point is that the upper boundary seems to be a better predictor of the center of the vortex-ring state region rather than the edge. The upper boundary was defined to begin at the point where the descent rate is equal to $0.707v_h$. This definition made the assumption that B, the tip loss factor, was equal to one. In other words, no tip loss was assumed to occur. A tip loss factor of 0.8 would move the boundary to an even higher rate of descent as can be seen from Figure 17. This descent rate corresponds to the point at which the *maximum* thrust fluctuations occur, another indication of, perhaps one of the stronger regions of vortex-ring state. [Ref. 16]

From a practical standpoint, the vortex-ring state boundary of Wolkovitch is not sufficient for use as a warning algorithm. An indication of the strongest thrust fluctuations is of no use to a pilot who wishes to avoid the phenomenon in the first place. The boundary must be conservative enough to keep the helicopter away from combinations of airspeeds and rates of descent that could lead to the worst of vortex-ring state. Additionally, encountering vortex-ring state at high forward airspeeds is inconsistent with experience and current flight data and would be contrary to generally accepted methods of escaping vortex-ring

state. In terms of Figure 21, the boundary is essentially too narrow and too long, i.e., it never closes in the horizontal axis.

2. Peters And Chen

Peters and Chen attempted to improve upon the inconsistencies and discrepancies of the Wolkovitch theory. Peters and Chen created a different flow model, see Figure 25, on which to build their boundary. They included a wake propagation angle in their analysis and ensured that their boundary provided a bridge to the windmill brake state. Despite the apparent success of their improvement to the Wolkovitch theory, their predicted vortex-ring state boundary is also insufficient for practical use.

Peters and Chen defined the vortex-ring state to be the region where the concept of a momentum slipstream is no longer valid, which can include the helicopter and windmill brake states. This definition may be scientifically accurate, but its resultant effects on the predicted boundary render it impractical. The new vortex-ring state boundary developed by Peters and Chen, as seen in Figure 26, begins immediately upon any descent from a hovering condition. This also indicates that for every angle of descent, there is a vortex-ring state region. This, too, is not consistent with known model test and flight data as well as flight experiences. Additionally, the critical horizontal velocity of $0.62v_h$ suggests that vortex-ring state is not possible for any steep angle of descent with a horizontal component of velocity greater than $0.62v_h$. This can be seen from the results of the H-34 experimental data shown in Figure 41. A data point interpreted to be in vortex-ring state is excluded from the Peters and Chen boundary due to the restrictive critical horizontal velocity. [Ref. 17]

An interesting feature in Figure 28 is that of the vortex-ring state contours. Peters and Chen attempted to provide contours of strength of

the vortex-ring state. This was based on their suggestion that Wolkovitch's upper boundary began at the center of the vortex-ring state region rather than the edge. In their present form, the contour lines are little more than interesting as Peters and Chen did not specify how they quantified them. Perhaps they were based on flow visualization or were derived from some value of thrust fluctuation. Without this knowledge it would be difficult to quantify contours of vortex-ring state strength for applicability to a warning system.

In summary, the predicted vortex-region of Peters and Chen is impractical for use in the implementation of the warning system. At low airspeeds the boundary is over-conservative predicting vortex-ring state upon a descent from a hover. At low airspeeds ($Vx > 0.62v_h$), however, the boundary is not conservative enough permitting flight at steep angles of descent with no penetration of a vortex-ring state region. Neither of these observations is supported by flight experiences. [Ref. 17]

3. Gao and Xin

The work of Gao and Xin attempted to formulate vortex-ring state boundaries that would be of practical use for a pilot. This was based on the need to better define the vortex-ring state boundaries following a series of accidents in China attributed to this phenomenon. Having reviewed the Peters and Chen theory, Gao and Xin decided to take a semi-empirical approach to obtaining vortex-ring state boundaries. A unique test apparatus was developed that improved upon some of the typical wind tunnel limitations in helicopter testing.

Gao and Xin modified the Peters and Chen criteria by defining vortex-ring state as occurring when the freestream velocity component opposite to the direction of the wake reaches a critical value experimentally determined to be $0.28v_h$. Using the momentum equations as described previously, Gao and Xin formulated a new vortex-ring state

boundary and provided a comparison with the Peters and Chen model as shown in Table 9.

Critical Values	V_Y/v_h	V_X/ v_h	Descent Angles (Degrees)
Peters And Chen	0	0.62	All
Gao And Xin	0.28	0.91	<= 40
Flight Experiences	≈ 0.25	≈ 1	< 50

Table 9. Boundary Comparison From Ref. [17]

The experimentally determined critical vertical descent velocity was obtained by noting the point at which the torque required began to increase with increasing descent rate for a vertical descent.

Another interesting conclusion of Gao and Xin was the finding that the highest degree of turbulence was associated with descent angles between 60 and 75 degrees. This experimental result could pose additional problems to the validity of the Peters and Chen boundary.

According to Gao and Xin, their boundary is in good agreement with model test results and flight experiences. From the H-34 comparison previously discussed, their boundary was the most inclusive to the points regarded as vortex-ring state. Furthermore, the Gao and Xin boundary included a majority of the region of roughness from flow visualization. From a practical standpoint, the Gao and Xin boundary represents the most realistic boundary for implementation of the warning system. A warning cannot be issued upon a descent from a hover nor at a moderate airspeed, two concerns of the Wolkovitch and Peters/Chen boundary.

All of these issues are critical for implementation. It is crucial that false alarms, or failures to detect vortex-ring state are reduced as much as possible, if not eliminated. It was felt that the vortex-ring state boundary

of Gao and Xin would allow the best possibility of achieving these requirements.

D. OTHER VORTEX-RING STATE INDICATORS

One of the most significant properties of vortex-ring state that a helicopter encounters is high vibration levels. These vibrations result from erratic thrust fluctuations and associated flapping of the rotor blades. The erratic blade flapping has been primarily attributed to the bursting of the airbody that surrounds the system as discussed earlier. The vibration levels of a helicopter in vortex-ring state can be severe. Walter Gerstenberger, longtime helicopter pioneer and former Chief of Dynamics at Sikorsky Aircraft, frequently referred to vortex-ring state as "the roughest regime of helicopter flight." John E. Yeates of the Langley Aeronautical Laboratory published a study on helicopter vibrations in several regimes of flight including the vortex-ring state. Though this study was published in 1958, its relevancy has not diminished. The data presented in this study provides valuable insight into the mechanical stresses that the helicopter experiences as well as into the characteristics of many of these flight regimes. These characteristics have helped to better define the behavior of the helicopter and consequently have provided the helicopter designer with valuable information. Unfortunately, many of the present day studies do not attempt to address vibration levels of helicopters experiencing vortex-ring state. Considering the *reported* frequency of vortex-ring state's occurrence, its analysis is either deemed as unimportant or too great of a safety risk to warrant the amount of time and money required to obtain the desired data.

1. Yeates' Vibration Study

Yeates' study was conducted utilizing a tandem rotor helicopter with vibration sensors as shown in Figure 43. Vortex-ring state vibrations were measured in the vertical channel using sensors mounted on the front

and rear rotor masts. Vertical vibrations sensed at these two important locations and were recorded in time history from using an oscillograph. Other helicopter parameters such as airspeed and rate of descent were measured with recording instruments and synchronized with the oscillograph through a common timing circuit. Yeates reported 95 percent of the vibratory response at the three-per-rev (3P) frequency, no corrections were applied to the data to include other harmonics. [Ref. 20]

Yeates, like Peters and Chen, defined the vortex-ring state to be the point where a definite momentum slipstream ceases to exist. He specified the traditionally defined limits of vortex-ring state, which extend from hover to that condition where rate of descent is equal to twice the average induced velocity. The flight test consisted of maintaining a constant rotor speed from hover up to a forward speed of 10 knots. Power was then reduced to allow the helicopter to begin a descent. Yeates observed that the helicopter began to wallow while the descent rate steadily increased. Pilot recovery was initiated by increasing forward airspeed by applying forward cyclic, or lowering the nose. [Ref. 20]

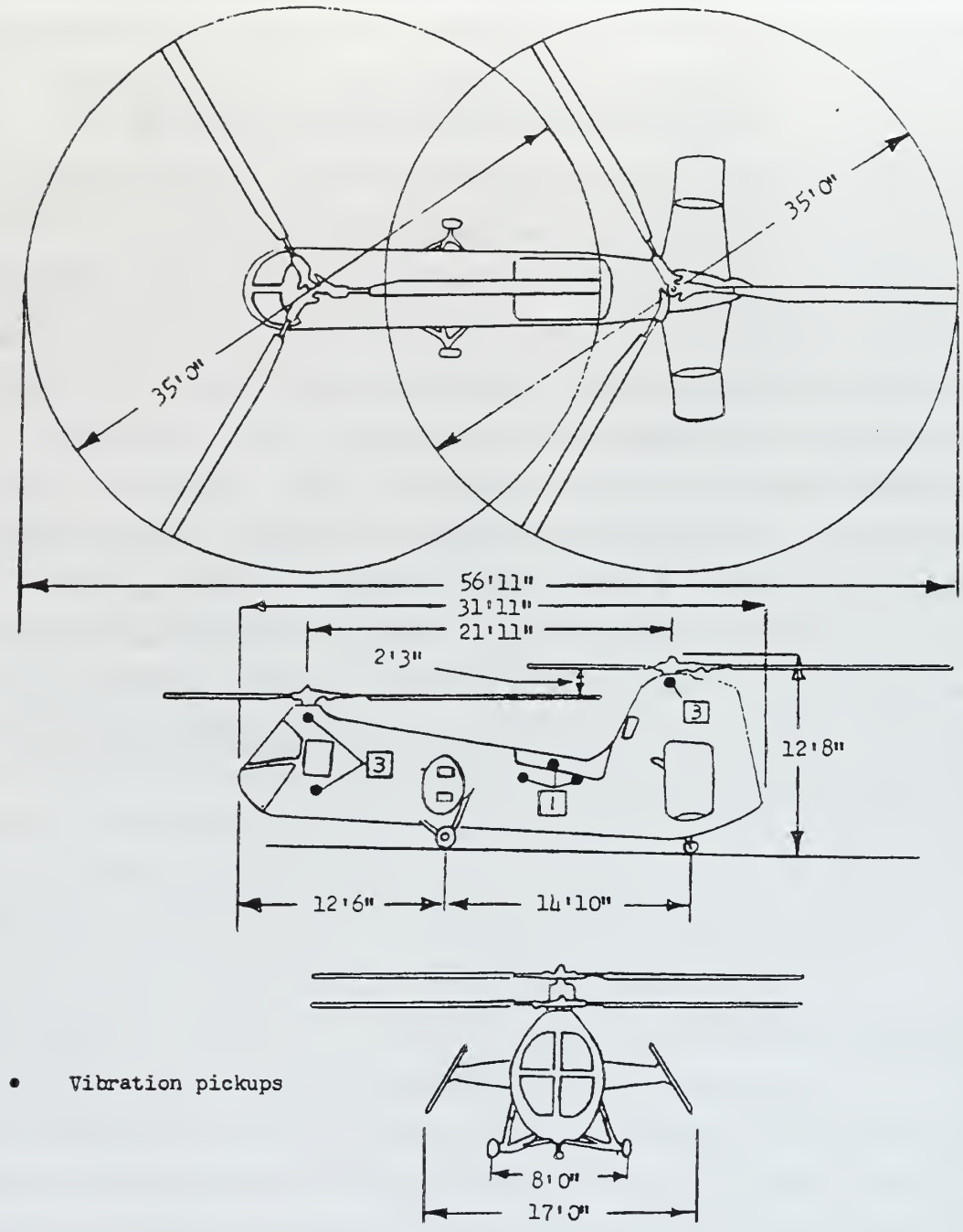

Figure 43. Test Helicopter Utilized For Vibration Investigation From Ref. [20]

a. Results

Figure 44 reveals the nature of helicopter vertical vibrations in a hovering condition. This plot provides a basis of reference when the vibration envelope of vortex-ring state is examined. As can be seen the vibrations are relatively low and do not demonstrate any significant fluctuating or erratic behavior.

The observable occurrence of vortex-ring state in Figure 44 extends between a nondimensional rate of descent of −0.23 to −1.25 at near zero forward airspeed. This region shows the pulsating unsteady nature of the vibration envelope. [Ref. 20]

Descent With Forward Airspeed Near Zero. Figure 45 shows the time histories of the vibration envelopes, which contain all frequency components of vibration, measured for a rate of descent that varies from 360 ft/min to 1,940 ft/min. This is equivalent to the nondimensional rates of descent Vv = −0.23 to −1.25. The vibration envelopes for both rotors show large irregular peaks in the vicinity of approximately 1,600-ft/min rate of descent. The envelope also displays random pulsating vibrations indicating, according to Yeates, the shedding of vortices. These pulsating vibrations were not reported to be the result of any pilot induced control input, or any rotor frequency. Beyond about 1,950 ft/min, or Vv = −1.25, the helicopter seems to have reached the end of any observable effects of vortex-ring state. [Ref. 20]

Descent With Forward Speed Near 10 Knots. Figure 46 shows the histories of the vibration envelopes for rates of descent that varied between 500 ft/min to 1,150 ft/min or Vv = −0.32 to Vv = −0.74 at a forward airspeed of approximately ten knots. The vibrations appear to have more regular occurring pulses. Yeates suggests that this is due to the regular shedding of the vortices and further states that this indicates the likely forward airspeed limit for the observable effects of vortex-ring state. He also noted that a helicopter in vortex-ring state at ten knots has

a higher mean level of vibration for the aft rotor and a lower mean level of vibration for the forward rotor. Finally, the test pilot for the study commented that control in the vortex-ring state was much easier with forward speed.

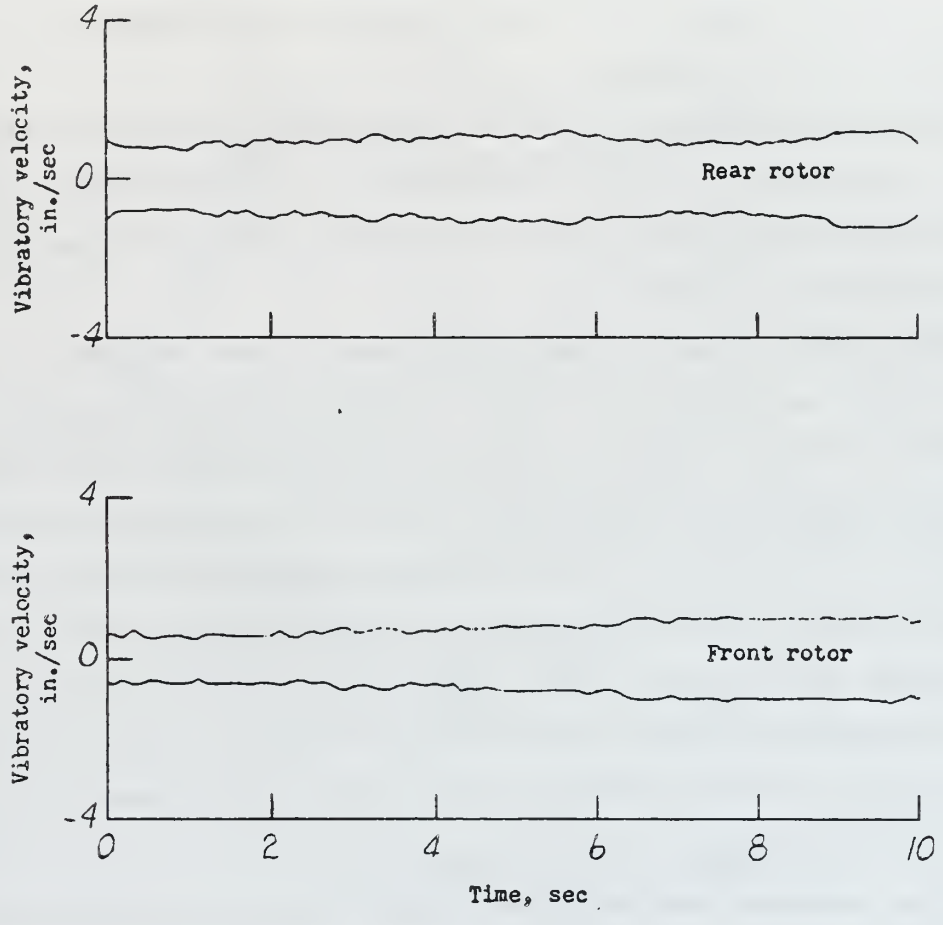

Figure 44. Time History Of Vertical Vibrations In A Hover From Ref. [20]

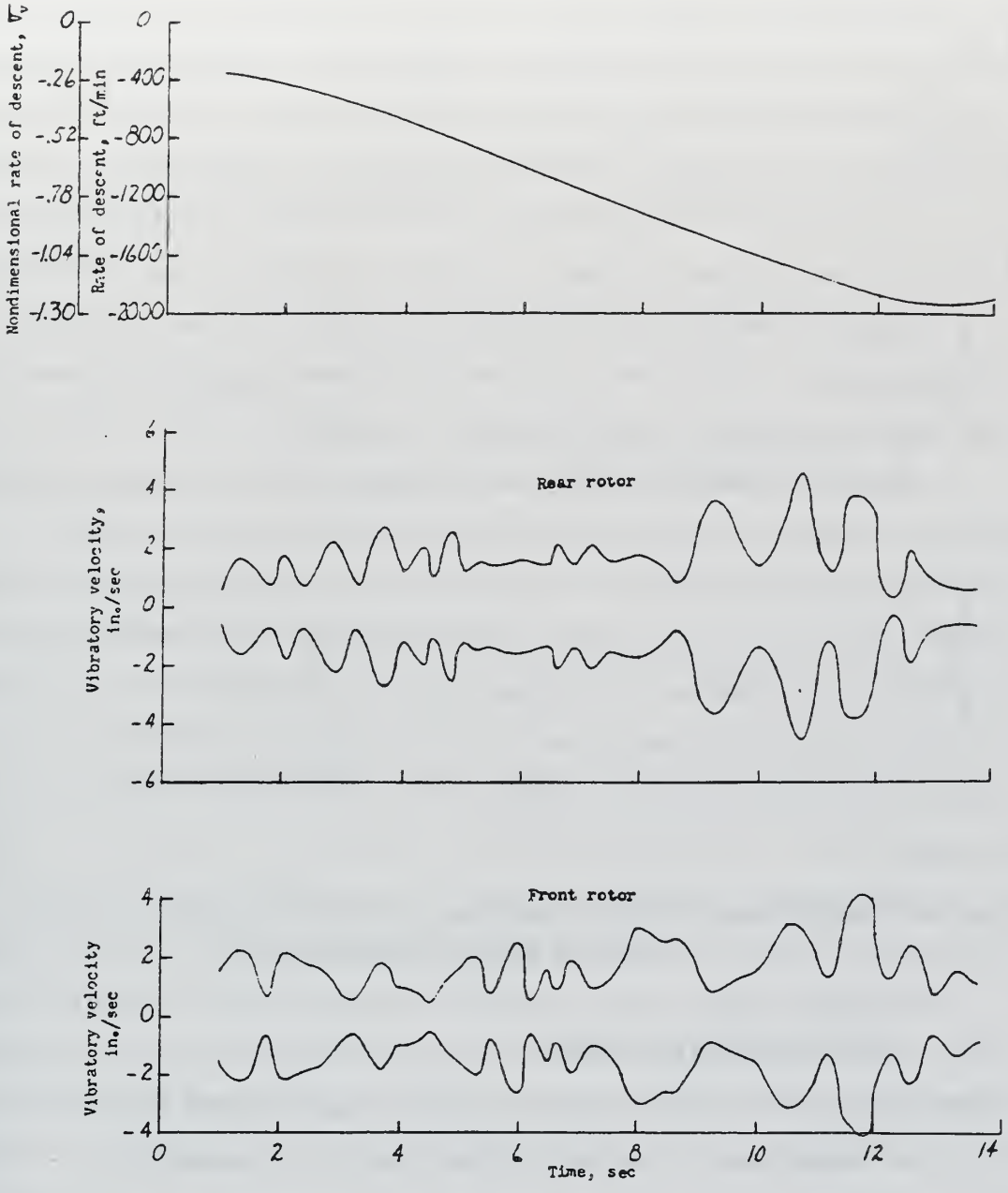

Figure 45. Time History Of Vibrations In Vortex-Ring State At Zero Forward Airspeed From Ref. [20]

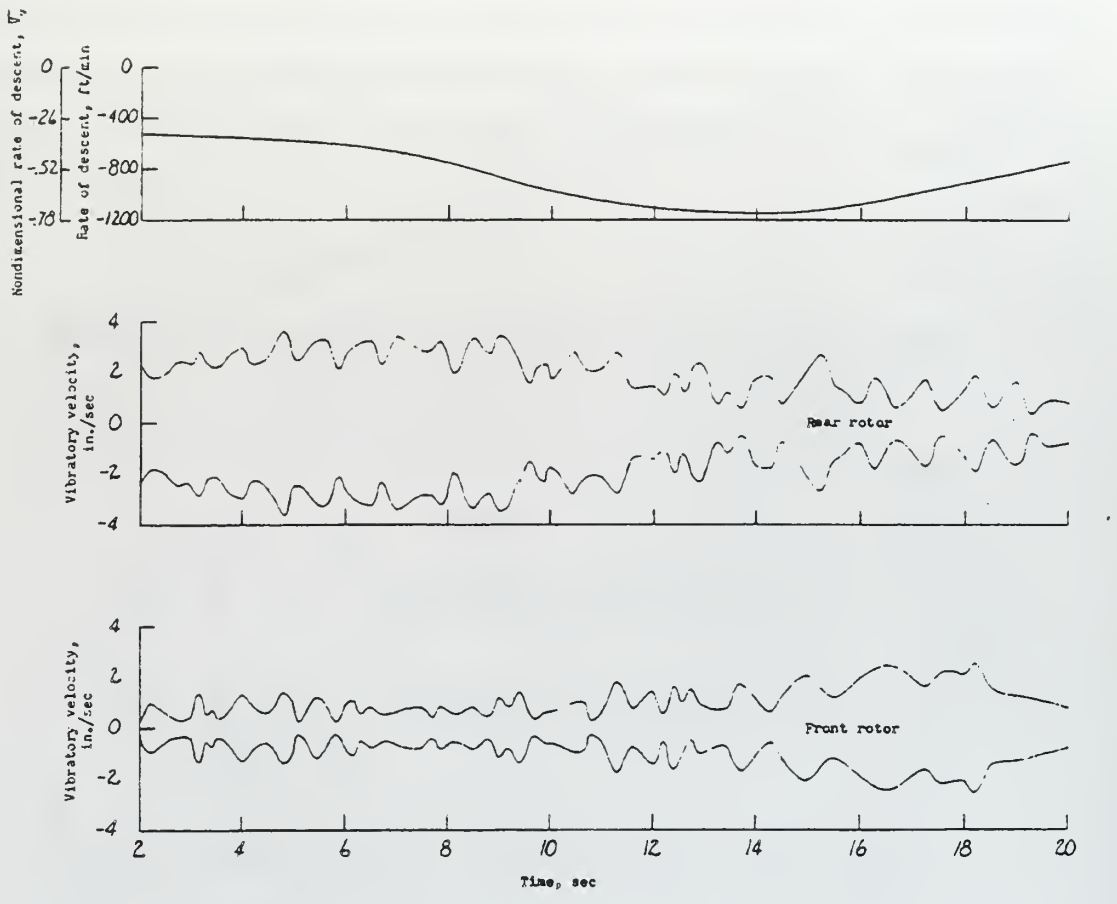

Figure 46. Time Histories Of Vortex-Ring State At A Forward Speed Of 10 Knots Forward Airspeed From Ref. [20]

2. H-34 Flight Test Data

The NASA TM X-952 provides a wealth of data for the partial power decent flight tests. This data includes section aerodynamic loading, harmonic analysis of blade root motions and aerodynamic loading, differential pressures, flapwise bending moments, and chordwise bending moments. Although relatively little vibration data is presented it is possible to examine many of these additional parameters to get a feel for the motion and loading of the blades at the partial power descent points where this data is provided. Given the thrust fluctuations, blade flapping and turbulent flow associated with vortex-ring state, one would

expect that the parameters listed above would support such unsteady and fluctuating behavior. This in turn could also serve to verify the probable existence of vortex-ring state beyond the pilot comments provided in Table 8. The NASA TM X-952 provides the time history of forward-speed dynamic pressure, pressure altitude, pitching and rolling angular velocities, and normal accelerations. Values for each of the parameters of aerodynamic loading, flap and chordwise bending moments, and differential pressures were averaged over three specific instances in the time history plots. Examples of the aerodynamic loading and flapwise bending moment data for flight 59 are shown in Tables 10 and 11.

Referring again to Table 8, flight 59 included a comment referring to the uncontrollability of the helicopter. It is safe to assume that this remark alludes to one of the strongest areas of vortex-ring state. In fact, looking at vortex-ring state boundary plots in combination with the H-34 partial power descent points, the point associated with flight 59 and its "out of control" remark lies almost directly in the middle of the vortex-ring state regions as well as the flow visualization area. (See Figures 40 through 42) Figure 46 shows the time history plot of flight 59 as presented in the NASA TM X-952. The time history plot of the normal acceleration reveals a maximum of about 1.2-g's. Other significant fluctuations can be observed in the pitch and roll axis as well as in the forward-speed dynamic pressure plot. It is already clear from a cursory glance at the time history plots that the helicopter displays some instability.

Table 10 shows tabulated flapwise, chordwise and torsional moment data averaged over three instances of time on the time history plots in Figure 46. $\psi_{Nominal}$ is the azimuth in degrees of the rotor blade without any lagging motion. This angle is measured in the direction of rotation from the downwind position. r/R represents the percent distance along the span of the rotor blade moving radially outwards. For flapwise bending

moments, a positive sign indicates compression in the upper surface of the blade; for chordwise bending moment, compression in the trailing edge of the blade; and for torsional moment, couple tending to rotate the blade leading edge upward. In order to illustrate the erratic behavior of vortex-ring state, a comparison of the flapwise bending moment data between smooth flight at 56 knots and flight in the assumed vortex-ring state was made. The vortex-ring state data came from flight 61 of the partial power descent data shown in Table 8. The flapwise bending moments of the two different flight regimes were plotted against the azimuth angles on the same graph. The results are shown in Figure 48. It is quite apparent that the vortex-ring state regime contains widely varying flapwise bending moments. Especially interesting are not only the changes in magnitudes of the flapwise moments in the vortex-ring state, but also the change in sign of the moments. This indicates a varying state of expansion and compression of the upper surface of the blade. Significant blade movement is a consequence of such rapidly changing compression and expansion.

Another parameter useful in examining the vibratory characteristic of the vortex-ring state, and the helicopter in general, is the harmonic analysis of the aerodynamic loading. The harmonics of the aerodynamic loads on the blade give rise to vibratory response of the blade [Ref. 21]. Since the blade is restrained at the root, the blade responses result in root shears, which feed from the rotorhead into the fuselage as vibratory shears and moments. During this transformation process the rotor system acts as a filter and allows frequencies of n/rev and 2n/rev to pass through. The n values are determined from the number of rotor blades the helicopter has (four for the H-34). The n/rev vibration is regarded as the most critical since the lower harmonics of the blade loading are considered to be much greater than the higher harmonics. From this conclusion it can be shown that the n/rev vibrations of the fuselage are a

result of the n-1, n and n+1/rev vibratory response of the blades in the rotating system. These result from n-1, n and n+1 per rev harmonics of the airloads acting on the blade. Therefore, primary contributors to the basic 4/rev vibrations of the H-34 are these airloads at 3P, 4P, and 5P harmonics of rotor speed, Ω. Two figures help to illustrate the importance of the aerodynamic blade loading and its harmonic analysis. First, a comparison was made between the section aerodynamic loading at r/R equal to 0.75 for the smooth flight of 56 knots and that of flight 61 from the partial power flight tests. As can be seen from Figure 49, the flight in the vortex-ring state (VRS) region contains more abrupt changes in airload as at various azimuth locations. These abrupt changes most likely result from blade-vortex interaction and include higher harmonic content. This higher harmonic content is a principal contributor to the vibrations experienced. [Ref. 21] Also, notice from Table 11 that lift is provided at ***all*** radial locations and at ***all*** $\psi_{nominal}$ angles. Even though this test flight seemingly represented one of the most hazardous vortex-ring state conditions, the rotor system is still generating lift everywhere. [Ref. 21]

The second figure shows the amplitude of the aerodynamic loading at the r/R = 0.75 position for harmonics of n= 3, 4, 5. As previously discussed, these harmonics are considered to be the primary source of fuselage vibration (at 4/rev). As can be seen from Figure 50, the aerodynamic loading due to the harmonics of the rotor system was much higher for the vortex-ring state case than the flight condition of 68 knots. This higher aerodynamic loading in the vortex-ring state directly contributes to the vibrations encountered in this regime.

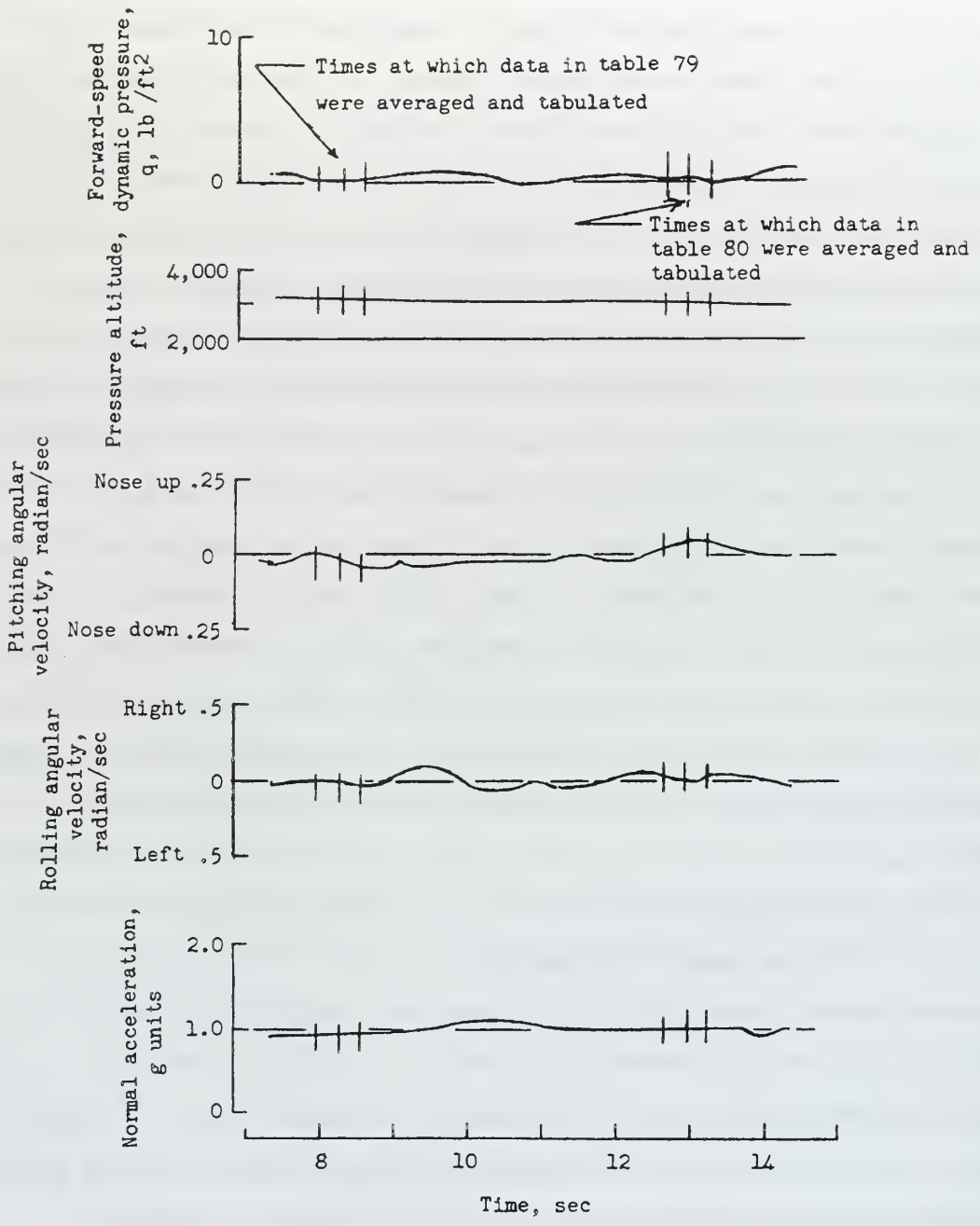

Figure 47. Time History Data For Flight 59, H-34 Partial Power Descent From Ref. [18]

(e) Flapwise bending moment

ψ_{nom}, deg	Flapwise bending moment, in-lb, at -							
	r/R = 0.150	r/R = 0.275	r/R = 0.375	r/R = 0.450	r/R = 0.575	r/R = 0.650	r/R = 0.800	r/R = 0.925
6	216	-899	-705	-2229	-4459	-7126	-6496	-3942
21	1584	-627	-2269	-4519	-5269	-6599	-5036	-3511
36	-730	-1832	-2423	-3956	-4054	-5534	-3797	-2650
51	-525	-1914	-2034	-2582	-2030	-3534	-3515	-2657
66	1049	388	136	-1151	-1661	-3465	-2563	-2672
81	1881	2071	1916	489	-473	-2430	-3619	-3745
96	1869	1667	1916	1443	1094	-1137	-2380	-3081
111	900	1394	1663	757	1366	774	-73	-2723
126	695	644	1483	1176	1745	784	-680	-3249
141	935	1378	2124	2025	1419	-211	-230	-2738
156	2371	1931	1980	1167	1419	903	-120	-2759
171	1299	1023	1907	1720	1340	207	1020	-1022
186	855	297	850	881	1463	-579	-2594	-3504
201	444	512	895	-26	-1274	-3365	-4189	-3730
216	1972	809	280	-1027	-1925	-4659	-6757	-4920
231	1049	330	127	-1142	-3025	-6002	-5837	-3847
246	1026	-83	-1049	-2792	-2910	-4321	-3865	-2745
261	137	-1378	-1365	-2201	-2497	-4251	-3504	-2540
276	-365	-800	-316	-1228	-2057	-4390	-4561	-3124
291	2246	883	45	-1447	-2180	-4131	-5042	-3854
306	1163	1097	1510	136	-1476	-3913	-4503	-3044
321	1641	611	479	-436	-130	-2132	-4383	-3789
336	843	446	624	-922	-1362	-2092	-2249	-2489
351	1892	-231	-723	-2029	-2330	-4868	-5026	-3292

(f) Chordwise bending moment

ψ_{nom}, deg	Chordwise bending moment, in-lb, at -			
	r/R = 0.150	r/R = 0.375	r/R = 0.575	r/R = 0.825
6	-1608	-33	7109	13139
21	-289	1188	8285	11831
36	-940	342	6165	13249
51	-2991	-423	5637	12389
66	-4750	-3810	4149	12435
81	-6964	-5161	2517	11666
96	-8836	-7066	2789	12554
111	-6475	-5763	1301	11364
126	-6785	-5600	3061	12526
141	-7387	-5193	2933	11666
156	-7078	-6431	1189	11035
171	-7061	-6756	1509	11529
186	-6475	-4363	3973	12654
201	-4033	-2149	5349	13039
216	-3392	-635	6133	13396
231	-3431	-1254	6533	13121
246	-1591	-537	5285	12417
261	-676	-895	5941	13286
276	-1119	-570	6021	12334
291	-1119	-1416	6117	13167
306	-794	-1172	6037	13057
321	-2682	-1172	7397	13661
336	-1217	-684	6357	13002
351	-1452	-309	7109	13524

(g) Blade torsional moment and pitch-horn load

ψ_{nom}, deg	Torsional moment, in-lb, at -		Pitch-horn load, lb
	r/R = 0.15	r/R = 0.50	
6	-723	-203	-58
21	-775	-199	-46
36	-520	-94	-30
51	-692	-201	-45
66	-806	-528	-43
81	-363	-206	11
96	-51	-29	47
111	-65	114	55
126	-184	-89	55
141	-300	-20	57
156	-113	-92	76
171	-261	-156	49
186	-457	-273	40
201	-249	66	48
216	-168	31	81
231	-65	148	72
246	-247	98	65
261	-274	89	33
276	-791	-199	-10
291	-622	-230	-19
306	-451	-160	-5
321	-336	-178	13
336	-457	119	-23
351	-768	-355	-50

Table 10. H-34 Flapwise Bending Moments For Flight 59 From Ref. [18]

(b) Section aerodynamic loading

ψ_{nom}, deg	Section aerodynamic loading, l, lb/in., at -						
	r/R = 0.25	r/R = 0.40	r/R = 0.55	r/R = 0.75	r/R = 0.85	r/R = 0.90	r/R = 0.95
6	5.35	9.08	11.48	12.35	13.71	12.80	11.67
21	5.33	9.27	11.33	12.05	13.55	12.99	14.18
36	4.40	9.06	10.65	11.89	12.88	12.60	14.45
51	4.83	8.83	9.67	11.35	13.16	11.40	10.62
66	4.00	8.54	10.10	11.87	14.36	14.64	13.98
81	3.53	8.12	10.89	13.37	17.02	17.13	17.00
96	3.44	7.50	9.95	13.69	18.45	19.59	21.19
111	3.47	6.95	9.62	16.08	21.72	24.41	23.45
126	2.88	5.55	7.89	15.31	21.09	26.04	26.40
141	2.62	5.54	6.92	14.07	20.11	27.12	26.21
156	3.02	5.80	7.26	11.21	15.55	20.32	19.95
171	3.27	5.95	7.46	11.28	13.82	14.53	14.47
186	3.27	5.70	6.89	11.85	15.98	15.51	15.71
201	3.17	6.15	8.41	14.05	20.07	19.37	18.86
216	3.66	7.54	10.13	16.88	20.15	19.41	17.55
231	4.33	9.18	12.27	16.05	18.19	17.19	17.39
246	4.76	9.40	11.81	15.18	16.02	15.19	13.86
261	4.59	7.43	10.55	14.25	15.56	14.13	13.06
276	4.55	7.62	10.22	12.12	15.31	13.53	13.16
291	3.57	7.73	10.12	14.02	15.47	14.62	13.29
306	4.24	7.93	11.27	14.92	17.48	16.11	14.19
321	4.10	8.63	11.44	14.05	16.34	15.14	12.73
336	4.83	9.31	12.19	14.82	16.96	15.21	13.29
351	4.37	8.81	11.77	13.84	16.12	14.09	11.57

Table 11. H-34 Arodynamic Loading Data For Flight 59 From Ref. [18]

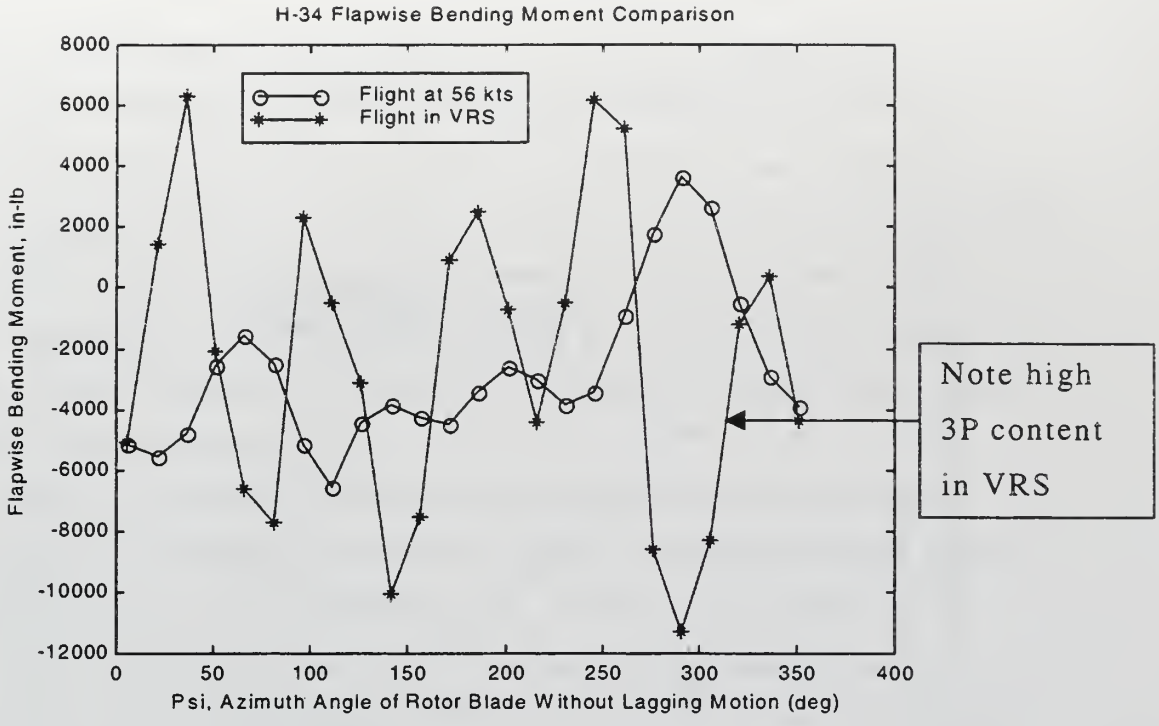

Figure 48. H-34 Flapwise Bending Moment Comparison

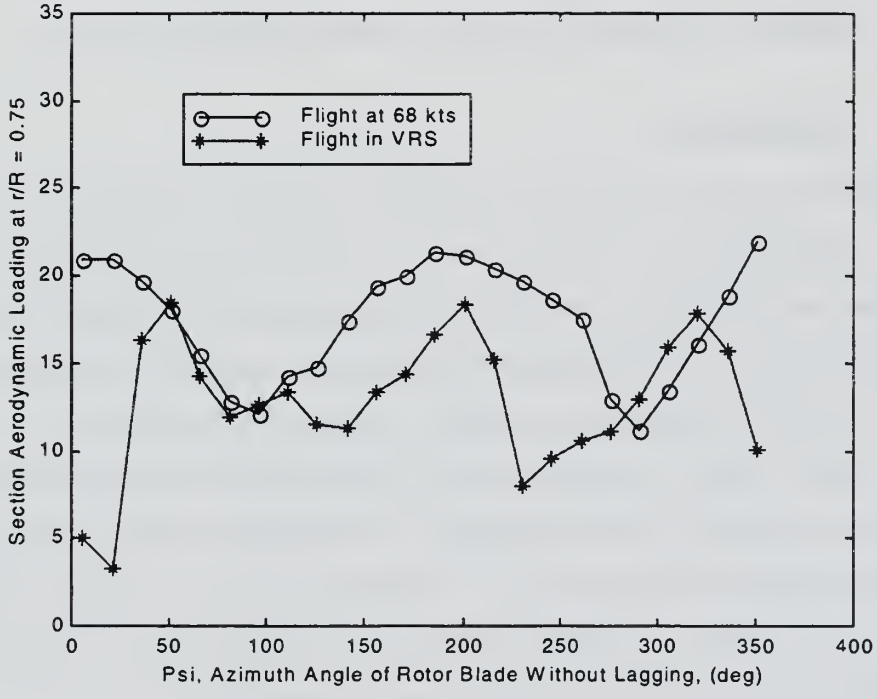

Figure 49. Aerodynamic Section Loading Vs. Azimuth Angle For Flight At 56 Kts And the Vortex-Ring State

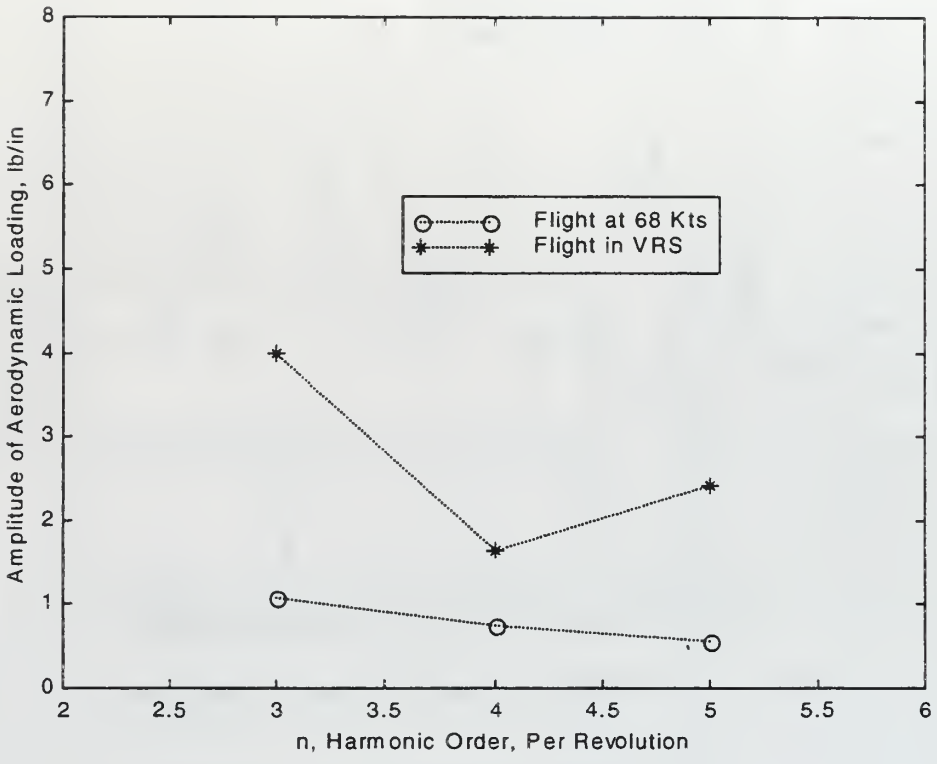

Figure 50. Aerdynamic Loading At Harmonics Of n = 3, 4, 5

3. Conclusion

Vibration can be an excellent indicator for the presence of vortex-ring state. Aerodynamic loading results in response of the blade. The resulting flap and chordwise bending moments produce vibratory shears at the blade root that are transmitted to the helicopter-fixed coordinate system as vibratory forces and moments, which in turn vibrate the helicopter. The volume of information contained in the NASA TM X-952 provides great insight to the helicopter's vibrational nature, rotor system lift, and blade stresses encountered in vortex-ring state. Vibration sensing equipment now in place with many Health and Usage Monitoring Systems (HUMS) could permit vibrations to be easily measured for use in a vortex-ring state warning system. Though the use of vibration data is promising in the aspect of developing a vortex-ring state warning system, there

remain some concerns. Some claim that the levels of vibrations experienced in vortex-ring state are not vastly different from those in translational lift, transition to landing, or turbulence associated with meteorological conditions. Second, the highest vibration levels associated with vortex-ring state are, again, likely to coincide with the maximum thrust fluctuations which occur towards the center of the vortex-ring state region. Use of vibrations to assess the occurrence of vortex-ring state, requires further investigation.

Time constraints of this research have not allowed complete investigation of helicopter vibrations for use as a complimentary method of vortex-ring state boundary prediction. There is a great deal of potential for use of vibration data in one form or another in the study of vortex-ring state. This is particularly true with the advent of helicopter HUMS systems that regularly monitor vibrations in all phases of flight, not just during maintenance related actions.

THIS PAGE INTENTIONALLY LEFT BLANK

V. IMPLEMENTATION

A. ALGORITHM DEVELOPMENT

The initial programming was completed in MATLAB in order to gain an appreciation for the structure and functionality desired. This was followed by the code's implementation utilizing C++. The program listings can be found in Appendix A. Finally, the warning system was implemented on the GADGHT system using a combination of National Instruments CVI and C. A discussion of the program implementation follows:

1. MATLAB Coding

The basic structure needed to determine vortex-ring state boundary penetration was relatively short. The most significant task was to represent the non-dimensional vortex-ring state boundary of Gao and Xin (see Figure 38) in a form that could be utilized in conditional tests. The data points for the Gao and Xin boundary were recorded in Microsoft Excel for use in plots already presented. A plot containing the boundary in non-dimensional form was used to formulate a polynomial equation that could be utilized in conditional testing. Several attempts to formulate an equation representative of the entire boundary fell short. It seemed that none of the curve fitting algorithms provided a satisfactory reproduction of the vortex-ring state boundary. In order to use the curve fitting algorithms contained within Excel it was necessary to break up the boundary into an upper and lower half. Gao's and Xin's boundary contained a minimum and maximum nondimensional vertical descent parameter (0.28 and 1.8) as well as a critical horizontal velocity parameter equal to 0.91. The upper half of the boundary contained all nondimensional rates of descent values from 0.28 to the value

corresponding to the maximum horizontal velocity component of 0.91. In a similar manner, the lower boundary was defined from a nondimensional rate of descent value of 1.8 to the value corresponding to the maximum horizontal velocity component of 0.91. A sixth order polynomial fit was selected to represent the upper and lower halves of the boundary. The equations produced by the Excel curve-fitting algorithm are shown below:

Upper boundary equation:

$Y = -40.66x^6 + 102.46x^5 - 96.842x^4 + 40.387x^3 - 7.0525x^2 + 0.1779x - 0.2864$

The mean square error, R^2=0.9979.

Lower boundary equation:

$Y = 62.743x^6 - 148.98x^5 + 130.5x^4 - 51.395x^3 + 10.099x^2 - 1.2784x - 1.795$

The mean square error, $R^2 = 0.9971$.

Y is the nondimensional rate of descent, and x is the nondimensional horizontal velocity.

Excel calculates the R^2 value as follows:

$$R^2 = 1 - \frac{SSE}{SST}, \text{ where}$$

$$SSE = \sum \left(Y_j - \hat{Y}_j\right)^2$$

$$SST = \left(\sum Y_j^2\right) - \frac{\left(\sum Y_j\right)^2}{n}$$

Once the boundary was defined, the input parameters and conditional calculations were constructed. The MATLAB code required user input for the following data: Air density in slugs/ft^3, rotor radius in ft, weight of the helicopter including fuel and crew in pounds, airspeed in knots, and rate of descent in fpm.

Following the input of the requested data, the first function of the program was to calculate the hover-induced velocity using the weight, rotor radius, and air density. Once this was completed the airspeed and rate of descent data provided by the program user could be nondimensionalized. This was completed by dividing the rate of descent

and airspeed by the hover induced velocity. Because the polynomial fit was accomplished using the nondimensional boundary points, it was essential that the aircraft data be converted into the same form.

The second half of the program involved conditional testing for boundary penetration. Since the boundary provided by Gao and Xin was not based on maximum thrust fluctuations there was no need to add a further cushion or "proximity warning" to the boundary. The first conditional test checked to see if the maximum horizontal velocity, or airspeed, was exceeded. If it was, a message was displayed that read, "NO VORTEX-RING STATE," and the program stopped. If the horizontal velocity was not exceeded, another test checked to see if the nondimensional y value was above or below the upper boundary. This was done by calculating the upper boundary y value, *yup*, for the nondimensionalized airspeed and then comparing this against the nondimensional value, y, computed from the user input. If y was greater than *yup*, then the point was above the upper boundary and a message was displayed, "NO VORTEX-RING STATE." If the y value was less than or equal to *yup*, then the point could be either above or below the lower boundary. The lower boundary value, *ylo*, was calculated in a similar manner as *yup*, substituting in the nondimensional airspeed for x in the equation. If the y value was located between the upper and lower boundaries a warning message was provided, "***VORTEX-RING STATE***." If the point was located below the lower boundary, then the,"NO VORTEX-RING STATE" message was displayed.

The C++ code developed duplicated the MATLAB code's functionality.

B. IMPLEMENTATION ON THE GADGHT UNIT

Once the algorithm had been coded and tested, the next step was implementing the warning system as a Microsoft Windows application on

the GADGHT unit. In order to test the system a second computer and Windows program was designed to represent the data that the aircraft's ARINC 429 busses would provide. This user interface as well as the Windows user interface for the vortex-ring state monitor application were developed with the time and assistance of the VH Systems Engineering Integrated Product Team.

The first step in the process of developing the windows based application for the vortex-ring state warning system was to define the data that would be obtained through the avionics architecture of the CH-60, in this case. The table below describes the data obtained through the ARINC-429 busses.

Data	Source	Limit/Range	Units	Accuracy
CH-60 Fuel Quantity – Internal Aux	AOP	0-797	Pounds	N/A
Fuel Quantity – No 1 Main	AOP	0-1226	Pounds	N/A
Fuel Quantity – No 2 Main	AOP	0-1226	Pounds	N/A
Fuel Quantity – ESSS Aux LH Inboard	AOP	0-1567	Pounds	N/A
Fuel Quantity – ESSS Aux LH Outboard	AOP	0-1567	Pounds	N/A
Fuel	AOP	0-1567	Pounds	N/A

Quantity – ESSS Aux RH Inboard				
Fuel Quantity – ESSS RH Outboard	AOP	0-1567	Pounds	N/A
Fuel Quantity – Roberston Aux Fore	AOP	0-1226	Pounds	N/A
Data	Source	Limit/Range	Units	Accuracy
Fuel Quantity – Roberston Aux Aft	AOP	0-1226	Pounds	N/A
Computed Airspeed	ADC	0-220	Knots	±7 from 15-30; ±5 at 50; ±3 at 80; ±2 from 100-220
Altitude Rate	ADC	±5000	Ft/min	± 32 or 5 % of vertical speed, whichever is greater
Static Air Temperature	ADC	-60 to 90	Degrees Celsius	± 1
Static Pressure	ADC	11.10-33.31	Inches of Hg	± 0.03

Table 12. Application Input Data

The next step was to develop the user interface to represent the aircraft. Screen captures of the software may be found in Appendix B. The aircraft simulator user interface allowed the user to specify fuel weights, static air temperature, static pressure, altitude rate, and airspeed. The units for these user inputs were consistent with data that would be taken from an actual CH-60 ARINC 429. Below the input area was a receive or display area that reflected the changes that the user made taken from the appropriate receive channel of the ARINC-429 card. This was instrumental in showing that the data supplied by the user was converted to correct ARINC 429 format and pulled off the ARINC-429 receive channel just as would be done in an actual aircraft implementation. A lunchbox computer housed the ARINC 429 card as well as the Windows-based simulation software.

The third major step was to develop the user interface for the vortex-ring state monitor itself. This is the program that runs on the GADGHT system. This program was developed to allow the user to select a helicopter type and enter a base weight. The helicopter type would set the rotor radius, used to calculate the hover induced velocity, and the information necessary to pull required data from whatever configuration (MIL-STD 1553 or ARINC-429) exists. The base weight would be the helicopter's weight including crew and equipment, but without fuel weight. The ARINC-429 provides the fuel weight for each tank used in the CH-60. The program currently defaults to a CH-60 and a base weight of 18,000 pounds. If a base weight other than 18,000 pounds is desired the user simply has to click on the base weight display window to bring up a numeric keypad in order to make a different entry. Clear and entry keys are also available on the keypad. Once 'ENT" has been selected the keypad will close and the entered weight will be displayed. Once this has been accomplished the user may select 'RUN' for the application to begin. A graph will be displayed on the same window as the entry information.

A boundary based on the current conditions entered on the aircraft simulator interface located on the lunchbox computer will be drawn. The helicopter's position in terms of airspeed and rate of descent will be shown on the graph with a helicopter icon. Any value outside of the range of the graph will be defaulted to the maximum value appearing on the graph. Thus, there is no confusion from what direction the helicopter is approaching the vortex-ring state boundary. Penetration of the vortex-ring state boundary will result in flashing background color of the graph. Simultaneously, an aural warning recorded on a wave file will be played on speakers for the demo, or sent into the ICS system on an aircraft. The program will not allow minimization of the main window while a penetration of the vortex-ring state boundary exists. Should the weight of the helicopter need to be updated, i.e., additional passengers, a 'STOP' button may be depressed in order to allow the base weight to be changed. The program may minimized while not in a warning by selecting the 'HIDE' button or closed completely by depressing the 'QUIT' button.

It is interesting to note the effect of pressure temperature and weight visually on the boundary. Such effects were previously discussed in this thesis. Screen captures of the simulation and application interface may be found in Appendix B. A block diagram of the setup may be found in Figure 51.

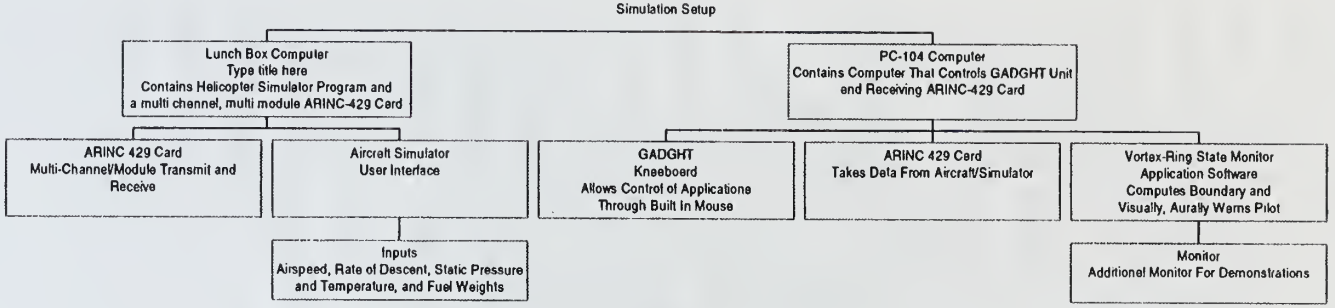

Figure 51. System Block Diagram

C. IMPLEMENTATION CONSIDERATIONS

1. Ease of Integration into Helicopter Avionics System

As was previously discussed, the use of the GADGHT unit in the implementation of the vortex-ring state warning system has permitted tremendous flexibility, and has significantly decreased development time. The GADGHT unit, as a stand-alone Windows based PC-104 computer, simply requires an interface capable of reading data from desired busses within the avionics architecture. The PC-104 computer and its associated memory contain and execute the application program used for this warning system as well as other pilot aid programs. Applications running within the GADGHT unit do not require on board computing power or modifications to an Operational Flight Programming (OFP). This is a considerable advantage as changes to an OFP can take as long as several years to complete. The use of such stand-alone computer systems provides increased functionality and is an inexpensive and rapid way of implementing needed pilot aids and safety devices.

2. Low Airspeed Sensing

Low airspeed measurement remains as one of the major obstacles in successful implementation of a vortex-ring state warning system. It has been a problem that has plagued the helicopter community for many decades particularly since many of the missions best suited for helicopters require operation in low airspeed environments. These missions include Search and Rescue (SAR), Vertical Replenishment (VERTREP), Ant-Submarine Warfare (ASW), and mine detection. [Ref. 22]
The pitot-static device used to sense airspeed in the helicopter is regarded as inaccurate in low airspeeds, due to the interference from the rotor wash. The flow field in the immediate vicinity of the airframe is disturbed by the main rotor downwash to the extent that there is no

location aside from above the rotor head that provides a "clean" location suitable for low airspeed measurement [Ref. 22]. Attempts have been made to improve the quality of low airspeed indications since the 1950s, but complexity, cost, reliability and aerodynamic drag factors have prevented their widespread use. A paper presented by Kelly McCool and Dr. David Haas suggests the use of a neural network based approach to helicopter low airspeed estimation. In their study, aircraft state parameters measured in the fuselage are used as inputs into a backpropagation network in order to predict the airspeed. These parameters are also fed into a learning vector quantization network to categorize sideslip angle into the four quadrants of helicopter motion; rearward, forward, as well as left and right sideward flight. The parameters are normally available on most platforms and do not require special instrumentation. These two networks were developed based on HH-60J and CH-46E flight test data. McCool and Haas were able to achieve low airspeed accuracy with the HH-60J of ± 5 knots in ground effect. Similarly for the CH-46E, airspeed accuracies were ± 5 knots for in ground effect flights while accuracies for out of ground effect flight were ± 8 knots. Sideslip angle was predicted correctly 92 percent of the time for the HH-60J in all quadrants above 15 knots. An average of 93.5 percent accuracy was obtained for the CH-46E above 15 knots in all quadrants.

It is vitally important that efforts such as those of McCool and Haas continue. Given the low airspeeds involved in defining the vortex-ring state boundaries it is crucial that the airspeed values used in determining vortex-ring state boundary penetration are as accurate as possible. A high a degree of confidence in the vortex-ring state warning system necessarily involves a high degree of confidence in the airspeed information it utilizes.

3. False Alarm Rates and Missed Warning Concerns

The vortex-ring state warning system must be capable of providing sufficient warning to enable corrective action to be taken in an ample amount of time. Equally important is that the helicopter crew is not warned about a vortex-ring state condition if one does not truly exist. This issue is not only a function of correctly working hardware and software, but one of the basic underlying theory as well. This system was implemented using the Gao/Xin boundary as it offered the best practical solution to the boundary dilemma. A more detailed analysis of their research was completed in a previous section. Hardware, software and the basic underlying theory are all possible sources of errors. This potential error leads to the requirement that flight-testing in order to verify the operational reliability of this system. Assuming the boundary, airspeed and rate of descent information is correct, the system must provide a warning based on the conditional testing performed in the software application. Beyond this verification of correctly functioning software and hardware, a more in-depth analysis of the theory must be completed in order to alter the boundary to better reflect actual vortex-ring state experiences.

4. Validation and Flight Testing

Concerns over operational reliability, particularly in the system's ability to detect a vortex-ring state boundary penetration as well as possible false alarms necessitate that the system meet some predetermined validation requirements. Satisfactory completion of these requirements would enable the vortex-warning system to be treated as a safety device instead of merely a pilot aid.

Currently, the application software has no error detection, data averaging, self-test features, or any filtering capability. The addition of these capabilities would create a much more robust detection system

permitting more reliable results. This, along with flight-testing would serve to validate the theory and software minimizing false alarms or missed warnings.

Actual flight testing for validation would involve flying the aircraft inside, outside and close to the boundary at several locations. Observation of the aircraft's performance and behavior to flight inside and close to the boundary would also be critical to expanding knowledge on the accuracy of the boundary. Because of the inherent risks involved with flying in vortex-ring state flight tests must be carried out with more than sufficient altitude for recovery. Additionally, explicit procedures for escaping vortex-ring state must be clear and concise to the pilots flying the aircraft in this regime. These flight tests could also be performed in varying wind conditions and azimuths, to check for possible effects this may have on the reliability of the warning system.

It has been the intention and ultimate goal of this research to develop this system in such a manner that it could be used in a similar fashion as a fixed wing stall warning, i.e., a safety device. It is recognized that validation of a vortex-ring state warning system will not be an easily achieved task. Nevertheless, it is the next step that this particular research will pursue.

VI. CONCLUSIONS AND RECOMMENDATIONS FOR FURTHER STUDY

Vortex-ring state has long been a difficult problem for helicopter aerodynamicists to analyze. The breakdown of a continuous slipstream has led to the inability of momentum theory to accurately predict helicopter behavior in the vortex-ring state. Three theories were examined for use in implementing a vortex-ring state warning system. The two theories of Wolkovitch and Peters/Chen proved to be impractical for use in the warning system due to the way their boundaries were defined. The third theory of Gao and Xin used a semi-empirical approach in combination with momentum theory to better define boundaries that could be used by helicopter pilots so they could understand when their aircraft might encounter vortex-ring state. Due to its practicality and supportive experimental results, it was decided that the theory of Gao and Xin would be well suited for this research.

Safety statistics were researched turning up a total of 33 mishaps/accidents attributed to vortex-ring state, including vortex-ring state of the tail rotor. While this number does not appear to be astronomical, several issues were raised in the safety research that would lead one to believe that this was not indicative of the actual problem. First, many of the databases have not been completely digitized. This forced searches using previously established keywords that did not include vortex-ring state. Only a search for some of the symptoms and synonyms of vortex-ring state revealed desired data. The only other method to thoroughly locate vortex-ring state data was to read every helicopter mishap, which was not accomplished. Additionally, the information obtained from the armed services as well as the NTSB was data that resulted in actual accidents or mishaps specifically attributed to

vortex-ring state. There were many other accidents that "appeared" to be the result of vortex-ring state, but were not explicitly stated as such. Also, how many times have pilots encountered this phenomenon and not had any accidents? Based on informal discussion with pilots, flight into vortex-ring state has happened more frequently than one might imagine. While speaking to a particular helicopter manufacturer, one of their engineers stated that he didn't believe and was fairly confident that their helicopter had not been flown into vortex-ring state. Yet, after informal discussions with some pilots that fly this aircraft, they claim to have experienced it and proceeded to describe characteristics that are often associated with vortex-ring state. A widespread misunderstanding and mysticism associated with this phenomenon most likely kept many pilots and commanding officers from sending out any hazard reports to document a vortex-ring state encounter. Surely, such a report would generate debate over the claim of encountering vortex-ring state because, again, it is poorly understood. Perceptions of what it is, how it behaves, how one gets into it, and under what conditions are extremely varied across the helicopter world. Another misconception is that a helicopter can be "designed" completely out of vortex-ring state. This is simply not true. Finally, the increasingly demanding missions of the modern helicopter actually puts it into profiles of flight that may be more susceptible to a vortex-ring state encounter. As a result it is believed that the magnitude of the problem is not well represented by the statistics presented earlier in this thesis.

A vortex-ring state warning system was developed and implemented using a Windows-based moving map PC-104 computer. Airspeed, rate of descent, pressure altitude, outside air temperature, and fuel quantity were read from the helicopter's avionics system (Two ARINC 429 busses) and fed into the vortex-ring state application software. Utilizing these parameters as well as the base weight and rotor radius the application

software determined if the helicopter was inside the vortex-ring state boundary. The application software was developed using C++ as well as National Instruments CVI and was modeled after a MATLAB program written by the author. If a boundary penetration is detected an aural and visual warning are supplied to the pilot through the Inter-Com system (ICS) and the moving map kneeboard display respectively. Features such as error detection, data averaging, self-tests, and filtering could improve the robustness of the code.

This thesis has only exposed the tremendous opportunity in the study of vortex-ring state. Very little work has been done in the area of vortex-ring state in recent years. Most studies were done many decades ago. The three theories studied in this thesis were published in 1972, 1982, and 1994. There still remains a great deal to be done in the development of theory used to predict the vortex-ring state boundary. A recommendation in this area could include the development of a three-dimensional boundary to represent this phenomenon. It would be reasonable to expect that a sufficiently large sideways or rearward velocity should allow one to escape the clutches of vortex-ring state as well as the critical horizontal (forward) velocity previously discussed. As mentioned by Benjamin Moore's article in *Rotor & Wing* [Ref. 2], forward application of cyclic control may not be possible depending on the environment one is operating in. Another recommendation is to determine the occurrence of vortex-ring state on an individual helicopter basis using the same precepts as laid out by Gao and Xin. In other words, given that the rotor torque on the helicopter rotor can be measured, one could test to see when the torque required increases with increasing descent rate. This was the vertical velocity point at which Gao and Xin defined their vortex-ring state boundary to begin. Additional recommendations include a more thorough study of vibration information as a confirmation or prediction of vortex-ring state, increased software development to allow visual

representations of the boundaries at "desired" operating conditions to serve as a planning aid, additional research into warning pilots on tail rotor vortex-ring state now that sideslip velocities are becoming available, increased study into low airspeed measurement devices, and further support of this research through actual flight testing and validation.

With the advance of avionics technology and improved aerodynamic researching tools, there is no longer any reason for ignorance or surprise when it comes to vortex-ring state. The time has come to end the misunderstandings that abound concerning vortex-ring state and to prevent mishaps, accidents or unintended flight into the worst of this phenomenon.

APPENDIX A. WARNING SYSTEM PROGRAMMING CODE

A. MATLAB PROGRAMMING CODE

```
clear screen
clear all
close all
rho=input('Air Density in slugs/ft3  ')
R=input('Rotor Radius in ft  ')
T=input ('Helicopter Weight in lbs  ')
vh=(T/(2*pi*rho*(R^2)))^0.5
xreal=input('Actual Airspeed in knots  ')
yreal=input('Actual Rate Of Descent in fpm  ')
x=xreal/vh/0.5925;
y=yreal/vh/60;

%    Test To See If Airspeed Lies Beyond Critical Horizontal Value
%    If it does, then print message
if x>0.91
  ['NO VORTEX RING STATE']
  break
end
yup=-40.66*x^6+102.46*x^5-96.842*x^4+40.387*x^3-
7.0525*x^2+0.1779*x-0.2864
ylo=62.743*x^6-148.98*x^5+130.5*x^4-51.395*x^3+10.099*x^2-
1.2784*x-1.795
if y>yup
  ['NO VORTEX RING STATE']

  break
```

```
end
if y<=yup
  if y>=ylo
    ['***VORTEX RING STATE****']

    break
  end
  ['NO VORTEX RING STATE']

end
```

B. C++ PROGRAMMING CODE

```
/***Vortex-Ring State Boundary Detection Source Code***/

//LCDR David J. Varnes
//Naval Post Graduate School, Monterey
//August, 1999

#include <iostream.h>
#include <stdio.h>
#include <math.h>

main()
{

//Variable Definition
// computed airspeed (knots), altitude rate (fpm), static presure (inches
HG), fuel Robertson fore (pounds)
```

```
// Fuel NO 1 main (pounds), fuel NO 2 main (pounds), rotor radius (ft),
base weight (pounds)

double compairspeedKT, altrateFPM, statpressHG, oatC, f_1mainLB,
f_2mainLB, f_robforeLB, base_weight, rot_radius;
double totalfuel, totalhelo, tempf, nondim_airspeed, nondim_altrate, vh,
density, yup, ylo;
float pi = 3.1415927f;

/** DATA ENTRY **/

/* Read initial Rotor Radius */

cout << endl
       << "Please Enter the rotor radius in feet:"
       << endl
       << "(To end program, enter 0 for the rotor radius)";

cin >> rot_radius;

if(rot_radius<0) {
      cout << endl
             << "Error - Please enter rotor radius again:";
      cin >> rot_radius;
}
/* Main data entry and calculation loop */

while (rot_radius>0) {

cout << endl
```

```
        << "Enter the base weight of the helicopter, with crew and
equipment, NO fuel, in pounds:";

cin >> base_weight;
cout <<  endl
    << "Enter Fuel Weight of helicopter in pounds:";

cin >> totalfuel;
cout <<  endl
    << "Enter OAT in degrees C:";

cin >> oatC;
cout <<  endl
    << "Enter Static Pressure in inches of HG:";

cin >> statpressHG;


cout << endl
    << "Enter Helicopter's Airspeed in knots:";

cin >> compairspeedKT;

cout << endl
    << "Enter rate of descent in fpm:";

cin >> altrateFPM;
```

```
//Calculation of Total Fuel Weight and total helicopter weight

//totalfuel=f_1mainLB + f_2mainLB + f_robforeLB;
totalhelo=totalfuel + base_weight;

//Calculation of Air Density from p=rhoRT in slugs/cubic-ft
//To Convert Inches of HG to lb/inches^2 multiply by 70.7262
//To Convert degrees C to degrees R convert to F and add 459/67

tempf=32.00000000+(1.8000000*oatC);
density=
(statpressHG*70.7262000)/(1716.0000000*(459.6700000+tempf));

//Calculation of Hover-Induced Velocity in fps

vh=sqrt(totalhelo/(2.0000000*pi*density*pow(rot_radius,2)));

//Calculation of Nondimensional airspeed and Nondimensional rate of
descent

nondim_airspeed=compairspeedKT/vh/0.5925000;
nondim_altrate=-altrateFPM/vh/60.0000000;

//Sixth Order Polynomial Approximations Upper and Lower Boundaries

yup=pow(nondim_airspeed,6)*(-
40.66)+pow(nondim_airspeed,5)*102.46+pow(nondim_airspeed,4)*(-
96.842)+pow(nondim_airspeed,3)*40.387+pow(nondim_airspeed,2)*(-
7.0525)+0.1779*nondim_airspeed-0.2864;
```

```
ylo=pow(nondim_airspeed,6)*62.743+pow(nondim_airspeed,5)*(-
148.98)+pow(nondim_airspeed,4)*130.5+pow(nondim_airspeed,3)*(-
51.395)+pow(nondim_airspeed,2)*10.099-1.2784*nondim_airspeed-1.795;

//Conditional Boundary tests

if(nondim_airspeed<=0.91)
{
      if((nondim_altrate<=yup)&&(nondim_altrate>=ylo))
      {
            cout << endl
               << "***VORTEX-RING STATE***" << endl;
      }

}
cout << endl
   << "vh";
cout << vh
   << endl;

cout << endl
   << "Nondimensional rate of descent value:";
cout << nondim_altrate
   << endl;

cout << endl
   << "Nondimensional airspeed value:";
cout << nondim_airspeed
   << endl;
```

```
cout << endl
    << "Upper Boundary polynomial rate of descent value";
cout << yup
    << endl;

cout << endl
    << "Lower Boundary polynomial rate of descent value";
cout << ylo
    << endl;

cout << endl
    << "Calculated Density in slugs/cubic-ft";
cout << density
    << endl;

cout << endl
    << endl;
cout << "Thank you for trying the Vortex-Ring State Program!";

cout << endl
    << "Please Enter rotor radius:";
cin  >> rot_radius;
if(rot_radius<0)   {
       cout << endl
              << "Error - Please enter rotor radius again: ";
       cin  >> rot_radius;
}
}
}
```

THIS PAGE INTETNIONALLY LEFT BLANK

APPENDIX B. SOFTWARE SCREEN CAPTURES

A. AIRCRAFT AVIONICS SYSTEM

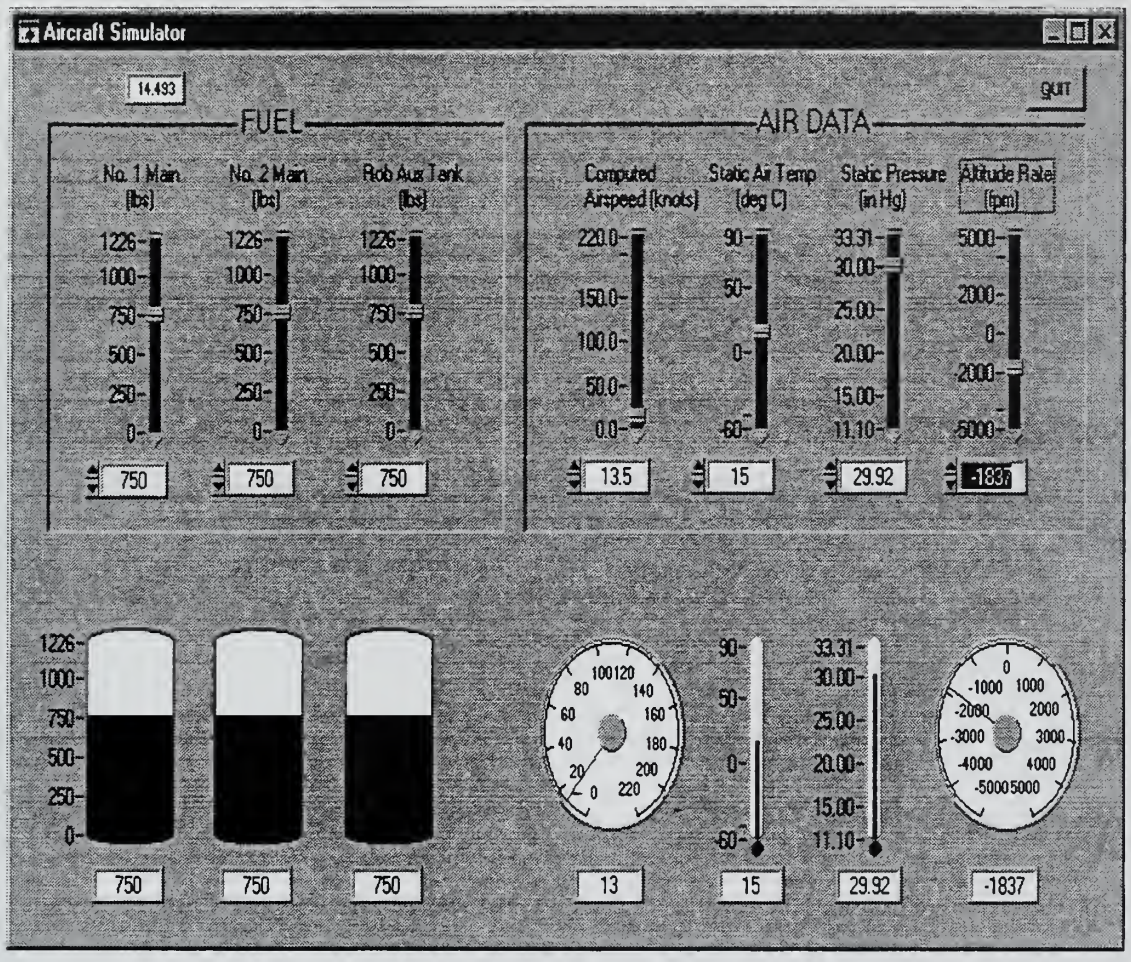

B. VORTEX-RING STATE MONITOR START UP WINDOW

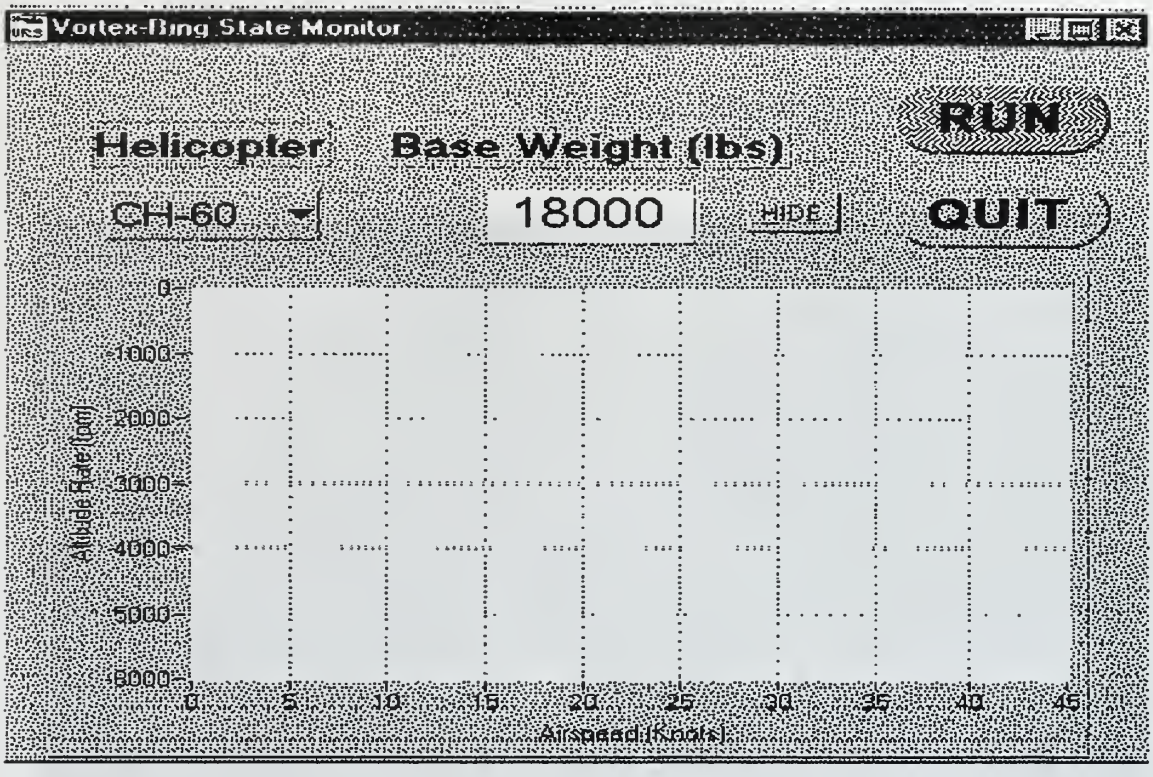

C. VORTEX-RING STATE MONITOR WARNING

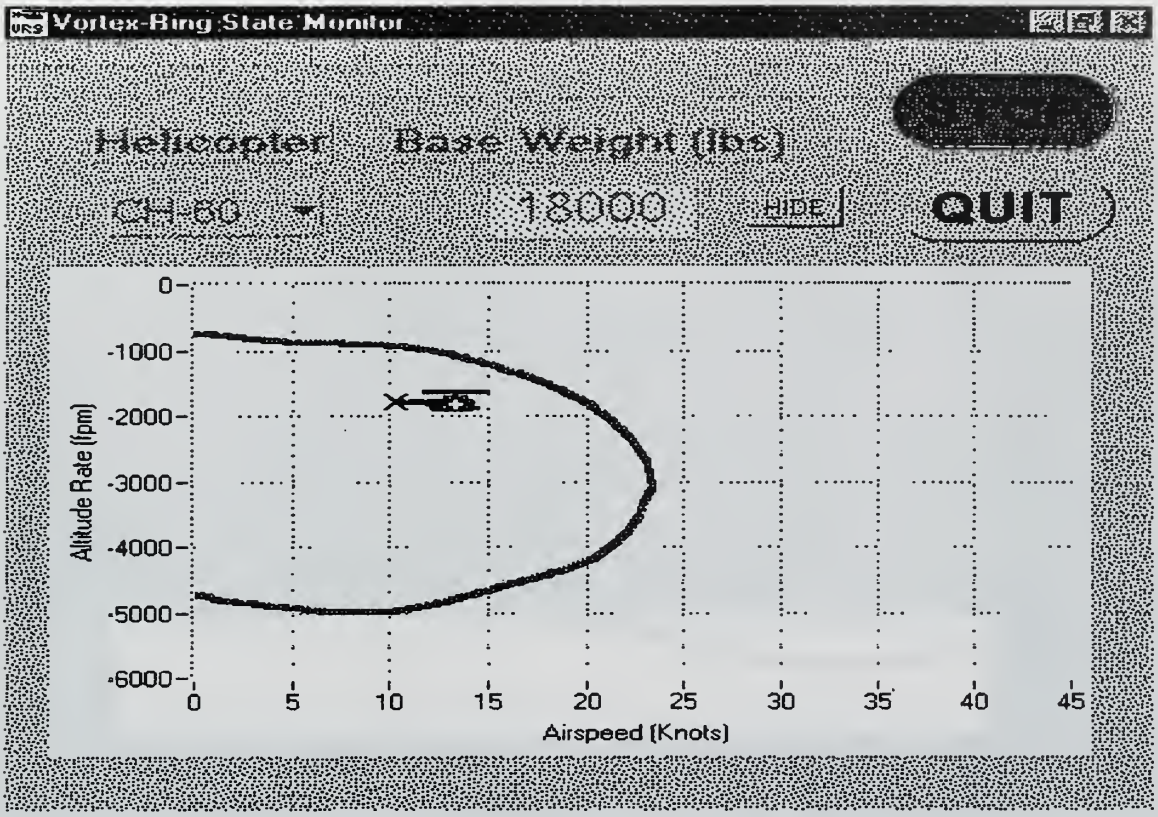

D. VORTEX-RING STATE MONITOR WARNING BACKGROUND FLASHING

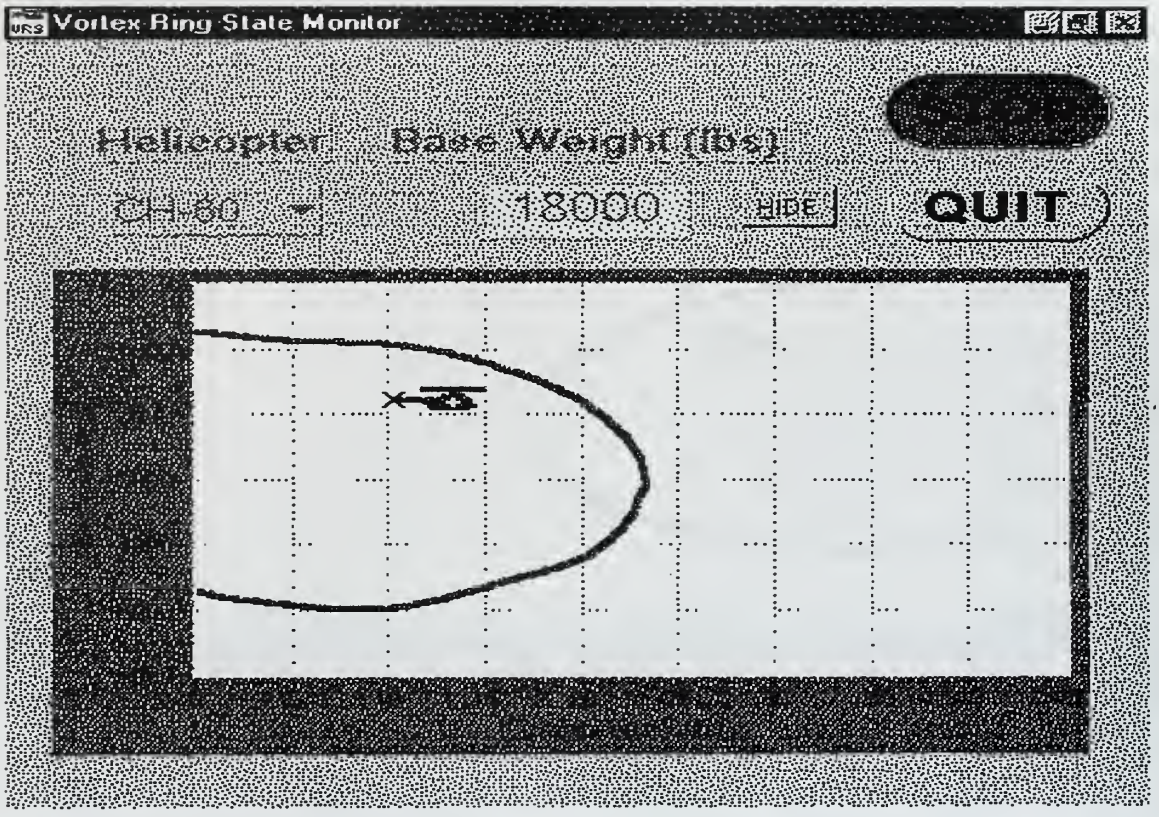

E. SIMULATION SETUP

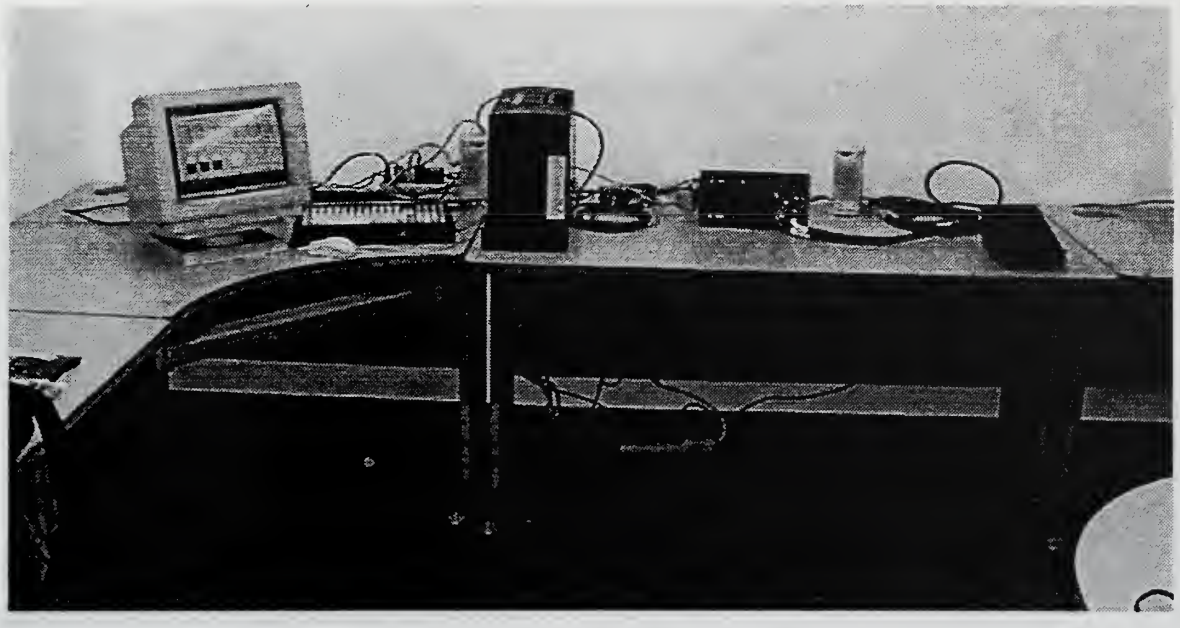

F. PC-104

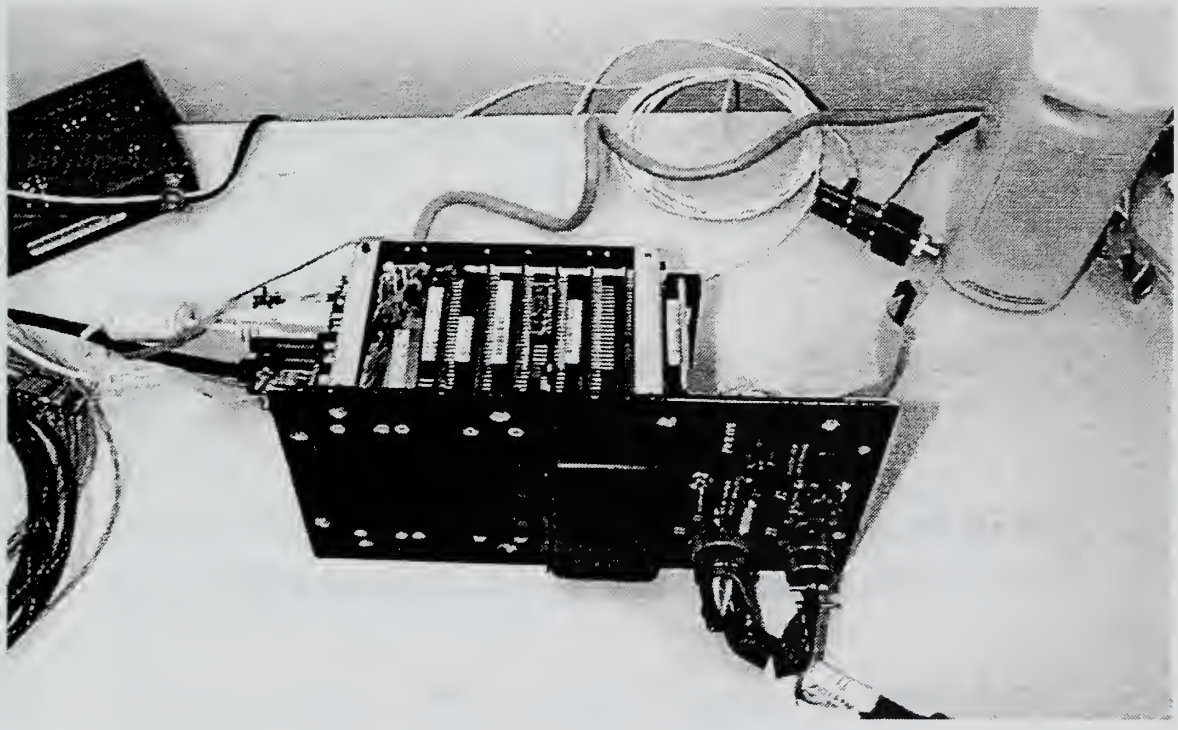

G. KNEEBOARD

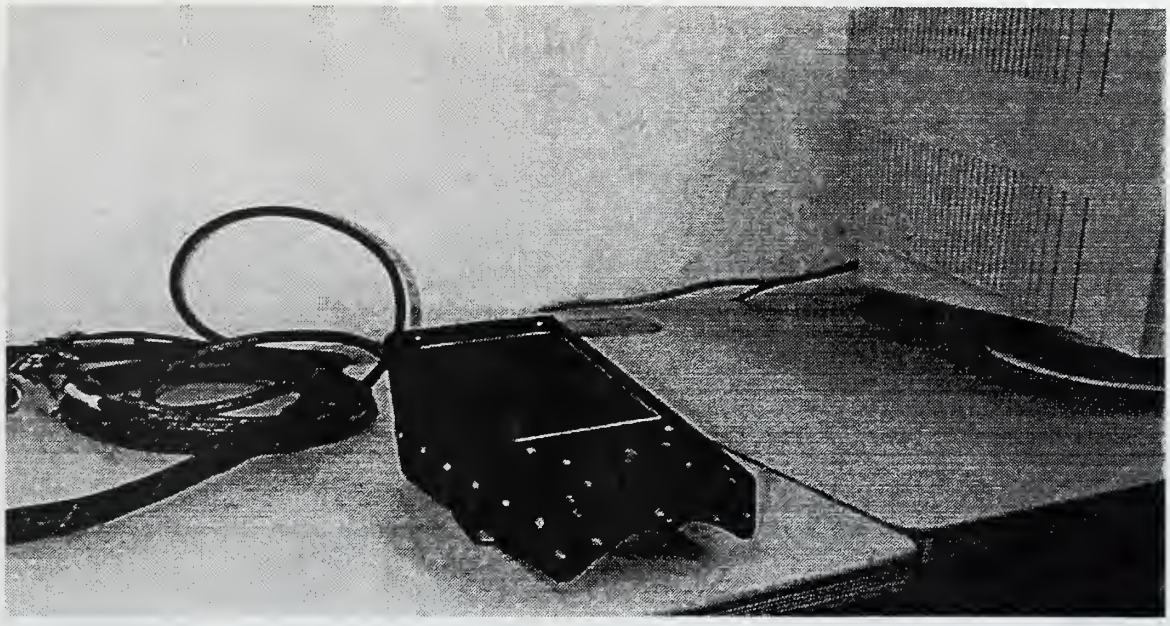

LIST OF REFERENCES

1. Headquarters Department of the Army, "Fundamentals of Flight," Field Manual (FM) NO. 1-203, US Army Adjutant General Publications Center, September 9, 1983.

2. Moore, B. H., "Dead Air", Rotor & Wing, Volume 33, Number 5, May 1999.

3. Chief of Naval Operations, "NATOPS Flight Manual, Navy Model HH-60H Aircraft," Department of the Navy, January 15, 1991.

4. Hurt, H. H., Jr., "Aerodynamics for Naval Aviators," NAVWEPS 00-80T-80, The Office of the Chief of Naval Operations, 1960.

5. Tomasic, J. E., Brown, S., "GADGHT Tomorrow's Moving Map Today," GADGHT Team, VH Systems Engineering IPT, June 1999. Tomasicje@navair.navy.mil, brownsb@navair.navy.mil.

6. Avshop.Net Website, http://www.avshop.net/avshop/410418000.html, Jeppesen MentorPlus FliteMap, January 10, 1999.

7. McLees, Lea, "FalconView Soars," Research Horizons Website, http://www.gtri.gatech.edu/rh-sf97/falcon.htm, 1997.

8. Stewart, W. B.Sc., "Helicopter Behaviour in the Vortex-Ring Conditions," A.R.C. R/M-3117, November 1951.

9. Telephone Conversation With Mr. Louie Allen, USAF Flight Safety Desk, 505-846-1193, May 1999.

10. Telephone Conversation With LT. McGuire, USCG Human Resources/Safety/Security/Environmental, 202-267-1884, May 1999.

11. IFR Envelope Plot, BO-105 Manual, European Rotorcraft Forum. Estimated 1985.

12. Kolwey, H. G., 2 Engine H-53 PerformanceVortex-Ring State Excel Spreadsheet Modified By LCDR David J. Varnes, Naval Postgraduate School, July 1999.

13. Prouty, Raymond W., "Helicopter Performance, Stability, and Control," PWS Publishers, 1986.

14. Johnson, Wayne, "Helicopter Theory," Dover Publications, Inc., 1980.

15. Wolkovitch, Julian, "Analytical Prediction of Vortex-Ring State Boundaries for Helicopters in Steep Descents," Journal of the American Helicopter Society, July 1972.

16. Peters, David, A., and Chen, Shyi-Yuang, "Momentum Theory, Dynamic Inflow, and the Vortex-Ring State," Journal of the American Helicopter Society, July 1982.

17. Gao, Zheng, and Xin, Hong, "An Experimental Investigation on Vortex-Ring State Boundary," First Russian Helicopter Society Annual Forum Proceedings, August 1994.

18. Scheiman, James, "A Tabulation of Helicopter Rotor-Blade Differential Pressures, Stresses, And Motions As Measured In Flight," NASA TM X-952, Langley Research Center, National Technical Information Service, March 1964.

19. Kolwey, H. G., Excel Spreadsheet of Wolkovitch Vortex-Ring State Boundary as Modified by LCDR David J. Varnes, August 1999.

20. Yeates, John E., "Flight Measurements of the Vibrations Experienced by a Tandem Helicopter in Transition, Vortex-Ring State, Landing Approach, and Yawed Flight," National Advisory Committee For Aeronautics, Technical Note 4409, Washington, September 1958.

21. Wood, Roberts, E., "An Introduction To Helicopter Dynamics," Department of Aeronautics and Astronautics, Naval Postgraduate School, Monterey, CA, class handout.

22. McCool, Kelly, M., Haas, David, J., "Prediction of Helicopter Airspeed and Slideslip Angle in the Low Airspeed Environment," Caderock Division, Naval Surface Warfare Center, Bethesda, MD, Presented at the American Helicopter Society 53rd Annual Forum, May 1997.

THIS PAGE INTENTIONALLY LEFT BLANK

INITIAL DISTRIBUTION LIST

No. of Copies

1. Defense Technical Information Center 2
   8725 John J. Kingman Rd., Ste 0944
   Ft. Belvoir, VA 22060-6218

2. Dudley Knox Library 2
   Naval Postgraduate School
   411 Dyer Rd.
   Monterey, CA 93943-5101

3. Department Chairman, Code AA 1
   Department of Aeronautics and Astronautics
   Naval Postgraduate School
   699 Dyer Road, Rm. 137
   Monterey, CA 93943-5107

4. Dr. Russ W. Duren, Code AA/DR 2
   Department of Aeronautics and Astronautics
   Naval Postgraduate School
   699 Dyer Road, Rm. 137
   Monterey, CA 93943-5107

5. Dr. Roberts E. Wood, Code AA/WD 1
   Department of Aeronautics and Astronautics
   Naval Postgraduate School
   699 Dyer Road, Rm. 137
   Monterey, CA 93943-5107

6. Naval Air Warfare Center, NRWATS 1
Attn: Mr. James E. Tomasic, Jr.
VH Systems Engineering IPT
Hangar 111, Suite 2A, Mail Stop #1
Patuxent River, MD 20670-5304

7. N80 1
Attn: Captain Tom Stites
Naval Air Force, U.S. Atlantic Fleet
1279 Franklin Street
Norfolk, VA 23511-2494

8. Captain John Mullarky 1
CH-60 FIT
NAS North Island
Coronado, CA

9. Commander (N02X) 1
Naval Air Force, U.S. Atlantic Fleet
Attn: Mr. Steve Kern, Science and Technology Advisor
1279 Franklin Street
Norfolk, VA 23511-2494

10. Office Of Naval Research 09N 1
Naval Science Assistance Program
Attn: Mr. John Edwards
BCT 3 Rm. 159
800 N. Quincy Street
Arlington, VA 22216-5660

11. Naval Warfare Center Aircraft Division 1
Rotary Wing Aircraft Test Squadron
Attn: Herman Kolwey 4K1400A MS1
22681 Saufley Road
Patuxent River, MD 20670-5304

12. Midwest Helicopters 1
Attn: Mr. Benjamin Moore
525 Executive Dr.
Hinsdale, IL 60521

13. LCDR David J. Varnes 2
321 Arloncourt Rd
Seaside, CA 93955